The role of magnetic susceptibility in magnetic resonance imaging: MRI magnetic compatibility of the first and second kinds

John F. Schenck
General Electric Corporate Research and Development Center, Schenectady, New York, 12309

(Received 17 November 1995; accepted for publication 28 February 1996)

The concept of magnetic susceptibility is central to many current research and development activities in magnetic resonance imaging (MRI); for example, the development of MR-guided surgery has created a need for surgical instruments and other devices with susceptibility tailored to the MR environment; susceptibility effects can lead to position errors of up to several millimeters in MR-guided stereotactic surgery; and the variation of magnetic susceptibility on a microscopic scale within tissues contributes to MR contrast and is the basis of functional MRI. The magnetic aspects of MR compatibility are discussed in terms of two levels of acceptability: Materials with the first kind of magnetic field compatibility are such that magnetic forces and torques do not interfere significantly when the materials are used within the magnetic field of the scanner; materials with the second kind of magnetic field compatibility meet the more demanding requirement that they produce only negligible artifacts within the MR image and their effect on the positional accuracy of features within the image is negligible or can readily be corrected. Several materials exhibiting magnetic field compatibility of the second kind have been studied and a group of materials that produce essentially no image distortion, even when located directly within the imaging field of view, is identified. Because of demagnetizing effects, the shape and orientation, as well as the susceptibility, of objects within and adjacent to the imaging region is important in MRI. The quantitative use of susceptibility data is important to MRI, but the use of literature values for the susceptibility of materials is often difficult because of inconsistent traditions in the definitions and units used for magnetic parameters—particularly susceptibility. The uniform use of SI units for magnetic susceptibility and related quantities would help to achieve consistency and avoid confusion in MRI.

Key words: magnetic susceptibility, image-guided therapy, electromagnetic units, magnetic field compatibility, positional accuracy, safety of MR imaging

TABLE OF CONTENTS

 0094-2405/96/23(6)/815/36/$10.00

I. INTRODUCTION

Magnetic susceptibility is a quantitative measure of a material's tendency to interact with and distort an applied magnetic field. This interaction is so weak in most substances that magnetic susceptibility is a relatively obscure property and usually is not an important consideration in the selection of materials for a given application. With the advent of magnetic resonance imaging (MRI), however, magnetic susceptibility has become a conspicuous topic in radiology and medical physics: In MR-guided surgery[1–31] it is important to the choice of materials for instrumentation and determines, in part, the positional accuracy of MR images;[32–35] it is an important source of image artifacts[36–68] and of the hazards associated with magnetic forces and torques on surgically implanted foreign bodies and external orthotic devices;[69–82] its variation on a microscopic scale within tissues provides an important MR contrast mechanism for endogenous brain iron,[83–105] cerebral hemorrhage,[106–108] bone marrow,[109–112] and other organs; it is the physical basis for the field of functional brain imaging[113–132] and it can be used to study water diffusion in tissues.[133–140] Susceptibility-dependent shifts in the MR resonant frequency can be used to measure susceptibility.[141–146] In addition to its role in MRI, magnetic susceptibility has important applications in chemistry and physics.[147–183] The fields of paleomagnetism and environmental magnetism have given magnetic susceptibility an important role in geophysics.[184–197]

Quantitative susceptibility data are not readily available for many materials and, when available, are often difficult to use. These difficulties stem from inconsistent conventions, with regard to definitions and units, which have become entrenched in the literature and traditions of the various disciplines concerned with magnetic susceptibility. The purpose of this paper is to aid in the quantitative use of susceptibility data in MRI and MR-guided surgery and to draw attention to, and facilitate the the use of, information available in other disciplines. The physical principles of magnetic susceptibility are presented and its role in determining MRI compatibility and the positional accuracy of MR images is described. Extensive, but not exhaustive, references are provided to help illuminate the historical development of the concept and to place the role of susceptibility in MRI within the context of related disciplines.

The symbols used in the paper are defined in Table I. Unless stated otherwise, SI units, or their standard decimal multiples and submultiples, are used throughout the paper. In both the SI and CGS systems susceptibility is a dimensionless quantity. Later it is explained why peculiar units such as emu/cc, gauss/oersted and erg/(cc-oersted^2) are often attached to the values reported for this dimensionless quantity. Efforts to establish the use the SI definition and units for susceptibility across disciplines have so far been generally unsuccessful. This is particularly true in the fields of radiology, theoretical physics, chemistry, and geology. In these fields it is easy to find papers and textbooks[192] published in the 1990s that use non-SI units for susceptibility and that quote numerical values that sometimes cannot be interpreted even after careful study of the context. Despite the underlying simplicity of the concept, it is likely that confusion involving the definition and units of susceptibility will continue for some time.

II. MRI MAGNETIC COMPATIBILITY DISTINGUISHED FROM MRI COMPATIBILITY

Magnetic compatibility is the subject of this paper but it is not the only aspect of MRI compatibility. The B_1 excitation field produces a strong radio-frequency electric field which interacts with all electrically conducting materials within the imager: As a result, the electrical conductivity, as well as the magnetic susceptibility of materials is relevant to MRI compatibility. Many materials with good magnetic compatibility, such as ceramics and thermoplastic polymers, are electrical insulators and do not produce artifacts or hazards associated with applied electric fields. Some metallic materials, such as copper, brass, and aluminum also have good magnetic properties and experimentally it is found that rather large masses of these materials can be accommodated within the imaging region without significant image degradation. Experience with dental fillings and implanted nonmagnetic metal prostheses has demonstrated that small amounts of internal, nonmagnetic metallic conductors can be tolerated both from patient safety and image quality considerations.[70–72,75,77,82]

A full discussion of compatibility with the electric fields associated with MRI is beyond the scope of this paper. It is noted, however, that induced currents in closed loop conductors are much larger than those in conductors without closed loops:[198] Consequently, devices containing closed metallic loops should be avoided in MRI. If metallic conductors are

TABLE I. Definitions of symbols. Some symbols are used for more than one purpose because of established conventions. In each case the meaning should be clear from the context. SI units are specified except where standard decimal multiples or submultiples are conventional and convenient.

Symbol	Quantity	Units	Comments
B	Magnetic induction or magnetic flux density	T	Frequently referred to simply as the magnetic field. B_0 is the static in an MR scanner. ΔB is the perturbation in B produced by a magnetized object. The non-SI unit gauss (G) is frequently used: 1 T is equivalent to 10 000 G.
BW	Receiver bandwidth	Hz	32 kHz is a typical value for MR scanners.
c	Speed of light	m/s	299 792 458 m/s (exact by definition).
C	Curie constant	K	$C=\mu_0 N m^2/(3k)$.
CGS	System of unit		The centimeter, gram, and second.
d_o	Particle size	m	Maximum diameter for a single domain particle: commonly given in μm.
d_s	Particle size	m	Maximum diameter for a superparamagnetic particle; commonly given in μm.
e	Electric charge	C	The electron charge is $1.602\,177\times10^{-19}$ C.
E	Electric field	V/m	ΔE is the perturbation in E produced by an electrically polarized object.
E	Energy	J	E_n is the energy of an atom in the nth excited state. E_o is the ground state energy.
emu	Electromagnetic unit	-	A unit of the CGS magnetic series. The precise meaning depends on the context.
esu	Electrostatic unit	-	A unit of the CGS electric series. The precise meaning depends on the context.
f_o	Resonant frequency	Hz	For protons at 1 T, $f_o=42.5775$ MHz.
FOV	Field of view	m	Usually expressed in cm; typically ranges from 8–48 cm.
g	Landé g factor	Dimensionless	$g=2.002\,319$ for electrons; $g=5.5857$ for protons.
G	Gradient magnetic field	T/m	The non-SI unit, G/cm is frequently used. A typical value is 10 mT/m or 1 G/cm. G_x is the gradient in the x direction: G_R is the gradient in the readout direction.
h	Planck's constant	J s	$h=6.626\,076\times10^{-34}$ J s.
H	Magnetic field strength	A/m	Not commonly used in MRI; by convention, $\chi=M/H$; H_{dm} is the demagnetizing field. In the CGS system the unit oersted (Oe) is frequently used for H.
J	Total angular momentum quantum number	Dimensionless	The possible values are integers or half-integers: 0,1/2, 1, 3/2, 2, 5/2 ... .
J	Current density	A/m^2	$J=\sigma E$ (conduction current); $J=dP/dt$ (polarization current).
k	Boltzmann's constant	J/K	$k=1.380\,658\times10^{-23}$ J/K.
L_{no}	Orbital angular momentum	J s	The angular momentum matrix element coupling excited state n to the ground state.
M	Magnetization	A/m	The magnetic dipole moment per unit volume. M is the source function for the fields of magnetized materials. M_s is the saturation magnetization for ferromagnets and M_o is the remanent magnetization.
m	Magnetic dipole moment	A m^2 orJ/T	For electrons, $m=9.284\,77\times10^{-24}$ J/T. For protons, $m=1.410\,61\times10^{-26}$ J/T; the symbol used for nuclear dipole moment is m_n.
m	Mass	kg	The electron mass is $m_e=9.109\,39\times10^{-31}$ kg; the proton mass is $1.672\,62\times10^{-27}$ kg.
MKS	System of units		The meter, kilogram and second. SI units include the ampere to form the MKSA (Giorgi) system.
MW	Molecular weight	g/mol	The mass in grams of one mole (6.022×10^{23}particles) of a substance.
N	Particle density	m^{-3}	N=particles/m^3; N_e=conduction electrons/m^3; N_p=paramagnetic ions/m^3; N_{SP}=superparamagnetic particles/m^3; N_n=nuclei/m^3; for protons in water at 37 °C, $N_n=6.641\times10^{28}$ protons/m^3.
N	Number of pixels across the FOV	Dimensionless	Typically, $N=128$ or $N=256$.
P	Electric polarization	C/m^2	The electric dipole moment per unit volume.
r	Radial distance	m	$\langle r^2\rangle$ is the mean-square-radius of the electron orbits in an atom.
S	Total spin quantum number	Dimensionless	The possible values are integers or half-integers: 0,1/2, 1, 3/2, 2, 5/2 ... .
T_E, T_R	Imaging parameters	s	T_E is the echo time (typically 10–200 ms); T_R is the recovery time (typically 0.01 to 4 s).
T_1, T_2	Relaxation times	s	T_1 is the spin-lattice (longitudinal) relaxation time: T_2 is the spin-spin (transverse) relaxation time.
T_o, T_c, T_N	Critical temperatures	K	T_o is the critical temperature in the Curie–Weiss law; T_C is the Curie temperature for ferromagnets($T_o=T_C$); T_N is the Nèel temperature for antiferromagnets ($T_o=-T_N$).
Z	Atomic number	Dimensionless	Z is the number of orbital electrons per atom.

TABLE I. (*Continued.*)

Symbol	Quantity	Units	Comments
α	Demagnetizing factor	Dimensionless	There is one demagnetizing factor for each principal axis of an ellipsoid, α_1, α_2 and α_3: $\alpha_1+\alpha_2+\alpha_3=1$.
γ	Domain–wall surface energy	J/m^2	For iron, $\gamma=2.9\times10^{-3}$ J/m^2.
γ	Gyromagnetic ratio	rad/(s T)	The resonant frequency, $f_o=2\pi\gamma B_o$: for protons $\gamma/2\pi=42.577\,47\times10^6$ Hz/T; for nuclei in general, $\gamma=2\pi g\mu_N/h$.
ϵ	Permittivity	F/m	$\epsilon_o=8.8542\times10^{-12}$ F/m is the permittivity of free space. $\epsilon_r=\epsilon/\epsilon_o$ is the relative permittivity or dielectric constant.
μ	Permeability	H/m	$\mu_o=4\pi\times10^{-7}$ H/m is the permeability of free space. $\mu_r=\mu/\mu_o$ is the relative permeability.
μ_B	Bohr magneton	J/T	Unit of magnetic moment; $eh/(4\pi m_e)=9.274\,015\times10^{-24}$ J/T.
μ_{eff}	Effective number of Bohr magnetons	Dimensionless	$\mu_{\text{eff}}=m/\mu_B$. For atoms (e.g., transition elements)with fully quenched orbital angular momentum, $\mu_{\text{eff}}=2\sqrt{S(S+1)}$.
μ_N	Nuclear magneton	J/T	$eh/(4\pi m_{\text{proton}})=5.050\,79\times10^{-27}$ J/T.
ρ	Mass density	kg/m^3	Using decimal sub-multiples of the SI units ρ can be expressed in units of g/cc.
σ	Electrical conductivity	Ω^{-1} m^{-1}	$J=\sigma E$.
χ	Susceptibility	Dimensionless	The terms magnetic susceptibility, volume susceptibility and susceptibility per unit volume are used loosely and interchangeably in the literature. $\chi=M/H$; $\Delta\chi=\chi-\chi_{\text{water}}$, χ_n is the nuclear susceptibility.
χ_e	Electric susceptibility	Dimensionless	For most materials this parameter is much larger than the magnetic susceptibility, χ.
χ_g	Mass susceptibility	m^3/kg	Defined as χ/ρ. The use of the SI submultiple unit cc/g for χ_g is often convenient.
χ_M	Molar susceptibility	m^3/mol	Defined as χMW/ρ. The use of the SI sub-multiple unit cc/mol for χ_M is often convenient.

placed inside, or are in superficial contact with, a patient's body, during MRI, the possibility of inadvertent current loops that use part of the patient's body as a conducting path should be considered and, if possible, avoided.

III. BASIC PHYSICS OF MAGNETIZATION AND SUSCEPTIBILITY

A. Susceptibility and permeability

For materials whose magnetization, M, depends linearly on the applied field, H, the susceptibility, χ, is defined by the formula $M=\chi H$, and is closely related to the permeability $\mu=\mu_r\mu_o$, which is defined by $B=\mu H$. Using $B=\mu_o(H+M)$, it is easy to show that $\chi=\mu_r-1$. Thus knowing the magnetic susceptibility of a material is equivalent to knowing its relative permeability and the two quantities are redundant. However, both of these parameters have firmly established realms of usage and it is a matter of tradition which of them is used in a given situation. For the common "magnetic" materials, $\mu_r\gg1$, and the susceptibility and relative permeability are essentially equal to one another. Historically, strongly magnetic materials have been described in terms of permeability rather than susceptibility. On the other hand, the majority of materials important in MRI are only weakly magnetic and have $|\chi|\ll1$: In these cases, the use of μ_r is numerically inconvenient. As an example, for water at 37 °C, $\chi=-9.05\times10^{-6}$, and $\mu_r=0.999\,990\,95$. This is likely the reason it is traditional to use the susceptibility, rather than the relative permeability, to characterize weakly magnetic materials.

B. Classification of magnetic materials

For most materials the magnetization can be expressed as a function of the applied field by $M=M_o+\chi H$. Here, M_o represents inherent magnetization that is present in some materials even in the absence of an applied magnetic field: The term χH accounts for magnetization induced by an externally applied field. This equation can be considered as the first two terms of a Taylor series representing the magnetization as a function of field strength. In some cases, particularly in strong fields, M does not vary linearly with H, and higher order susceptibility coefficients corresponding to terms in the magnetization proportional to quadratic, cubic and higher powers of H are required; however, in MRI, the linear term almost always suffices.

Although this approach is not sufficient for MRI, materials are traditionally classified into three categories with regard to their magnetic properties—hard magnetic materials, soft magnetic materials, and nonmagnetic materials. The hard magnetic materials have a nonzero, remanent magnetization M_o that can range from near zero to values as high as 1.05×10^6 A/m for neodymium–iron–boron alloys. M_o is not truly constant but can be changed by application of an intense magnetic field. Field-induced changes in M_o persist to some degree when the magnetizing field is removed and, therefore, for a given hard magnetic material M_o can have a range of values—including zero. The M_o exhibited by these materials depends on the history of their field exposure. Magnetic hardness, defined as the the ability to resist field-induced changes in M_o and to maintain a high remanent magnetization, tends to correlate with mechanical hardness.

Good permanent magnet materials include the high carbon steels, alnico (an alloy of aluminum, nickel, iron, cobalt, and other metals), barium ferrite, samarium–cobalt alloys, and neodymium–iron–boron. Some common, naturally occurring, minerals such as magnetite or lodestone (Fe_3O_4) and hematite (Fe_2O_3) can maintain permanent magnetic moments over geological time spans.[186–195] Generally speaking, hard magnetic materials are anathema to MRI and, unless otherwise stated, it is assumed in this paper that $M_o=0$.

Soft magnetic materials are not magnetized ($M_o=0$) unless they are subjected to an applied magnetic field. However, their susceptibility is very large and they exhibit easily detected forces and torques in the presence of a strong magnetic field. Materials in the nonmagnetic category have such small susceptibilities that no forces and torques are normally apparent when they are placed in an applied field. However, field-induced magnetization can be demonstrated in all materials by use of the proper sensing equipment—and MRI is sensitive to the fields produced even by very small magnetizations. There is no precise susceptibility value that separates soft magnetic materials from nonmagnetic materials, but a reasonable criterion, which is used in this paper, is to classify as magnetic materials all those substances with either a nonzero value for M_o or with an absolute value of susceptibility greater than 0.01. By these criteria, the vast majority of common materials, including essentially all plant and animal tissues, are nonmagnetic. However, the term nonmagnetic is meaningful only in a relative sense, and, although it is often attempted, it is incorrect to regard all nonmagnetic materials as automatically MR compatible.

FIG. 1. MRI magnetic incompatibility. Ferromagnetic components within this radio-frequency power amplifier became magnetized when it was inadvertently moved too close to a 1.5 T superconducting magnet and the magnetic forces overcame the ability of the workmen moving the power supply to restrain it. A block and tackle apparatus was required to remove it from the magnet bore and the incident caused a magnet quench. (Photograph courtesy of Dr. W. A. Edelstein.)

C. Magnetic aspects of MRI compatibility

The parameters χ and M_o determine, from a magnetic standpoint, the suitability of a material for use in or near an MR imaging system. Bulk samples of hard (large M_o) and soft (large χ) materials experience strong magnetic forces in the presence of intense magnetic fields. Unless firmly anchored to supporting structures, these materials should be excluded from the vicinity of MRI systems for safety reasons alone (Fig. 1). Thus it is reasonable, as is commonly done, to lump the hard and soft magnetic materials together as magnetically incompatible with MRI (Table II). In some cases, it may be acceptable to use very small magnetic objects (such as a magnetic screw in a large, nonmagnetic frame) or a dilute dispersion of small magnetic particles in a nonmagnetic matrix (such as superparamagnetic contrast agents), but the consequences of such choices should be carefully considered.

Hard and soft magnetic materials can easily be identified and excluded from consideration by testing with a small permanent magnet. In nature, however, overtly magnetic materials are relatively uncommon, and the vast majority of materials appear inert to casual testing with permanent magnets and exhibit varying degrees of compatibility with MRI. Although these "nonmagnetic" materials exhibit a continuous range of magnetic properties, to simplify the discussion they are classified in Table II into MR compatibility groups of the first and second kinds. The susceptibility of the materials of the first kind is large enough that, when they are within or near the imaging region, the induced magnetization significantly degrades the MR image. Therefore, magnetic field compatible materials of the first kind can be considered safe from the standpoint of mechanical forces but they are not acceptable if stringent image quality criteria are imposed. The susceptibility of the second group is sufficiently close to that of human tissues that they may be used within the imaging region without substantial degradation of image quality.

The distinction between MR compatibility of the first and second kinds is particularly relevant to the design of instruments for MR-guided therapy. It is important that these instruments—scalpels, cannulas, endoscopes, implants, and so on—do not impede surgical procedures or impair patient safety by exhibiting extraneous forces or torques in or near the magnet. This requirement is met by both kinds of MR magnetically compatible materials. For instrumentation, such as anesthesia equipment, that is used in the vicinity of the scanner but not directly within the imaging region, it is necessary only that the materials used possess MR magnetic

TABLE II. MRI magnetic compatibility for MRI applications. χ_{water} is taken as -9.05×10^{-6} and is a close approximation to the susceptibility of human tissues. The precise susceptibility boundaries between the classes is approximate and will vary with the application. In theory, if M_o were not precisely zero, but sufficiently small, a material could exhibit magnetic field compatibility of the first kind ($M_o<\sim10^4$ A/m) or of the second kind ($M_o<\sim10$ A/m).

Conditions	Property	Examples	Comments
$M_o\neq0$ and/or $\lvert\chi\rvert>10^{-2}$	MRI magnetic incompatibility	Iron, cobalt, magnetic stainless steel, nickel	These materials experience strong magnetic forces and torques and create image distortion and degradation even when they are located far from the imaging region.
$10^{-5}<\lvert\chi-\chi_{water}\rvert<10^{-2}$	MRI magnetic compatibility of the first kind	Titanium, bismuth, nonmagnetic stainless steel	These materials do not experience easily detectable forces or torques, but they can produce marked image distortion and degradation if they are located close to the imaging region.
$\lvert\chi-\chi_{water}\rvert<10^{-5}$	MRI magnetic compatibility of the second kind	Water, human tissues, copper, zirconia	These materials produce no easily detected forces or torques and very limited or negligible image distortion or degradation even when located close to the imaging region.

compatibility of the first kind. However, instruments used directly in the imaging region should not excessively degrade the image or reduce its positional accuracy. This requires the use of magnetically compatible materials materials of the second kind. The failure to distinguish between these two forms of magnetic compatibility has led to confusion and impaired the development of instruments for MR-guided surgery. The degree of image degradation that can be tolerated depends on the details of each surgical procedure. The criteria in Table II are a reasonable guide for the initial evaluation of the suitability of a material. However, in a given application, the precise values for the acceptable susceptibility values may be somewhat more or less stringent.

To quantify the forces involved in MR-guided therapy, the magnetic forces (F_m) on a surgical instrument made from nonmagnetic stainless steel with a density of 8 g/cc (8000 kg/m^3) and $\chi=0.01$ can be compared with its weight. The weight is $F_g=\rho g V$, where $g=9.80$ m/s^2 is the acceleration of gravity and V is the instrument's volume. In an MR scanner a magnetic force,

$$F_m=(\chi V/\mu_0)B\ \partial B/\partial r,$$

tends to pull the instrument into the region of strongest field. Here, $\partial B/\partial r$ is the field gradient at the position of the instrument. The ratio of magnetic to gravitational forces is given, in terms of the material properties χ and ρ, by

$$F_m/F_g=(1/\mu_0 g)B\ \partial B/\partial r(\chi/\rho).$$

The maximum value for $B\ \partial B/\partial r$ along the axis of the MR scanners with strongest fields (4T) now in use[199] is on the order of 8.8 T^2/m. In this unusually strong magnet the maximum value for F_m/F_g is 0.89 and the magnetic force is slightly less than the weight. The value of B ∂B/∂r is approximately proportional to the square of the main field and for a conventional scanner, operating a lower field, the force ratio can be much smaller: At 0.5T, F_m/F_g is about 1/64 of that calculated above. Magnetic torques that tend to align the instrument with the field are also present. These torques depend on the shape of the instrument and are usually more powerful than the translational forces. However, in either situation, if $\lvert\chi\rvert<0.01$, the magnetic forces and torques on "nonmagnetic" stainless steel instruments, although possibly inconvenient, are ordinarily manageable even at the center of the scanner; however, such instruments do produce serious image artifacts.

The size and location of an object, as well as its magnetization and susceptibility, are important in determining its MR compatibility. If a magnetic object is extremely small (e.g., much smaller than an image voxel) it may not significantly affect the imaging process and the magnetic forces and torques may be insignificant even if it is located directly within the imaging region. Also, as the induced field of an object falls off rapidly with the distance, r, away from the object ($\Delta B\propto 1/r^3$), larger and more strongly magnetized objects can be tolerated if they are sufficiently far from the imaging region.

D. Thermodynamic and symmetry constraints on susceptibility values

In principle, paramagnetic materials, which, by definition, have $\chi>0$, can exhibit arbitrarily large susceptibility values. However, from energy conservation, it can be shown that, for diamagnetic materials ($\chi<0$), the minimum possible susceptibility value is $\chi=-1.0$.[200] This, in turn, requires that the relative permeability of all materials is greater than, or equal to, zero. Susceptibility values near the limiting value of -1.0 are found only in superconducting materials and at cryogenic temperatures; therefore, this limiting value of diamagnetic susceptibility is not encountered in MRI.

Many crystalline materials are anisotropic and magnetize more readily in some directions than in others. In this case, M, is not necessarily parallel to H, and the susceptibility is a tensor, not a scalar, quantity. This tensor is defined, in Cartesian coordinates, by $M_i=\chi_{ij}H_j$. Irrespective of the physical mechanism responsible for a material's magnetic response, it can be shown that the susceptibility tensor is symmetric ($\chi_{ij}=\chi_{ij}$): If a material did not meet this require-

TABLE III. Volume, mass and molar susceptibility.

Quantity	Symbol	Definition	MKS Units	CGS Units[a]
Susceptibility[b]	χ	$\chi=M/H$		emu/cc
Mass susceptibility	χ_m	$\chi_m=\chi/\rho$	m^3/kg[c]	emu/g
Molar susceptibility	χ_M	$\chi_M=\chi MW/\rho$	m^3/mol[c]	emu/mol

ρ=density; MW=molecular weight in g/mol in the CGS system and kg/mol in the MKS system.

[a]Within the CGS system several alternatives to the listed units are used as discussed in the text.
[b]The terms volume susceptibility and magnetic susceptibility are often used interchangeably with the term susceptibility.
[c]The units cc/g for χ_m and cc/mol for χ_M are also used within the mks system using the rationalized value for χ.

ment it could be used to construct a perpetual motion device.[201] Symmetric tensors have only six, not nine, independent components, and at every point in a material there is a set of principal axes such that only the diagonal elements ($i=j$) of the tensor are nonzero. It is usually assumed that the susceptibility is measured under conditions of thermal equilibrium at a constant temperature, T: At low temperatures and at high frequencies paramagnetic spin systems sometimes achieve thermal equilibrium among the spins but not with the lattice. In this case a distinction is made between the conventional, or isothermal susceptibility, $\chi=(\partial M/\partial H)_T$, measured at constant temperature, T, and the smaller, adiabatic susceptibility, $\chi_s=(\partial M/\partial H)_s$, measured at constant entropy, S.[161,202] With few exceptions, the materials relevant to MRI are isotropic and are at a fixed temperature: As a result χ may ordinarily be taken to be a scalar and isothermal quantity.

E. Conventions and systems of units for magnetic quantities

A substantial effort has gone into devising electromagnetic units that permit the fundamental formulas to be expressed simply and elegantly and, at the same time, are of a convenient order of magnitude for practical use.[203–221] One approach has been based on the CGS (centimeter, gram, second) set of mechanical units, while a second has used the MKS (meter, kilogram, second) units. The MKS system, supplemented by the ampere as a fundamental electrical unit to form the MKSA system, has been adopted in the SI international system of units. The MKSA system is based on a suggestion of Giorgi:[203] It utilizes the defined constant μ_0 and incorporates the proposal of Heaviside[222–225] to rationalize the units by utilizing a factor, 4π, in the denominator of the fundamental force laws.

To facilitate the analysis of the forces present in the vicinity of magnetized materials Kelvin[148] introduced in 1848, as a mathematical convenience, two magnetic fields, B and H. In the CGS units used by Kelvin, $B=H+4\pi M$. Using this definition B and H are identical in free space where $M=0$, but differ inside magnetized matter where $M\neq 0$. The fields B and H have been retained on roughly equal footing in the theory of magnetism: They are formally distinguished by referring to B as the magnetic flux density or the magnetic induction and H as the magnetic field strength, magnetic intensity, or magnetizing force; in practice, however, either quantity is often referred to simply as the magnetic field. Confusion between B and H is common,[226,227] although this could be avoided by adherence to the original definitions.[155,228] To create the MKS system, Giorgi (1901) redefined Kelvin's B and H so that $B=\mu_o(H+M)$ and in these (SI) units $B=\mu_o H$ in free space. As discussed below, in the CGS system it was decided in 1930 to use differing units for B (gauss) and H (oersted).

For many applications, and MRI is an example, B and H are more or less redundant with B being generally more useful and fundamental. Lorentz showed[150,173,180] that the field B represents the *average* field of force inside an object comprised of atoms and molecules and that the field H does not have such an interpretation. Use of the field H might not be necessary at all in MRI except that Kelvin chose to define the susceptibility as M/H rather than M/B; from a modern perspective, M/B might have been a preferable definition.[173] Traditionally, the demagnetizing factors, to be discussed below, are also defined in terms of H rather than B.

In both the CGS convention with $B=H+4\pi M$ and in the Sommerfeld[164,182] or MKSA (SI) convention with $B=\mu_o(H+M)$, the volume susceptibility is defined by $\chi=M/H$. By definition, then, χ is dimensionless in both systems, but

$$\chi_{\mathrm{MKSA}}=4\pi\chi_{\mathrm{CGS}}.$$

It is easy to recast the definition of susceptibility so that it is no longer dimensionless. For example, the Kennelly convention, sometimes used in magnetic materials research,[164,182] takes $B=\mu_o H+M$. In this case, the tesla (T) is the unit for both M and B, and $\chi=M/H$ is not dimensionless, but has the units as H/m, the same as μ_o.

F. Volume susceptibility, Mass susceptibility, and Molar susceptibility

One source of confusion regarding the published susceptibility data is loose usage of the term susceptibility for any of three distinct concepts—the volume, mass, and molar susceptibilities (Table III). The quantity ordinarily implied by the term susceptibility is the volume susceptibility which is dimensionless in both the SI and CGS systems. The mass and molar susceptibilities are defined in terms of magnetization per unit mass or per mole of material and are not dimensionless. A numerical susceptibility value is ambiguous un-

TABLE IV. Susceptibility using various definitions and systems of units. Ideally, susceptibility data is presented using dimensionless SI units. This table illustrates the variety of equivalent forms in which the susceptibility of water and the paramagnetic compound, Mohr's salt, might occur in the literature.

Parameter	Water[a] (37 °C)	Mohr's salt[b] (25 °C) (Ferrous ammonium sulfate)
Volume susceptibility (χ)		
SI units	-9.05×10^{-6}	750×10^{-6}
CGS units	-0.72×10^{-6}	59.7×10^{-6}
	-0.72×10^{-6} emu/cc	59.7×10^{-6} emu/cc
	-0.72×10^{-6} G/Oe	59.7×10^{-6} G/Oe
	-0.72×10^{-6} erg/(cc Oe^2)	59.7×10^{-6} erg/(cc Oe^2)
	-0.72×10^{-6} erg/(cc G^2)	59.7×10^{-6} erg/(cc G^2)
	-0.72×10^{-6} emu/(cc Oe)[c]	59.7×10^{-6} emu/(cc Oe)[c]
Mass susceptibility ($\chi_g=\chi/\rho$)		
SI units	-9.09×10^{-9} m^3/kg	0.402×10^{-6} m^3/kg
	-9.09×10^{-6} cc/g	402×10^{-6} cc/g
CGS units	-0.723×10^{-6} cc/g	32.0×10^{-6} cc/g
	-0.723×10^{-6} emu/g, etc.	32.0×10^{-6} emu/g, etc.
Molar susceptibility ($\chi_M=\chi$MW$/\rho$)		
SI units	-1.64×10^{-10} m^3/mol	158×10^{-9} m^3/mol
	-1.64×10^{-4} cc/mol	158×10^{-3} cc/mol
CGS units	-1.30×10^{-5} cc/mol	125×10^{-4} cc/mol
	-1.30×10^{-5} emu/mol, etc.	125×10^{-4} emu/mol, etc.

[a]For water at 37 °C, $\rho=0.933$ g/cc$=993.3$ kg/m^3, and MW$=18.015$.
[b]For Mohr's salt at 25 °C, $\rho=1.864$ g/cc$=1864$ kg/m^3, and MW$=392.13$.
[c]In this convention the term emu is used for the electromagnetic unit of dipole moment.

less it is clear whether it represents a volume, mass, or molar susceptibility and whether the SI, CGS, or some other system of units is employed.

G. Superfluous units for susceptibility

Although the standard definitions assure that the volume susceptibility is dimensionless, there is a tradition, particularly in the CGS system, of attaching superfluous units to it. The most common of these units are the emu/cc, the gauss/oersted, and the erg/cc-oersted.[2] Other variants, including some based on the MKSA system, are sometimes encountered. The origin of the term oersted is described below. Dimensional analysis demonstrates that these units can be considered as obliquities which camouflage the dimensionless character of χ; they originated during the tangled historical development of the electromagnetic units.[203–231] Table IV displays some of the many forms in which the susceptibility of two materials, water and the paramagnetic salt, ferrous ammonium sulfate, might be found in the literature.

The terms emu (electromagnetic units) and esu (electrostatic units) are used to designate two versions of CGS units for electricity and magnetism. The terms emu or esu are often attached to electrical and magnetic measurements to indicate which system is being used. Over time, the terms emu and esu sometimes have come to be treated as though they designated specific units rather than systems of units; for example, it is common to attach the term emu/cc to CGS values of the volume susceptibility. To have correct dimensions, the term emu, when used this way, must be taken as equivalent to a cubic centimeter (cc):[181] This leads to the units emu/g for the mass susceptibility, and emu/mol for the molar susceptibility. An additional complication is that the usage of the term emu is not fixed. For example, emu is sometimes used as a CGS unit of magnetic dipole moment. Under this convention the unit of magnetization is the emu/cc[229] and the volume susceptibility is given the unit emu/cc-gauss or emu/cc-oersted. In this case emu is not equivalent to a cc as above, but is either a cc-oersted or a cc-gauss.

Some authors have held that the units to be used for physical quantities are not simply to be determined by convenience and mutual agreement, but are of fundamental physical significance that can be elucidated by theory and experiment.[230,231] In particular, Rücker argued that the permeability, defined as B/H in CGS units, was not dimensionless as ordinarily assumed: Instead, somehow the "true units" of permeability were actually unknown, had been "suppressed" by its mode of derivation, and might be discovered by further research. This view was widely criticized:[159] Planck wrote that the goal of determining "··· the 'real' dimensions of a physical quantity ··· has no more sense than inquiring into the 'real' name of an object;" [209] Birge wrote, "the attempt on the part of certain subsequent writers to incorporate Rücker's philosophy into electromagnetic theory has resulted in a devastating variety of treatments." [211] Nonetheless, in 1930 and 1932 international committees determined by ballot:[206–208] "that B and H are quantities of fundamentally different nature; that $\mu=B/H$ is not a pure number; that the unit gauss is to be used only for B and M; and that a new unit, the oersted, is to be used for H." In this case the CGS unit for $\chi=M/H$ becomes the gauss/oersted (G/Oe). Whether it is worthwhile to consider

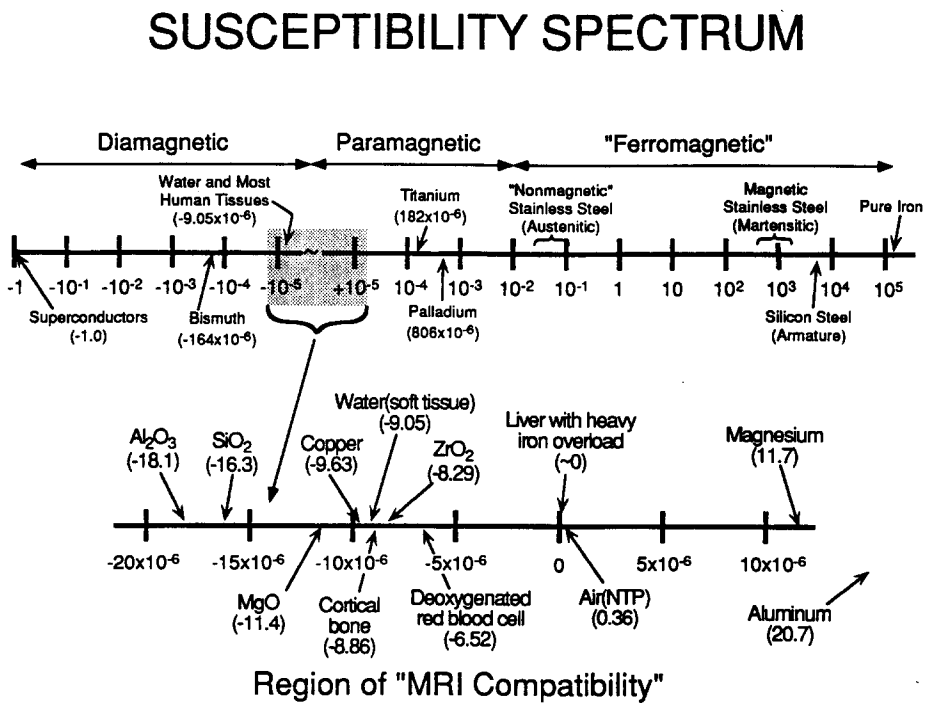

FIG. 2. Susceptibility spectrum. The upper diagram uses a logarithmic scale to indicate the full range of observed magnetic susceptibility values: It extends from $\chi=-1.0$ for superconductors to $\chi>100\,000$ for soft ferromagnetic materials. The bottom diagram uses a linear scale (in ppm) to indicate the properties of some materials with $|\chi|<20$ ppm. The susceptibilities of most human tissues are in the range from -7.0 to -11.0 ppm.

the gauss and the oersted as different units is contentious; formally, they both have the dimensions of $g^{1/2}/(cm^{1/2}\ s)$ and their ratio is dimensionless, or, perhaps, of "suppressed" dimensions. The term oersted does not appear to serve a purpose that the term gauss does not, other, perhaps, than to raise awareness of the need to properly distinguish B and H inside materials.[164] Despite the dubious rationale for its use, the oersted is deeply entrenched in the literature of magnetism: At any rate, when used as a CGS unit for the volume susceptibility, the unit G/Oe may be replaced by unity without changing the physical implications of any calculation.

The CGS unit of energy is the erg which is equivalent to the $g\ cm^2/s^2$. The work, W, required to magnetize an object of volume V is (in CGS units), $W=1/2\chi VH^2$. If this formula is solved for χ, a formal CGS unit for susceptibility is found to be the erg/(cc-oersted^2) or, equivalently, the erg/(cc-gauss^2). This unit is used for the volume susceptibility by some authors and its analog, the erg/(gauss^2-mol),[232] is also used as a unit for molar susceptibility. Substituting the expressions for the erg and oersted or gauss in terms of fundamental units shows that this unit is, again, an obfuscation tending to conceal the fact that χ, in CGS units, is dimensionless.

H. Magnetic susceptibility of common materials

The magnetic susceptibilities of materials vary over several orders of magnitude (Fig. 2). Tables V and VI summarize published susceptibility values for a wide variety of materials. These have been taken from several sources[233–242] and converted, where necessary, to SI units. To facilitate the calculation of mass and molar susceptibilities, the molecular weights, and densities are also tabulated. Susceptibility values for ferrous ammonium sulfate[171,233] and for nickel chloride solution[171,234] have been included in Table V to show the magnitude of the room-temperature paramagnetism that can be achieved in paramagnetic salts and in concentrated solutions of transition metal ions. Oxygen is paramagnetic and its presence makes the susceptibility of air slightly positive: This very small effect can be used to measure the concentration of oxygen in gas mixtures.[243–245]

The formal definition of susceptibility as the dimensionless ratio, M/H, does not provide an intuitive insight into the physical implications of its numerical magnitude. For illustration note that a field with $B=1.5$ T corresponds to $H=1.19\times10^6$ A/m: In this applied field water and human tissues have $M\approx-10.8$ A/m; titanium has $M=217$ A/m; and nonmagnetic stainless steels have M in the range from 4200–8000 A/m. If, as usually the case in MRI, the absolute value of $\chi\ll1$, a more intuitive visualization of the physical consequences of a given susceptibility value can be developed by considering the induced field that results when an object is placed in a uniform external field, B_o. Only ΔB_z, the component parallel to B_o, is relevant to MR and, in the region of the magnetized object, ΔB_z takes on both positive and negative values: The induced field is strongest inside the object and on its surface; although it depends on the sample's shape, it is always in the range

$$-\chi B_o<\Delta B_z<\chi B_o.$$

TABLE V. Susceptibilities of selected weakly magnetic materials. In the absence of pathological iron deposition, the susceptibilities of the various human soft tissues are estimated to be within ±2 ppm (~20%) of χ_{water}. Most tissues are probably within 1 ppm of this value.

Material	Density (g/cc or, 10^{-3} kg/m^3)	Atomic or molecular weight[a]	Susceptibility ($\times 10^6$)
Graphite[b] (perpendicular to atomic planes)	2.26	12.011	−595
Carbon[b] (polycrystalline graphite)	2.26	12.011	−204
Bismuth	9.75	208.98	−164
Antimony	6.691	121.75	−67
Indium	7.31	114.82	−51
Thallium	11.85	204.38	−37
Gold	19.32	196.97	−34
Mercury	13.546	200.59	−28
Beryllium	1.85	9.012	−24
Silver	10.50	107.87	−24
Gallium	5.907	69.723	−23
Tin (α-gray)	5.75	118.71	−23
Carbon (diamond)	3.513	12.011	−21.8
Phosphorus (white)	1.82	30.973	−20
Selenium	4.79	78.96	−19
Phosphorus (red)	2.20	30.973	−18.5
Alumina (Al_2O_3)	3.97	101.96	−18.1
Silica (SiO_2)	2.64	60.08	−16.3
Lead	11.35	207.2	−15.8
Zinc	7.13	65.39	−15.7
Pyrex Glass (Corning 7740)			−13.88
Sulfur (α)	2.07	32.066	−12.6
Sulfur (β)	1.957	32.066	−11.4
Magnesia (MgO)	3.58	40.30	−11.4
Copper	8.92	63.546	−9.63
Water (37 °C)	0.933	18.015	−9.05
Human Tissues	~1.00–1.05		~(−11.0 to −7.0)
Silicon Nitride (Si_3N_4)	3.44	140.28	~−9.0
Graphite[b] (parallel to atomic planes)	2.26	12.011	−8.5
Zirconia (ZrO_2)	6.49	123.22	−8.3
Whole Blood (deoxygenated)[b]	1.057		−7.90
Germanium	5.323	72.61	−7.1
Red blood cell (deoxygenated)[b]	1.093		−6.52
Silicon	2.33	28.0855	−4.2
Liver (severe iron overload)[c]			~0.0
Hemoglobin Molecule (deoxygenated)[c]	1.335	64 650	+0.15
Air (NTP)	0.001 29	28.97	0.36
Tin (β-white)	7.31	118.71	2.4
Rubidium	1.532	85.468	3.8
Cesium	1.873	132.91	5.2
Potassium	0.862	39.098	5.8
Sodium	0.971	22.99	8.5
Magnesium	1.74	24.305	11.7
Yttria (Y_2O_3)	5.01	225.81	12.4
Aluminum	2.70	26.98	20.7
Calcium	1.55	40.078	21.7
Tungsten	19.3	183.85	77.2
Zirconium	6.49	91.22	109
Nickel chloride in water[d]	1.255		116
Yttrium	4.47	88.91	119
Molybdenum	10.22	95.94	123
Rhodium	12.41	102.906	169
Tantalum	16.65	180.95	178
Titanium	4.54	47.88	182
Niobium	8.57	92.91	237
Nitinol (50% titanium, 50% nickel)	6.5		245
Platinum	21.45	195.08	279
Chromium	7.19	51.996	320
Vanadium	6.11	50.94	384
Ferritin (total molecule)[c]	1.494	929 850	520
Mohr's salt[e]	1.864	392.13	750

TABLE V. (*Continued.*)

Material	Density (g/cc or, 10^{-3} kg/m^3)	Atomic or molecular weight[a]	Susceptibility ($\times 10^6$)
Palladium	12.02	106.42	806
Ferritin core[c,f]	2.727	449 850	2011
Stainless Steel (nonmagnetic, austenitic)	8.0		3520–6700

[a]Based on the atomic mass unit: $1.660\,540\times10^{-27}$ kg (1/12 the mass of ^{12}C).
[b]References 355 and 356.
[c]Estimated (Ref. 122).
[d]Concentrated aqueous solution at 20 °C; 23.15 wt. % $NiCl_2$. From Refs. 171 and 234.
[e]Ferrous ammonium sulfate ($FeSO_4(NH_4)_2SO_4\cdot6H_2O$) at 17.2 °C. From Refs. 171 and 233.
[f]The nominal composition of the core is $(FeOOH)_8\cdot FeO\cdot H_2PO_4$.

The maximum field perturbation, ΔB_{max}, is related to χ, in SI units, by the formula

$$\chi \approx \Delta B_{max}/B_o:$$

For spheres, the exact expression is $\chi=3/2\Delta B_{max}/B_o$. Therefore, the susceptibility in SI units is a rough, but simple, measure of the degree to which an object can perturb an applied field. An object with $\chi=1\times10^{-6}$ (1 ppm), produces a maximum perturbation of about ±1 ppm in the surrounding field and in the resonant frequency. If the susceptibility is 10 ppm, the effect is ten times as large and so on.

A soft magnetic material with $\chi\gg1$, although subject to saturation, can produce an induced B field that is locally larger than the applied field: Superconductors, which have $\chi=-1$, can completely cancel an applied field in their interior ($\Delta B_{max}=-B_o$). Most materials, have $\chi\ll1$, and produce only very small fractional perturbations in applied fields; however, because of its sensitivity to tiny variations in the static field, even very small susceptibility values are important to MRI.

TABLE VI. Susceptibilities of strongly magnetic materials.[a] For the materials with field-dependent susceptibilities the maximum differential values are tabulated. The initial susceptibility values at small applied fields are usually smaller than the tabulated values. The susceptibilities of these materials are variable and depend on crystal perfection, residual strains, and impurity content. The measurement of high susceptibility values is difficult because of the strong demagnetizing fields associated with them (Ref. 163).

Material	Density (g/cc)	Atomic or molecular weight	Susceptibility
α-Fe_2O_3 (hematite)	5.277	159.70	1.46×10^{-3}
γ-FeOOH (lepidocrocite)	4.0	88.85	2.12×10^{-3}
α-FeOOH (goethite)	4.28	88.85	2.65×10^{-3}
Fe_3O_4 (magnetite)	5.18	231.54	70
Cobalt	8.9	58.933	250
Nickel	8.9	58.69	600
Stainless steel (magnetic, martensitic)	7.8		400–1100
Mumetal[b]	8.76		100 000
Iron	7.874	55.847	200 000
Supermalloy[c]	8.77		1 000 000

[a]Data adapted from Refs. 163, 235, 237, 238, and 267.
[b](16% Fe, 5% Cu, 2% Cr, 77% Ni).
[c](16% Fe, 5% Mo, 79% Ni).

I. Comparison of electric and magnetic susceptibilities

The electric susceptibility, χ_e, is analogous to the magnetic susceptibility, χ. It is defined by the relation $P=\chi_e\epsilon_0E$. P is the electric polarization induced by the applied electric field, E. The electric susceptibility is dimensionless and is related to the dielectric constant or relative permittivity, $\epsilon_r=\epsilon\epsilon_0$, by $\chi_e=\epsilon_r-1$. A fundamental difference between the electric and magnetic properties of materials is that χ_e is typically on the order of 1–10, while the magnetic susceptibility is orders of magnitude smaller, on the order of 10^{-5} to 10^{-3}. For example, silica (SiO_2) is diamagnetic with a magnetic susceptibility of -16.3×10^{-6} while its electric susceptibility is 2.78: A sample of silica perturbs an applied electric field 170 000 times more than an applied magnetic field. For water, the magnetic susceptibility is -9.05×10^{-6} and the electric susceptibility is 80 giving a ratio of 8.8×10^6. This discrepancy between electric and magnetic susceptibilities explains why most materials appear inert to applied magnetic fields even though they interact strongly with applied electric fields. A physical explanation of the discrepancy between the sizes of the electric and magnetic susceptibilities is that most materials are diamagnetic and, in a sense, diamagnetic forces may be considered as relativistic corrections to electric forces. This leads to an estimate of the value of the diamagnetic susceptibility, $\chi\approx(v/c)^2$, where v is the orbital velocity of the atomic electrons.[246] These velocities are on the order of c/300 and this estimate gives the correct order of magnitude for χ for those materials whose susceptibility is dominated by the diamagnetism of the orbital electrons and electron spin is not involved.

Another difference between the electric and magnetic properties of materials is that there are no magnetic currents associated with the motion of free magnetic poles within materials analogous to the electric currents associated with the motion of electric charges in electrical conductors. The mobility of electrical charges in metals and electrolyte solutions causes them to completely screen static applied electric fields from their interiors: It also leads to Joule heating in closed conducting circuits. There is no analog to this type of screening or to Joule heating associated with the application of a static magnetic field to an object.

J. Magnetic susceptibility at high frequencies and in intense fields

The standard definition of magnetic susceptibility, $\chi = M/H$, implies a steady state magnetization, M, induced by a steady state applied field, H. Although this definition is adequate for most MRI applications, generalized definitions of susceptibility are required for rapidly time-varying and/or intense driving fields. If H varies rapidly with time, the magnetization lags behind it and the ratio M/H is time dependent. A time-dependent susceptibility is an awkward concept and such situations are ordinarily analyzed using the frequency domain rather than in the time domain. $H(t)$ and $M(t)$ are written as Fourier integrals and the analysis is based on the linear response, $M(\omega)$, to a driving field with a constant amplitude and a sinusoidal time dependence, $H(\omega) = H_0 e^{j\omega t}$. The frequency-dependent susceptibility is defined by,[247–252] $\chi(\omega) = M(\omega)/H(\omega)$. The conventional susceptibility as normally used in MRI is $\chi(0)$, the limit of $\chi(\omega)$ as $\omega \rightarrow 0$. In general, the response $M(\omega)$ is not in phase with $H(\omega)$ and, consequently, $\chi(\omega)$ is a complex number.

Apparently, there have been no extensive studies of $\chi(\omega)$ for living tissues. On theoretical grounds, it is expected that $\chi(\omega) \approx \chi(0)$ for human tissues at least up to the frequency of the B_1 fields used in MRI. At low frequencies the induced magnetic field produced by a material is governed by the applied magnetic field and the magnetic susceptibility; at very high frequencies, however, magnetic susceptibility loses this significance[250] because the alternating electric field accompanying the alternating magnetic field is dominant in determining both the induced electric and magnetic fields. The applied magnetic field induces a magnetic field proportional to $\chi(\omega)$, but the electric field also induces magnetic fields through the action of conduction currents ($J = \sigma E$) and polarization currents ($J = dP/dt = \omega \chi_e \epsilon_0 E$). Electric susceptibilities (dielectric constants) are much larger than magnetic susceptibilities and at sufficiently high frequencies the magnetic response to the electric field overwhelms the response to the magnetic field. In MRI the magnetic field induced by the tissue response to the radio-frequency B_1 field, is determined by the dielectric constant and the electrical conductivity at the B_1 frequency (~1–200 MHz), and the magnetic susceptibility contribution to the induced magnetic field is negligible. Consequently, in the analysis of the response of tissues to radio-frequency fields, the magnetic susceptibility is usually taken as zero ($\mu_r = 1$).

Superposition does not apply when a material is exposed to the extremely intense driving fields encountered in laser physics and nonlinear optics and, when driving fields of more than one frequency are applied simultaneously, nonlinear susceptibility tensors that are functions of multiple frequencies are required. Systematic approaches have been developed to the choice of units and to the analysis of the complex symmetry constraints on the components of these tensors.[251] In principle, the nonlinear generalizations apply to both the electric and magnetic susceptibilities, but for the reasons discussed above, the nonlinear electric susceptibility tensors are more relevant to laser physics than their magnetic counterparts. However, nuclear magnetic resonance itself is commonly treated in terms of the time-dependent magnetic susceptibility of the nuclear spin system.[252] Although it is usually not made explicit, this treatment involves a nonlinear susceptibility tensor: The frequency-dependent magnetization of the nuclear spin system depends on the amplitude and orientation of both the static field, B_o and the radio-frequency field, B_1.

K. Microscopic mechanisms of magnetic susceptibility

1. Magnetization at the nuclear, atomic, and molecular levels

The orbital motion of electrons and the spins of electrons and nuclei respond to applied magnetic fields. The totality of these responses determines the overall susceptibility of a material.[253] Table VII summarizes, using SI units, expressions that relate the susceptibility to atomic properties for ten mechanisms by which materials become magnetized. In general, precise, quantitative calculations of susceptibility, starting from first principles, are not possible. Table VIII provides estimates of the components of the overall susceptibility values for copper and water; these two materials have nearly the same total susceptibility, but the underlying magnetization mechanisms are different.

2. Field-induced changes in electron orbits: Langevin diamagnetism, Landau diamagnetism, and Van Vleck paramagnetism

In an applied magnetic field, the orbital motion of the electrons around every atom is modified slightly. In accordance with Lenz's law, this induced change in motion creates a magnetic field opposed to the applied field. This mechanism is present in all materials and produces a negative magnetization that is relatively weak and temperature-independent known as the Langevin diamagnetism.[254,255] This is the "default mechanism" that determines the susceptibility of every material unless it is overridden by some more powerful mechanism.

Using quantum mechanical perturbation theory, it can be shown that excited states of electron orbital motion can make an additional positive contribution to the induced magnetization. By symmetry this effect is zero in monatomic molecules but provides a relatively weak, temperature-independent, contribution to the susceptibility of some polyatomic molecules. This is the Van Vleck paramagnetism[256] or "high frequency" paramagnetism. Ordinarily it provides only a relatively small correction to the Langevin diamagnetism.

In metals the conduction electrons are not confined to individual atoms but are free to move over extended regions of the lattice. Again, by Lenz's law, the field-induced modification of the motion of the conduction electrons results in a negative contribution to the magnetization known as the Landau diamagnetism.[257]

TABLE VII. Formulas and expressions for the basic mechanisms of susceptibility.

Mechanism	Susceptibility (χ)	Comment
Superconductivity	-1	This is the Meissner effect. It is normally observed only at cryogenic temperatures.
Landau diamagnetism	$-\mu_o e^2(3N_e/8\pi)^{1/3}/(6\pi m_e)$[a]	This effect is produced by changes in the orbital motion of conduction electrons.
Langevin diamagnetism	$-\mu_o e^2 NZ\langle r^2\rangle/(6m_e)$	The susceptibility "default mechanism." It is temperature independent and present in all materials.
Van Vleck paramagnetism	$\mu_o Ne^2/(6m_e^2)\ \Sigma(L_{no})^2/(E_n-E_o)$	A temperature-independent correction to the Langevin effect. The sum is over the orbital electron excited states.
Curie paramagnetism	$\mu_o N_p m^2/(3kT)$	This is the dominant effect in solutions and salts of transition metal ions.
Pauli paramagnetism	$\mu_o e^2(3N_e/8\pi)^{1/3}/(2\pi m_e)$[a]	Produced by the alignment of conduction electron spins in metals. Numerically, it is three times the Landau term.
Nuclear paramagnetism	$\mu_o N_n m_n^2/(3kT)$	This effect is very small at normal temperatures because nuclear moments are very small.
Curie–Weiss paramagnetism	$C/(T-T_o)$	Paramagnetic behavior above the critical temperature, T_o; T_o is negative in antiferromagnets. C is the Curie constant.
Alignment of ferromagnetic domains	$\mu_o M_s^2 A^2/3\gamma$[b]	The source of very high susceptibility in soft ferromagnetic materials.
Superparamagnetism	$\mu_o N_{SP}(M_s V)^2/(3kT)$	The susceptibility of an individual particle, of volume V, is $\mu_o M_s^2 V/(3kT)$.

[a]The expressions given are valid in the free electron gas-approximation to the conduction electron properties.
[b]Reference 176, p. 143; A=domain–wall area; $M_s=1.71\times10^6$ A/m for iron at 300 K.

3. Field-induced spin alignment: Curie paramagnetism, nuclear paramagnetism, and Pauli paramagnetism

Electrons and those atomic nuclei with nonzero spins possess intrinsic magnetic moments. These moments tend to align parallel to applied magnetic fields and to produce a positive magnetization. For orbital electrons the paramagnetic response caused by spin alignment is much stronger than the diamagnetic response of the orbital motion; however, because of the exclusion principle, the electrons in most atoms are present as spin-up and spin-down pairs that have a zero net magnetic moment and do not contribute to the susceptibility. Electron spin paramagnetism requires the presence of atoms or molecules with unpaired electrons. The tendency of the unpaired spins to align with the applied field is balanced by the tendency of fluctuating magnetic fields, generated by thermal agitation within the material, to produce a random spin orientation. This leads to a positive contribution to the susceptibility, known as Curie paramagnetism, that increases as the temperature decreases.[156,157,171,172,173,178] Unpaired electrons are present in the transition metal elements with unfilled d shells (e.g., iron and manganese) and in rare earth elements with unfilled f shells (e.g., gadolinium and dysprosium). Salts (e.g., ferrous ammonium sulfate or) or solutions (e.g., copper sulfate or nickel chloride in water) containing these ions can be strongly paramagnetic, particularly at low temperatures. The molecules of some gases,[156,172] e.g., O_2, NO, NO_2, and ClO_2, contain unpaired electrons and are paramagnetic. Free radicals are short lived chemical species that possess unpaired electrons; they contribute to paramagnetism but are usually present only in very small concentrations. Nuclei with nonzero spins also obey the Curie law, but, nuclear magnetic moments are much smaller than those of electrons and the nuclear contribution to bulk paramagnetism is negligible at normal temperatures: Special methods, such as nuclear magnetic resonance, are required to observe nuclear magnetism.

The spins of the conduction electrons in metals are also aligned by an applied field, but the exclusion principle permits field alignment only for electrons near the Fermi surface. This contribution to the metallic susceptibility is called the Pauli paramagnetism.[258] For the ideal case of a free electron gas, the Landau and Pauli effects can be calculated exactly (Table VII) and the Pauli paramagnetism is opposite in sign and exactly three times the magnitude of the Landau

TABLE VIII. Estimates of the magnetic susceptibility component for water and copper (25 °C). Data from Refs. 158, 165, and 302.

Water		Copper	
Susceptibility mechanism	Calculated value	Susceptibility mechanism	Calculated value
Langevin diamagnetism	-10.12×10^{-6}	Langevin diamagnetism	-25.1×10^{-6}
Van Vleck paramagnetism	$+1.10\times10^{-6}$	(core electrons)	
Nuclear paramagnetism	$+0.0039\times10^{-6}$	Landau and Pauli paramagnetism (conduction electrons)	$+15.6\times10^{-6}$
Total	-9.02×10^{-6}	Total	-9.5×10^{-6}

diamagnetism: Thus an ideal free electron gas is paramagnetic and the susceptibility is two-thirds of the Pauli paramagnetism. In real metals the energy band structure modifies these results: Metals, such as bismuth, with small effective masses for the electrons near the Fermi surface, exhibit strong Landau diamagnetism.[259–261] Theoretical calculations of the susceptibility of the conduction electrons in metals require the evaluation of electron exchange and correlation effects and are not yet capable of great precision.[262–265] To summarize, the susceptibility of nonferromagnetic metals is a superposition of the diamagnetism of the core ions with negative (Landau) and positive (Pauli) contributions from the conduction electrons: Thus metals with filled inner shells can be either weakly paramagnetic (e.g., titanium, aluminum) or weakly diamagnetic (e.g., copper, silver, lead).

4. Spontaneous magnetization

The largest susceptibility values occur in materials which have unpaired spins on some or all of their atoms and which, in their minimum energy state, have these spins locked into an ordered array. The term ferromagnetism is used as a generic term for any magnetically ordered phase; however, many distinct spin patterns occur in nature and, when it is necessary to distinguish among them, specific terms are used: ferromagnetism (e.g., iron, nickel, cobalt, martensitic stainless steel);[163,179] antiferromagnetism (e.g., chromium);[172] ferrimagnetism (e.g., magnetite);[172] canted ferromagnetism (e.g., hematite);[266–268] and so on. Spontaneous magnetization is destroyed if the substance is heated above a critical temperature, called the Curie temperature, T_C, for ferromagnets and the Néel temperature, T_N, for antiferromagnets. Above the critical temperature these materials are paramagnetic with susceptibility[186,269] given by $\chi = C/(T - T_C)$ for ferromagnets and $\chi = C/(T + T_N)$ for antiferromagnets.

Magnetically ordered materials are organized in a domain pattern:[163,179,270] In each domain the spins are locked into an ordered array and each domain is magnetized to its saturation value, M_s. Domain sizes vary from material to material and range from submicron values to several microns. The magnetizations of adjacent domains are oriented in different directions to minimize the total magnetic energy: Cancellation of the external fields produced by adjacent domains permits soft magnetic materials containing multiple domains to have a bulk magnetization close to, or equal to, zero even though the individual microscopic domains are intensely magnetized.

Domain walls are present between adjacent domains: They are regions of high energy where the spin alignment is disrupted. When a magnetic material is placed in an external field, domain wall motion occurs: Domains aligned with the field grow at the expense of other regions resulting in a surplus of regions magnetized to saturation in the direction of the applied field. This leads to the extremely high susceptibilities characteristic of soft ferromagnetic materials[271,272] (Table VI). Bulk samples of such materials are so magnetic that they are not normally useful or even tolerable in MRI: It is common, however, to have very small grains or crystals of ferromagnetic materials distributed in a nonmagnetic matrix. In this case, the ferromagnetic component can be sufficiently diluted that the overall susceptibility, while possibly quite paramagnetic, is compatible to some degree with MRI.

5. Single domain particles and superparamagnetism

Domain walls are energetically unfavorable; consequently, below some critical size, d_0, very small magnetic particles contain only a single domain. The susceptibility of a heterogeneous material containing small, single domain magnetic particles dispersed in a nonferromagnetic matrix differs markedly from that of the bulk magnetic material. There are energy barriers to the rotation of the magnetization of a single domain particle that depend either on particle shape (shape anisotropy) or crystal structure (magnetocrystalline anisotropy). The response of a dispersion of single domain particles with randomly oriented magnetizations to an applied field can exhibit two distinct patterns depending on the particle volume and the temperature. Domain wall motion is not possible in a single domain particle: Thus the susceptibility of stable single domain particles results from field-induced redirection of the magnetization against the energy barriers and is relatively small compared to its value for larger multidomain magnetic particles which magnetize by domain wall motion. However, if the grain size is less than a second critical value, d_s, such that the energy barriers to rotation of the magnetization are small compared to the thermal energy, kT, the magnetization, driven by thermal agitation, jumps rapidly between various directions of minimum energy. Just as in Curie paramagnetism, an applied field tends to align the magnetization of the individual grains against the thermal agitation. The resulting susceptibility is much greater than would occur if the magnetic atoms were distributed uniformly through the matrix rather than as clusters of magnetized grains: This behavior is termed superparamagnetism.[273–293]

The average time, τ, between jumps of the magnetization direction is taken as

$$\tau = \tau_0 e^{E/kT},$$

where τ_0 is a constant on the order of 0.1 to 100 ns and E is the energy barrier that must be overcome to change the direction of the magnetization. The magnitude of the energy barriers varies greatly from one material to another and is proportional to V, the particle's volume. As τ depends exponentially on the temperature and the volume, it is extremely sensitive to these two variables. For a fixed temperature, there is a blocking volume such that a dispersion of particles smaller than this value cannot sustain a remanent magnetization when the applied field is removed: For a fixed volume, there is a blocking temperature above which the dispersion also cannot sustain a remanent magnetization. For temperatures above the blocking temperature and for volumes below the blocking volume, the susceptibility is superparamagnetic; otherwise stable single domain behavior is observed. At suf-

TABLE IX. Critical particle sizes for superparamagnetic and single domain behavior (20 °C).[a] The transition from superparamagnetic to stable single domain behavior occurs at d_s and the transition to multiple domain behavior begins at d_o. The blocking volume is $\pi d_s^3/6$. Data from Refs. 196, 197, and 267.

Material	d_s (μm or 10^{-6} m)	d_o (μm or 10^{-6} m)	Curie temperature (°C)	Saturation magnetization (A/m)
Iron	0.008–0.026	0.017–0.023	770	1.71×10^6
Magnetite (Fe_3O_4)	0.025–0.030	0.05–0.06	585	0.48×10^6
Hematite (Fe_2O_3)	0.025–0.030	15	680	0.0025×10^6

[a]For $d<d_s$, particles are superparamagnetic; for $d_s<d<d_o$, particles have the susceptibility of stable single domains; for $d>d_o$, particles have the susceptibility of multiple-domain ferromagnets.

ficiently high temperatures, $d_s>d_0$ and stable single domain behavior is not observed for any particle size.

Table IX compares the single domain properties of pure iron and the magnetic iron oxides, hematite and magnetite. Single domain particles large enough to be above the blocking volume at all temperatures to which they have been exposed are present in many rocks: They are important in geology because they maintain for millions of years information on the direction of the earth's magnetic field at the time they cooled through their blocking temperature or, in the case of grains growing by chemical deposition, at the time they grew through their blocking volume.[185–195,277–279] The magnetic properties of igneous rocks are dominated by single domain crystals of magnetite. Small grains of hematite cause the red coloration of many sedimentary rocks and soils derived from them, and are major contributors to their susceptibility. At normal temperatures, hematite has a canted spin structure[266–268] which leads to a high degree of cancellation between adjacent spins and a saturation magnetization much less than that of iron and magnetite. The size range for stable, single domain behavior at room temperature is narrow for magnetite but large for hematite. Superparamagnetic dispersions of iron oxides are important to MRI because of their ubiquitous occurrence and potential for contamination of many experimental situations.

Superparamagnetic agents can be used as MRI contrast agents.[281–287] When present in the blood, or other tissues, these particles are free to physically rotate into alignment with the applied field even if the particle is larger than d_s. Therefore, the relatively low susceptibility seen with stable, single domain behavior for particles in a solid matrix is not expected and superparamagnetism should be present for all particles smaller than d_0. Because of the large magnetic moment per particle, superparamagnetic particles become fully oriented at relatively low field strengths, and, depending on particle size, the magnetization usually saturates at fields below those used for MR imaging.

IV. SUSCEPTIBILITY OF SPECIFIC MATERIALS

A. Water

The susceptibility of water[294–304] is basic to the magnetic properties of living tissues and the NMR relaxation times of water in tissues[305–311] are fundamental to MRI. Plant and animal tissues contain 65%–99% water and the other tissue components, ions, macromolecules, organelles, and so on, occur in such low concentrations and/or have susceptibilities so close to that of water that the susceptibilities of all human tissues, at both the organ and cellular levels, are close to that of water. This is fortunate for MRI because, if the amplitude of these microscopic-scale variations in magnetic susceptibility were as large as several ppm, the diffusion of water molecules through the resulting field inhomogeneities could shorten relaxation times sufficiently to preclude the practicality of MRI.

It was once thought that the susceptibility of water had a complicated temperature dependence.[294–298] However, precise measurements, using superconducting quantum interference devices (SQUIDS), indicate only a very small, smooth and practically linear variation of the mass susceptibility of water with temperature.[303,304] Although relative susceptibilities can be measured with great accuracy, it appears that the absolute susceptibility has not been measured for any solid or liquid substance with a precision better than approximately $\pm 0.001 \times 10^{-6}$. Water itself is often used as a reference material for the measurement of the susceptibility of other materials, but the absolute value of the susceptibility of water is not known with great precision. At present, the best estimate[312] for the susceptibility of pure water at physiological temperature (37 °C or 310 K)[313,314] is found by taking the mass susceptibility in CGS units at 20 °C to be -0.720×10^{-6} cc/g and to calculate the susceptibility using the variation of the density of water with temperature and the linear approximation to the measured variation of the mass susceptibility of water with temperature,[303]

$$\chi_g(T)/\chi_g(20\ ^\circ\mathrm{C}) = 1 + 1.388\ 10 \times 10^{-4}(T\text{-}20),$$

where T is in °C. Therefore, the mass susceptibility at 37 °C is -0.7217×10^{-6} emu/g or 1.0024 more diamagnetic than at 20 °C. Converting to SI units and taking the density of water to SI units and taking the density of water as 998.23 kg/m^3 at 20 °C and 993.35 kg/m^3 at 37 °C, $\chi = -9.032 \times 10^{-6}$ at 20 °C and $\chi = -9.053 \times 10^{-6}$ at 37 °C: For practical purposes, in this paper the volume susceptibility of water at 37 °C is taken as -9.05×10^{-6}.

The susceptibility of water is mainly due to Langevin diamagnetism, but there is a small positive contribution from Van Vleck paramagnetism (Table VIII). The observed temperature variation is very small as is expected from nominal temperature independence of these two mechanisms. The protons in the hydrogen atoms of the water molecules contribute an additional, but very small, temperature-dependent paramagnetism which is insignificant ($\chi_n = +0.0039 \times 10^{-6}$) at 37 °C. Also, some of the oxygen nuclei are of the isotope ^{17}O which has a nuclear magnetic moment and, in principle, contributes to the susceptibility; because of the small mag-

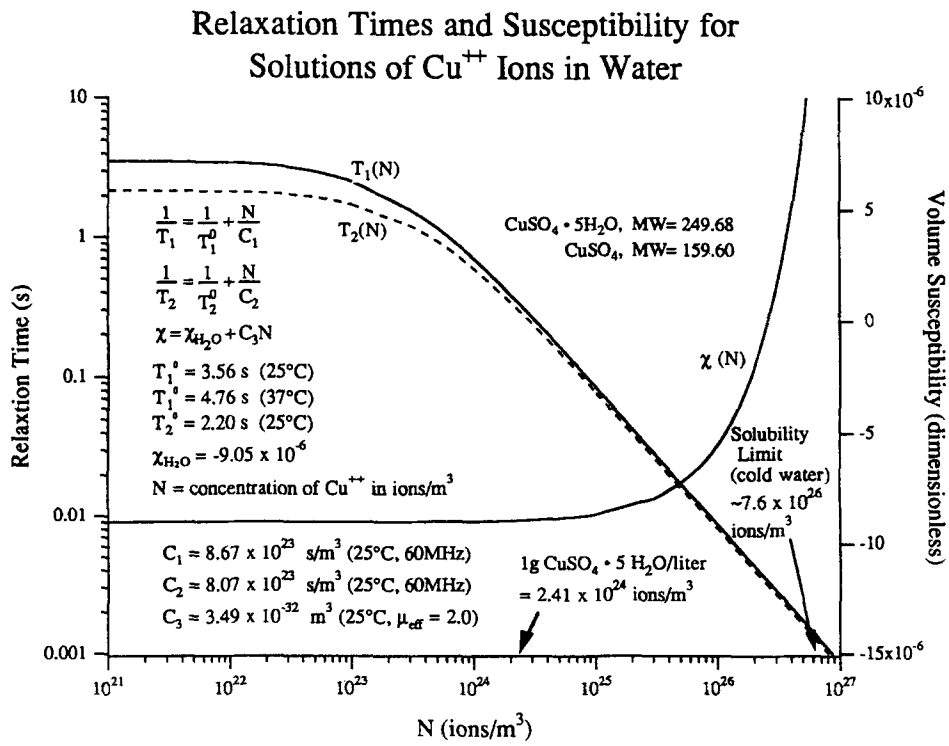

FIG. 3. Calculated values for the relaxation times and magnetic susceptibility of copper sulfate solutions. Copper sulfate (blue vitriol) solutions, with concentrations of 1–2 g/l (1–2 kg/m^3), are commonly used to provide MRI test solutions with convenient values of the relaxation times. The magnetic susceptibility of copper sulfate solutions is close to that of water until very high concentrations—not useful for MRI—are reached.

netic moment of this nucleus (in magnitude, 0.463 that of the proton) and the small natural abundance (0.038%) of the isotope, this contribution to the susceptibility of water and tissues is negligible.

For most experimental purposes pure water has inconveniently long NMR relaxation times and it is common to use water that is lightly doped with copper sulfate, or some other transition metal[315] salt, to provide standard imaging solutions with convenient values of T_1 and T_2 (Fig. 3). Because copper ions are paramagnetic, the susceptibility of these solutions is a function of the salt concentration. For very dilute solutions the T_1 and T_2 values are the same as those of pure water:[308,309] At higher concentrations the relaxation times decrease linearly with increasing copper concentration. The formulas for the relaxation times in Fig. 3 are taken from literature values[163] appropriate to 63 MHz (1.5 T). For solutions with 1 g/l of hydrated copper sulfate (blue vitriol) (1 kg/m^3), T_1=327 ms and T_2=290 ms. There is no appreciable increase in susceptibility until much larger concentrations are reached. The T_2 relaxation times of these concentrated solutions are too short to be useful for MRI. Therefore, at the concentrations useful in MRI, the susceptibility is dominated by the water component of the solution and the relaxation times are dominated by the copper ions.

B. Biological tissues

1. General aspects of tissue susceptibility

Only a few quantitative studies of the magnetic susceptibilities of living plant and animal tissues have been reported.[122,316–318] These measurements on gross tissue specimens are difficult because (i) the susceptibilities are very small, (ii) tissues are very heterogeneous, and (iii) it is difficult to work with living tissues in a susceptometer. There have, however, been many many susceptibility studies of tissue extracts and biochemical components, such as lipids and hemoglobin.[319] Water is the predominant component of most tissues and the susceptibility of most tissues appears to be within $\pm 10\%$–20% that of water; i.e., $-11.0\times10^{-6}<\chi_{\text{tissue}}<-7.0\times10^{-6}$. This is not simply an obvious consequence of the high water concentration in tissues. A single paramagnetic molecule (e.g., O_2) or ion (e.g., Fe^{++} or Fe^{+++}) can cancel the diamagnetism of hundreds or thousands of water molecules; however, the tissue concentrations of the paramagnetic species are too small to overcome the dominant diamagnetism. Common electrolyte ions, such as Na^+, K^+, and C^-, are weakly diamagnetic[320] but their concentrations are too small to contribute significantly to tissue susceptibility. Those proteins which do not contain transition metal ions probably all have susceptibilities close to that measured[312] for the iron-free apohemoglobin molecule: $\chi=-9.91\times10^{-6}$. Lipids are also diamagnetic with χ near that of water: The average susceptibility for stearic acid[321,322] is -10.0×10^{-6}.

2. Hard tissues

There are few reports on the susceptibilities of hard tissues such as nails, teeth, and cortical bone. Because of their low water content it might be expected that these suscepti-

bilities would differ significantly from those of soft tissues. Evidence from MRI indicates that this is unlikely. If the susceptibility of cortical bone varied as much as 10 ppm from that of the surrounding soft tissues, obvious image distortion would be present in the vicinity of large bones. The absence of such artifacts is consistent with a recent report[33] giving $\chi=-8.86\times10^{-6}$ for cortical bone; another report[111] suggests that bone is slightly more diamagnetic than water with $\chi=-12.82\times10^{-6}$.

3. Iron and other transition metals in trace concentrations

The body contains trace amounts of several paramagnetic transition metal ions such as copper, manganese, and cobalt. Iron, however, is about 30 times more abundant in the body than all the other paramagnetic ions combined, and the paramagnetic component of the susceptibility of human tissues is essentially entirely determined by the tissue iron concentration. The total body iron content is variable, but a representative value for a 70 kg human is 3700 mg. Iron ions free in solution are toxic and almost all iron in the body is bound to other molecules: There is approximately 2500 mg in the blood as hemoglobin; 1000 mg in specific storage tissues (e.g., liver, spleen, and the basal ganglia of the brain) as ferritin or hemosiderin deposits or chelated with small molecular weight molecules such as citrate; about 170 mg in the myoglobin of the skeletal muscles; 3 mg bound to the transport protein transferrin; and the rest is in various trace locations.[122] Even in its most magnetic configuration (Fe^{+++}, $S=5/2$, $\mu_{eff}=5.92$), 3700 mg of iron uniformly distributed throughout the body (volume$\approx$0.07 m^3=70 l), would have a negligible effect on susceptibility; by the Curie law, $\Delta\chi\approx0.16\times10^{-6}$. The body iron, however, is concentrated in certain tissues: These can have susceptibilities in the range of 1–10 ppm more positive than iron-free tissues.

4. Blood and hemoglobin

A molecule of deoxyhemoglobin is approximately spherical and consists of four protein chains each containing one paramagnetic iron ion, Fe^{++}, in the $S=2$ spin state. When combined with four paramagnetic oxygen molecules, each with $S=1$, the resultant oxyhemoglobin molecule has no net spin ($S=0$) and is slightly more diamagnetic than water.[312,319] Hemoglobin has a molecular weight of 64 650; a density of 1.335 g/cm^3 (1335 kg/m^3); a radius of approximately 27 Å (2.7×10^{-9} m); and a volume of 1.97×10^{-26} m^3. Random, thermally generated magnetic fields cause the magnetic moment of the iron atoms in deoxyhemoglobin to fluctuate rapidly, but the time-averaged susceptibility is given by the Curie law. The susceptibility of the four iron atoms in the molecule is $+10.1\times10^{-6}$ at 37 °C; combining this with the diamagnetic susceptibility of the apoprotein matrix, -9.91×10^{-6}, gives $\chi\approx+0.2\times10^{-6}$ for an individual deoxyhemoglobin molecule. A single red blood cell (rbc) has a volume of 90.1×10^{-18} m^3 and contains about 2.8×10^8 hemoglobin molecules: Accounting for the dilution of the hemoglobin molecules by the intracellular water, gives $\chi\approx-6.52\times10^{-6}$ for a fully deoxygenated rbc. If the hematocrit is 0.45, $\chi\approx-7.90\times10^{-6}$ for fully deoxygenated whole blood, in good agrement with reported values.[113,117] The small difference, about 1.5 ppm, between the susceptibility of deoxygenated blood and that of surrounding tissues is the basis of functional MRI.

5. Ferritin and hemosiderin

The majority of the nonheme iron in the body is stored in ferritin or in the related, but less well characterized compound, hemosiderin. They provide an important form of field-dependent contrast in MRI.[83–108,323] The accepted model of the ferritin molecule consists of a mineralized core surrounded by a protein shell: The spherical core, with a radius of approximately 4.0 nm (40 Å), consists of mineralized iron oxide and phosphate and contains up to 4500 iron atoms in the Fe^{+++} state. At very low temperatures the cores are probably magnetically ordered as single domain superantiferromagnets[288] and may exhibit unusual quantum tunneling of the magnetization between low-energy directions.[289–293] At body temperature, however, ferritin is probably above the Néel temperature and paramagnetic.[324,325] Assuming paramagnetic behavior with $\mu_{eff}=3.78$ for the core, and a diamagnetic outer protein shell with $\chi\approx-9\times10^{-6}$, gives a susceptibility for the fully iron-loaded ferritin molecule of $+520\times10^{-6}$.

In histology, the total iron concentration (c) is commonly specified in units of mg of iron per gram of wet tissue and for tissues containing deposits of storage iron,[122]

$$\chi\approx\chi_{water}+(1.30\times10^{-6})c\rho,$$

where ρ is the tissue density in g/cm^3. For normal liver, $\rho=1.05$ g/cm^3, and $c=0.21$ mg/g, the calculated $\chi\approx8.76\times10^{-6}$: For a severe iron overload, as in hereditary hemochromatosis, $c=6.6$ mg/g, and $\chi\approx0.0\times10^{-6}$. Thus even organs with very high iron concentrations, have susceptibilities, except in extremely pathological states, only a few ppm less diamagnetic than that of water.

6. Ferromagnetic particles in human tissues

Evidence has been presented for the presence of extremely small endogenous ferromagnetic particles, possibly with biological and/or pathological significance, in human lung, brain, and other tissues.[326,327] However, the low level of observed biological effects even in intense applied fields,[122] the ubiquitous presence of contaminating ferromagnetic particles in the air[195] and in the workplace environment of some occupations,[328–334] along with evidence for migration of these particles through the body,[335] suggest such particles may originate from external contamination.

7. Paramagnetism of oxygen dissolved in tissues

The oxygen molecule (O_2) is paramagnetic[172] with $S=1$ and $\mu_{eff}=2.83$; therefore, the susceptibility of all tissues will be somewhat increased by their oxygen content. The SI unit for pressure is the n/m^2 or Pascal (Pa) with 1 atmosphere (atm)=1.0133×10^5 Pa; in physiology, however, the partial

pressure of oxygen, pO_2, is usually specified in mm of Hg. In equilibrium with pure oxygen at 1 atm (760 mm of Hg), water and tissues contain 1.09×10^{-3} mol/l (6.56×10^{23} molecules/m^3) of dissolved oxygen. From the Curie law, at 37 °C, the contribution of physically dissolved oxygen (not bound to hemoglobin or myoglobin) to the paramagnetic susceptibility[122] is given by

$$\chi_{\text{oxygen}}\approx5.82\times10^{-11}\ pO_2.$$

Even for a tissue saturated with oxygen at atmospheric pressure (pO_2=760 mm of Hg), the paramagnetic correction to the tissue susceptibility is only ~0.04 ppm: Even under hyperbaric conditions, oxygen dissolved in tissues does not make a significant contribution to the tissue susceptibility.

C. Stainless steel

Stainless steels are a group of iron-based alloys containing 10%–30% chromium and 0.03% to roughly 1.2% carbon: other elements, e.g., nickel, molybdenum, titanium, and aluminum, are commonly added to achieve various desirable characteristics. A chromium-rich surface oxide forms spontaneously when these steels are exposed to oxygen in the atmosphere and this forms a corrosion-resistant passivating film: In the presence of oxygen this film heals spontaneously whenever it is broken resulting in the rust-resistant property that distinguishes stainless steel from iron. The susceptibility of stainless steel[336–349] is important in MRI because these steels are widely used in surgical instruments, implants, and in other medical devices. The magnetic behavior of stainless steel varies over a wide range and depends on the details of the composition and the metallurgical treatment.

One important class of stainless steels is comprised of the martensitic or α phase steels: They contain chromium in the 10.5% to 18% range and have a carbon content up to 1.2%; they have a distorted body-centered-cubic (bcc) lattice structure; and at room temperature they are ferromagnetic with Curie temperatures in the range of 300 to 900 °C. Many of them are members of the so-called 400 series. These and the related ferritic steels are known as "magnetic" stainless steels: They experience strong forces and torques in magnetic fields and their magnetism is easily demonstrated by use of a hand-held permanent magnet. They usually are not permanent magnets because of the random orientation of their ferromagnetic domains. Domain alignment gives these materials large initial susceptibilities which are in the range of 100 or more: These materials are completely incompatible with MRI. Many surgical instruments and other common objects, e.g., paper clips and refrigerator door panels, are made from magnetic stainless steels.

Another class of stainless steels is comprised of the austenitic or γ phase steels: These alloys have 16% to 20% chromium along with large amounts of nickel (up to 35%) and manganese (up to 15%) and other alloying elements. Examples include the 300 series of stainless steels. They have a face-centered-cubic (fcc) structure which is thermodynamically metastable: If an austenitic stainless steel is cold worked, it may spontaneously revert to the more stable, and ferromagnetic, martensitic crystal structure. Austenitic steels are paramagnetic at room temperature with susceptibilities in the range of 0.001 to 0.020: They have an antiferromagnetic phase at cryogenic temperatures with T_N on the order of 10 to 50 K.[345–349] These steels are inert when casually checked with a hand-held permanent magnet, and therefore, exhibit magnetic field compatibility of the first kind: They are commonly used as coil forms for superconducting magnets and as construction materials for cryostats. Their susceptibility is sufficiently large that they substantially disrupt MR images of objects in their immediate vicinity. It is important to recognize that there is no form of stainless steel that exhibits magnetic field compatibility of the second kind. It is also important to recognize that, when heavily cold worked, the susceptibility of the commonly used nonmagnetic 316 stainless steel increases from 0.003 to 9,[339] a factor of 3000, because of conversion to the martensitic structure. Thus an instrument or implant nominally expected to exhibit magnetic compatibility of the second kind could, during the manufacturing process, be converted to a dangerous, magnetically incompatible, device.

D. Carbon, graphite, and carbon fibers

Carbon fiber composites[350–354] consist of a tough network of graphite-like carbon fibers immersed in an inert matrix material such as epoxy resin. They are used in aerospace and other demanding applications because of their low density, high strength, and high stiffness. In surgical applications they have been used as trochars, endoscope cannulas, and in other applications: They can be sterilized and are nontoxic. Experimentally,[355] biopsy needles made from carbon fiber composites have shown good magnetic compability with MRI. Crystalline graphite has a layer structure and the susceptibility is diamagnetic and highly anisotropic.[356–358] The susceptibility orthogonal to the atomic layers is 70 times greater than that parallel to the layers which is very close to that of human tissues. The precise value of the overall magnetic susceptibility of the composites depends on the details of the manufacturing process and on the matrix material. The electrical resistivity is on the order of 10^{-5} to 10^{-4} Ω m which means that these materials are 2 or 3 orders of magnitude less conductive than metals which have resistivity in the range of 10^{-8} to 10^{-7} Ω m. In addition to the desirable electrical and magnetic properties, the mechanical properties such as Young's modulus, tensile strength, and fracture resistance are suitable for surgical applications.

E. Environmental materials

Most materials encountered in everyday experience are weakly diamagnetic with susceptibilities similar in magnitude to that of water. Frequently, however, samples of these materials are found to be paramagnetic because of the presence of small amounts of strongly magnetic contaminants: Most commonly the naturally occurring iron oxides. In particular, magnetite and hematite are widespread in the natural environment and in manufactured materials. These oxides are found in some ceramics: They also cause the paramag-

netism found in most soil samples and in many rocks,[184–197] inks and pigments,[241] cosmetics and tattoos,[332–335] U.S. paper currency,[359] and paintings.[360]

V. INDUCED MAGNETIC FIELDS AND DEMAGNETIZING EFFECTS

A. Optimum susceptibility matching

Ideally, if a foreign object, such as a surgical instrument is introduced into the region of MR imaging it should not perturb the pre-existing field by changing the initial magnetization. For objects to be located in the region outside the patient the ideal susceptibility is $\chi=0$: Technically, the ideal value is $\chi=\chi_{\text{air}}=+0.36\times10^{-6}$, but this distinction is not significant in practice. For objects, such as biopsy needles, to be embedded within the patient's tissues, which are assumed to have a susceptibility equal to that of water, the change in the induced magnetization is proportional to $\Delta\chi=\chi-\chi_{\text{water}}$,: In this case, ideally, $\Delta\chi=0$ and $\chi=-9.05\times10^{-6}$. Therefore, materials with the same susceptibility as tissues, rather than materials with zero susceptibility, are the goal for internal applications. In practice, however, many compromises with this ideal susceptibility criterion are required. One approach to MRI magnetic compatibility is to make hybrid instruments and devices using a combination of paramagnetic and diamagnetic materials such that the resultant device has the optimum overall susceptibility value. One difficulty with this approach is the unavailability of diamagnetic materials with large negative susceptibilities to balance the large paramagnetic susceptibilities frequently encountered.

B. Induced magnetization and induced magnetic fields

When an irregularly shaped object, e.g., a human being or a surgical device, is placed in an initially uniform magnetic field, $B_o=\mu_o H_0$, it becomes magnetized and produces an induced field which distorts the original field. Within the object, the induced field opposes the applied magnetic field and is known as H_{dm}, the demagnetizing field. In the general case, the induced magnetization varies from point-to-point and is determined by the sum of the applied and the induced magnetic fields. Precise calculation of the magnetization and the total field perturbation involves a self-consistent solution to a partial differential equation boundary value problem that usually requires numerical methods.[58,59,61,63,66,68] In many practical cases this complicated procedure can be avoided: The response of any ellipsoidal object, with uniform susceptibility, placed in a uniform external field produces a uniform internal field and magnetization which can be calculated by using algebraic rather than differential equations. This result is due to Poisson (1824). It is a consequence of the inverse square law for the force between magnetic poles: It would not be true for other types of force law. Spheres and cylinders are special cases of ellipsoids and ellipsoids can be used to approximate a wide variety of other shapes, ranging from flat disks to needles. If the fields of an irregularly shaped object are required, and if it is possible to find an ellipsoid that approximates the object's shape. A simple, closed-form first approximation to the induced fields can be determined algebraically. Stoner[361] noted that, "The ellipsoid is troublesome to deal with; but it is easier than anything else."

C. Demagnetizing factors for ellipsoids

If a field is applied along a principal axes of an ellipsoid and the susceptibility is isotropic, the induced internal field is parallel to the applied field and is given by

$$H_{\text{dm}}=-\alpha M,$$

where α, the demagnetizing factor, is a shape-dependent number between zero and one.[361–364] A general ellipsoid has three distinct principal axes and the sum of the three demagnetizing factors is always equal to one: The three principal axes of a sphere are equivalent, and therefore, the demagnetizing factor for any direction must be 1/3. For cylinders transverse to the applied field, $\alpha=1/2$; and for long cylinders parallel to this field, $\alpha=0$. The total internal field H is uniform and is the sum of the applied field, $H_0=B_o/\mu_o$, and the demagnetizing field, H_{dm}. Using $M=\chi H$ and $B=\mu_o(H+M)$ the total internal fields are given by

$$B=B_o(1+\chi)/(1+\alpha\chi),$$

$$\mu_o H=B_o/(1+\alpha\chi),$$

$$\mu_o M=B_o\chi/(1+\alpha\chi).$$

For strongly magnetic materials, with $\chi\gg1$, the internal B field and the magnetization are *independent of the susceptibility* and are determined only by the shape of the object. For $|\chi|\ll1$, M is parallel to the applied field and is equal to $\chi B_o/\mu_o$; *independent of the shape of the ellipsoid.* This is a consequence of the fact that $H_{\text{dm}}\ll H_0$ and, as a result, H_{dm} has a negligible effect on M. The internal B and H fields, however, do depend on both the shape and susceptibility. If the external field is not parallel to a principal axis, the field within an ellipsoid is not parallel to the applied field even if the susceptibility is isotropic. In this case the applied field may be resolved into components along the principal axes and the total field computed by vector superposition.

A general ellipsoid has three independent principal axes and three different demagnetizing factors, but it is simple and often sufficient to consider only ellipsoids of revolution: They have two equal principal axes and, therefore, two of the demagnetizing factors are equal. If the semimajor axis parallel to the axis of revolution is b and the two perpendicular semiaxes are a, the demagnetizing factors can be expressed in terms of the aspect ratio, $r=b/a$: for $r=1$ the ellipsoid is a sphere; for $r>1$ it is a prolate spheroid; for $r<1$ it is an oblate spheroid; for $r\gg1$ the ellipsoid is needlelike and approximates a long thin cylinder; for $r\ll1$ the ellipsoid is disklike and approximates a flat, circular plate. The demagnetizing factor for the direction parallel to the axis is α_b and is given by

$$\alpha_b=1/T^2(r/T\ \log[r+T]-1)\quad\text{for } r\geqslant1,$$

$$\alpha_b=1-(r/S)^2(\sin^{-1}[S]/(rS)-1)\quad\text{for } r\leqslant1.$$

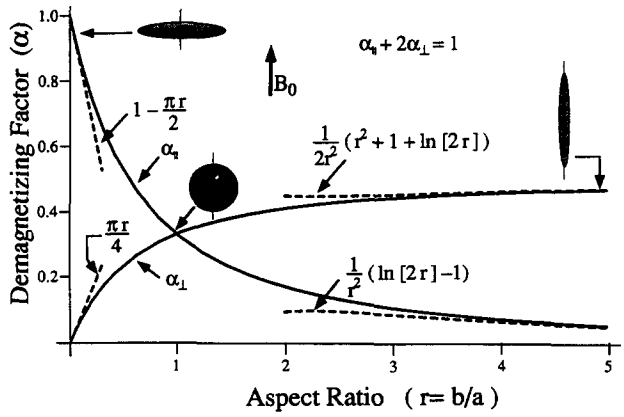

FIG. 4. Demagnetizing factors for ellipsoids of revolution. $\alpha_\parallel$ is the demagnetizing factor in the direction parallel to the axis of revolution and $\alpha_\perp$ is the demagnetizing factor perpendicular to this axis. The semiaxis along the axis of revolution is b and in the transverse direction it is a: $r=b/a$ is the aspect ratio of the ellipsoid. For $r=b/a \gg 1$ the ellipsoid is needle-shaped and for $r \ll 1$ it is disk-shaped: the approximate expressions for these limiting cases are given by the dashed lines.

Here, $T=(r^2-1)^{1/2}$ and $S=(1-r^2)^{1/2}$. The limiting cases are $\alpha_b \to 1-\pi r/2$ for $r \ll 1$ and $\alpha_b \to 1/r^2(\log[2r]-1)$ for $r \gg 1$. The demagnetizing factors for the axes perpendicular to the axis of revolution are $\alpha_a = 1/2(1-\alpha_b)$. These expressions and approximations for the demagnetizing factors are shown graphically in Fig. 4. Table X summarizes the demagnetizing factors and internal fields for various ellipsoids of revolution.

The total susceptibility, χ_{av}, of a dispersion of small ferromagnetic particles in a weakly magnetic matrix can be approximately estimated in terms of the volume fraction, f, which is occupied by the ferromagnetic grains.[190] Because of demagnetizing effects, the field H inside the grains is much less than the applied field and the average susceptibility of the whole specimen is $\chi_{av}=f\chi/(1+\alpha\chi)$, where χ is the intrinsic susceptibility of the individual grains. For cases, such as magnetite, which have $\chi \gg 1$, $\chi_{av}=f/\alpha$. If the particles are approximately spherical, $\alpha \approx 1/3$, and the volume fraction of magnetic grains is estimated as $f \approx \chi_{av}/3$. This implies that if a MR-compatible ceramic with $\chi \approx -10$ ppm, is contaminated with small magnetite particles occupying only 0.1% of its volume, the susceptibility will be increased to approximately 3000 ppm.

D. Fields of magnetized circular cylinders and spheres

The fields internal to an ellipsoid in a uniform external field are given by the above formulas: The effects of the induced magnetization on MRI, however, depend on the field external to the ellipsoid. For an ellipsoid, of volume V and magnetization M, the far field is simply that of a dipole with a dipole moment of MV. The effects of the induced fields are largest near the object's surface, however, and here the fields cannot be expressed in terms of simple functions but instead require ellipsoidal harmonics[365–367] which are not easy to use. There are two special cases, spheres and circular cylinders, for which both the internal and external fields can be written in terms of simple functions: These expressions can

TABLE X. Internal fields and demagnetizing factors for ellipsoids of revolution. It is assumed that the applied field, B_o, is not large enough to cause magnetic saturation.

				Circular cylinder		Thin circular disk	
		General ellipsoid of revolution	Sphere	B_o perpendicular to axis	B_o parallel to axis	B_o perpendicular to axis	B_o parallel to axis
Demagnetizing factor		α	1/3	1/2	0	0	1
B	General case	$\frac{1+\chi}{1+\alpha\chi}B_o$	$\frac{3+3\chi}{3+\chi}B_o$	$\frac{2+2\chi}{2+\chi}B_o$	$(1+\chi)B_o$	$(1+\chi)B_o$	B_o
	$\lvert\chi\rvert \ll 1$	$(1+(1-\alpha)\chi)B_o$	$\left(1+\frac{2\chi}{3}\right)B_o$	$\left(1+\frac{\chi}{2}\right)B_o$	$(1+\chi)B_o$	$(1+\chi)B_o$	B_o
	$\chi \gg 1$	B_o/α	$3B_o$	$2B_o$	$(1+\chi)B_o$	$(1+\chi)B_o$	B_o
$\mu_o H$	General case	$\frac{1}{1+\alpha\chi}B_o$	$\frac{3}{3+\chi}B_o$	$\frac{2}{2+\chi}B_o$	B_o	B_o	$\frac{1}{1+\chi}B_o$
	$\lvert\chi\rvert \ll 1$	$(1-\alpha\chi)B_o$	$\left(1-\frac{\chi}{3}\right)B_o$	$\left(1+\frac{\chi}{2}\right)B_o$	B_o	B_o	$B_o(1-\chi)$
	$\chi \gg 1$	$B_o/(\alpha\chi)$	$3B_o/\chi$	$2B_o/\chi$	B_o	B_o	B_o/χ
$\mu_o M$	General case	$\frac{\chi}{1+\alpha\chi}B_o$	$\frac{3\chi}{3+\chi}B_o$	$\frac{2\chi}{2+\chi}B_o$	χB_o	χB_o	$\frac{\chi}{1+\chi}B_o$
	$\lvert\chi\rvert \ll 1$	χB_o	χB_o	χB_o	χB_o	χB_o	χB_o
	$\chi \gg 1$	B_o/α	$3B_o$	$2B_o$	χB_o	χB_o	B_o

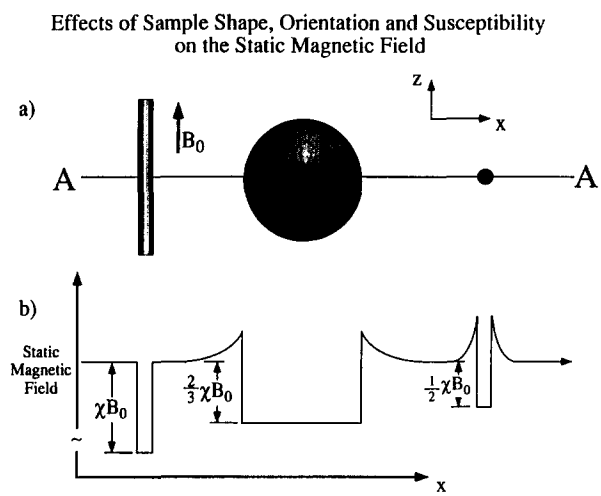

FIG. 5. Effects of sample shape, orientation and susceptibility. In the upper panel a sequence of a long cylinder parallel to B_o, a sphere, and a long cylinder transverse to B_o are indicated. The lower panel indicates the variation of the z-component of the resulting magnetic field along the line AA. The susceptibility is negative and is the same for all three samples. The field perturbation is determined by the sample shape and orientation, as well as by the susceptibility.

serve as the basis for the analytic treatment of susceptibility-dependent image artifacts for simple geometries:

(i) For circular cylinders transverse to B_o (radius a: axis along the y direction),
$\Delta B_z = \Delta\chi/2 B_o$ inside the cylinder and
$\Delta B_z = \Delta\chi/2 B_o a^2(z^2-x^2)/(x^2+z^2)^2$ outside the cylinder;

(ii) For circular cylinders parallel to B_o (radius a; axis along the z direction),
$\Delta B_z = \Delta\chi B_o$ inside the cylinder and
$\Delta B_z = 0$ outside the cylinder;

(iii) For spheres (radius a) centered at the origin,
$\Delta B_z = 2\Delta\chi/3 B_o$ inside the sphere and
$\Delta B_z = \Delta\chi/3 B_o a^3(2z^2-x^2-y^2)/(x^2+y^2+z^2)^{5/2}$
outside the sphere.

In the above equations it is assumed that $|\chi| \ll 1$. It is seen that a long cylinder parallel to the applied field does not perturb the external field at all. Figure 5 illustrates the important fact that objects of the same susceptibility produce different field perturbations depending on both their shape and their orientation with respect to the main magnetic field. The contours of constant ΔB_z for transverse cylinders and spheres are shown in Fig. 6. Perspective plots of these functions are shown in Figs. 7 and 8. Although, as mentioned above, the external field of a general ellipsoid cannot be found in terms of simple functions, the boundary conditions on the surface of the ellipsoid (B_z continuous at the poles, H_z continuous at the equator) can be used to find the maximum (polar) and minimum (equatorial) values of the external field for the general ellipsoid of revolution

$$\Delta B_z^{\text{pole}} = B_o \Delta\chi(1-\alpha)/(1+\alpha\Delta\chi)$$

and

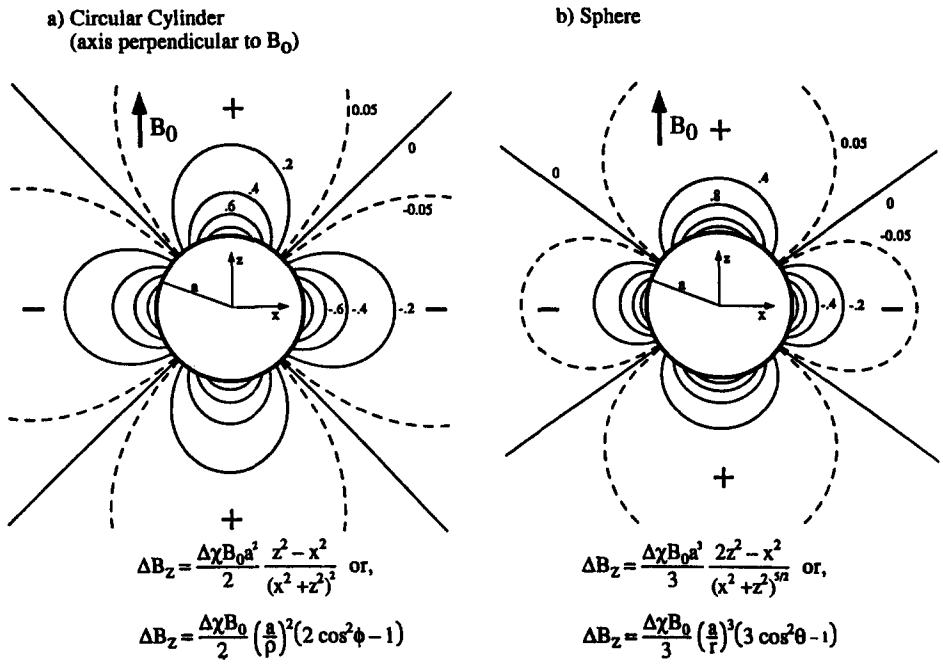

FIG. 6. Contours of ΔB_z. Quantitatively accurate contours of $\Delta B_z/(\alpha\Delta\chi B_o)$ are shown for a cylinder transverse to B_o (a), and for a sphere (b). For the cylinder ($\alpha = 1/2$) the contour intervals are 0.2, and the range is from -1.0 to 1.0. For the sphere ($\alpha = 1/3$) the contour interval is 0.2 between -1.0 and 0.0, and 0.4 between 0.0 and 2.0. Both objects produce fields that are negative in some regions (decreasing the applied field) and positive in others (increasing the applied field). The spherical and cylindrical coordinates are defined in Fig. 9. For the cylinder, $-\Delta\chi B_o/2$ (equator) $< \Delta B_z(x,y,z) < +\Delta\chi B_o/2$ (poles). For the sphere, $-\Delta\chi B_o/3$(equator) $< \Delta B_z(x,y,z) < +2\Delta\chi B_o/3$ (poles).

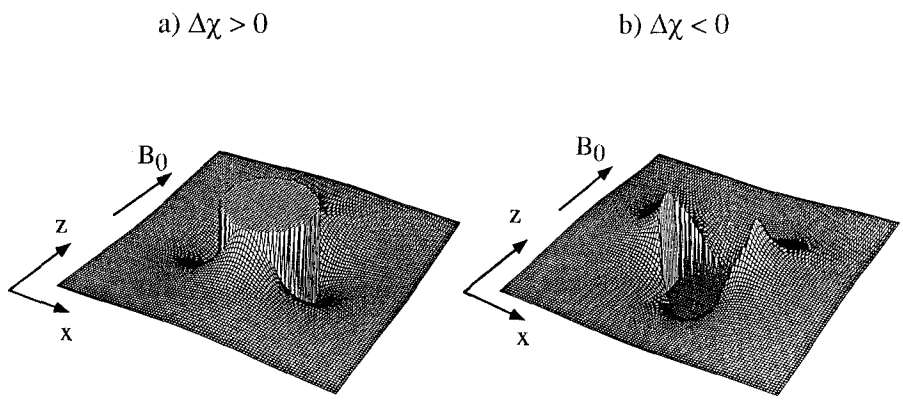

FIG. 7. Perspective view of ΔB_z for a cylinder transverse to the applied magnetic field. The field is shown for $\Delta\chi>0$ (a) and for $\Delta\chi<0$ (b). The cylinder axis is parallel to the y axis. The field discontinuity at the surface is zero at the poles of the cylinder and is a maximum ($\Delta\chi B_o$) at the equator. If an MR imaging slice is selected perpendicular to the y axis it will not be planar but will mirror the shape of the above surfaces.

$$\Delta B_z^{\text{equator}} = -B_o\alpha\Delta\chi/(1+\alpha\Delta\chi),$$

and for $\Delta\chi \ll 1$,

$$\Delta B_z^{\text{pole}} \approx B_o(1-\alpha)\Delta\chi \quad \text{and} \quad \Delta B_z^{\text{equator}} = -B_o\alpha\Delta\chi.$$

The total range of ΔB_z when $|\chi| \ll 1$ is the difference between the polar and equatorial values, $\Delta\chi B_o$, as indicated earlier. The poles are defined as the points where the principal axis parallel to B_o intersects the surface.

E. Magnetic field lines

Magnetic field lines provide a convenient means of visualizing the fields: For a uniformly magnetized transverse cylinder the field lines can be calculated, using cylindrical coordinates, from the differential equation, $1/\rho\ d\rho/d\phi = B_\rho/B_\varphi = \cos\varphi/\sin\varphi$. This is easily integrated to give the equations of the field lines as $\rho = c\ \sin\phi$, where c is a constant: These curves are circles passing through the origin and centered on the x axis at $x = c/2$ and $z = 0$. For magnetized spheres, the field lines are given, using spherical coordinates, by the equation, $1/r\ dr/d\theta = B_r/B_\theta = 2\cos\theta/\sin\theta$. This integrates to the equation for the field lines, $r = c\ \sin^2\theta$, where, again, c is an arbitrary constant. The field lines for spheres and transverse cylinders are shown in Fig. 9.

VI. SUSCEPTIBILITY AND MR IMAGE DISTORTION

A. Standard imaging techniques

MRI uses an intense, static magnetic field, B_o (ordinarily in the range from 0.02 to 4.0 T) in the z direction, a radio-frequency field, B_1, perpendicular to z, and three independent gradient fields to create image information. Ideally, each of the three gradient fields has a z component which is perfectly linear (i.e., proportional to x, y, or z) over the field of view. The gradient fields are used to manipulate the frequency and phase of the precessing spins as a function of position. The frequency of the NMR signal arising from any given point is proportional to the z component of the magnetic field at that point. In the ideal case,

$$B_z = B_o + G_x(t)x + G_y(t)y + G_z(t)z.$$

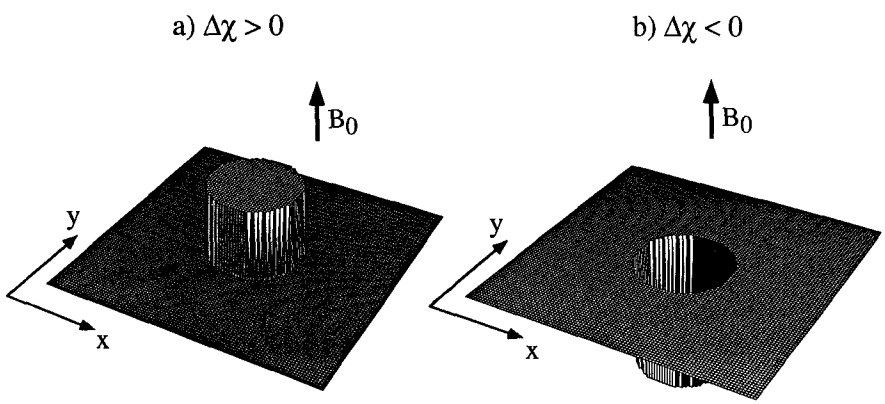

FIG. 8. Perspective view of ΔB_z for a cylinder parallel to the applied magnetic field. This field is shown for $\Delta\chi>0$ (a) and for $\Delta\chi<0$ (b). The field is not perturbed outside the cylinder. There is a uniform discontinuity in $B_z(\Delta\chi B_o)$ at the cylinder's surface. There is no image distortion outside the cylinder but MR-active spins within the cylinder map to an offset z location ($\Delta z = \Delta\chi B_o/G_R$).

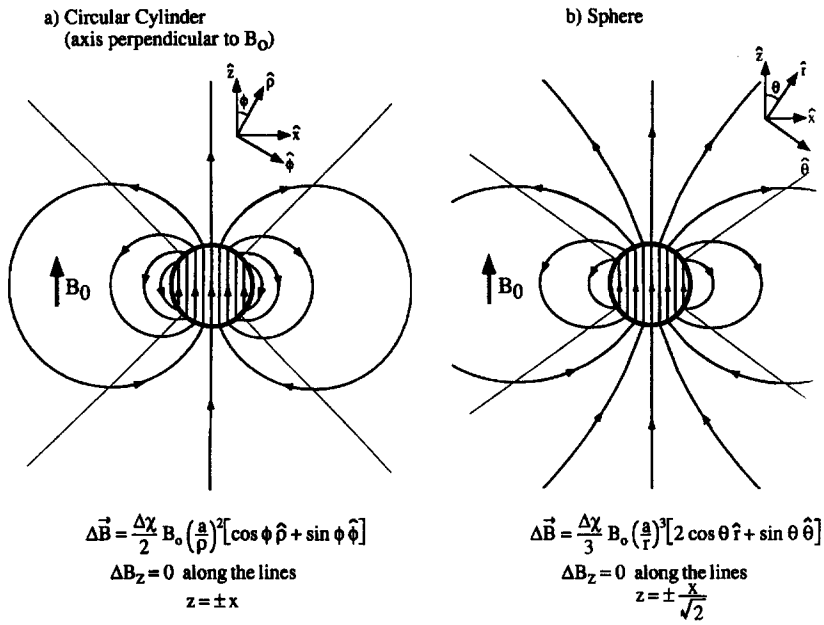

FIG. 9. Magnetic field lines. Quantitatively accurate field lines are shown (a) for a uniformly magnetized circular cylinder transverse to B_o and (b) for a uniformly magnetized sphere. Cylindrical coordinates ($\rho^2=x^2+z^2$, $\cos\phi=z/\rho$, $\sin\phi=x/\rho$) are used in (a) and spherical coordinates ($r^2=x^2+y^2+z^2$, $\cos\theta=z/r$, $\sin\theta=(x^2+y^2)^{1/2}/r$) in (b). Outside the cylinder the field decreases as $1/\rho^2$; outside the sphere the field decreases as $1/r^3$. In each case the locus for $\Delta B_z=0$ is a pair of straight lines.

Here, $G_x(t)x$, and so on, are the time-dependent values of the gradient fields. These fields are applied as three independent series of pulses with maximum amplitudes ranging from 10–40 mT/m (1–4 G/cm). In two-dimensional MRI the gradients are used to select the slice to be imaged and to encode position information into the phase and frequency of the MR signal. In practice, B_o is not perfectly uniform and the fields of the gradient coils are not perfectly linear; however, to the extent that these imperfections are fixed properties of the imager, they can be calculated from the coil geometry. It is then often possible to compensate in the reconstruction algorithms for these known sources of imaging errors.

B. Macroscopic field perturbations and positional accuracy

When objects, including the patient, with nonzero magnetic susceptibilities are present in the imaging region, an additional, usually time-independent, magnetic field is present. The z component of the total field is then given by

$$B_z = B_o + G_x(t)x + G_y(t)y + G_z(t)z + \Delta B_z(x,y,z),$$

where $\Delta B_z(x,y,z)$ is the z component of the field produced by the magnetization of the patient and whatever other objects are located within and adjacent to the region of imaging. This field cannot easily be measured or predicted. It depends on the position, size, shape, orientation, and susceptibility of each object present. If the susceptibilities are known, it can be calculated in closed mathematical form for ellipsoidal bodies, and using numerical methods, it can be calculated for bodies of general shape.[58,59,61,63,66,68] The imaging consequences of $\Delta B_z(x,y,z)$ depend on its magnitude and spatial extent in comparison to those of the gradient fields. Figure 7 indicates the effect of the field perturbation on slice selection: The induced field can alter the thickness and give a "potato-chip" appearance to the selected slice.

In most MRI pulse sequences the in-plane position information is encoded by two different mechanisms: In the readout direction the position information is frequency encoded; orthogonal to the readout direction the position information is phase encoded. A discrete series of gradient pulses is used to produce position-dependent phase shifts in the phase-encoding direction. The field $\Delta B_z(x,y,z)$ interferes with the frequency encoding process but does not affect the imaging results of the phase encoding; therefore, the induced field distorts the image in the readout, but not in the phase-

TABLE XI. Readout gradient (G_R) as a function of the field of view (FOV). The quantity $\Delta x=\Delta\chi B_o/G_R$, is a measure of the susceptibility effect on positional accuracy. It is tabulated assuming that $\Delta\chi=9.05\times10^{-6}$ and $B_o=1.5$ T; Δx corresponds to ≈4.6 pixels for each FOV.

FOV (cm)	Pixel size (mm)	G_R (G/cm)	G_R (mT/m)	$\Delta\chi B_o/G_R$ (mm)
8	0.3125	0.941	9.41	1.44
16	0.625	0.470	4.70	2.89
20	0.7825	0.376	3.76	3.61
24	0.9375	0.314	3.14	4.32
32	1.25	0.235	2.35	5.78

[a]The bandwidth (BW) is taken as 32 kHz and G_R=BW/(γFOV), where γ=42.58 MHz/T or 4.258 kHz/G. The total field variation across the FOV is 7.52 G or 7.52×10^{-4} T corresponding to a field change of 0.0294 G or 2.94×10^{-6} T per pixel (N=256). For B_o=1.5 T, f_o=63.87 MHz, and the fractional change of field is 501 ppm across the FOV, or, equivalently, 1.96 ppm per pixel. The frequency change across the FOV is BW=32 kHz and across a pixel it is BW/N=125 Hz.

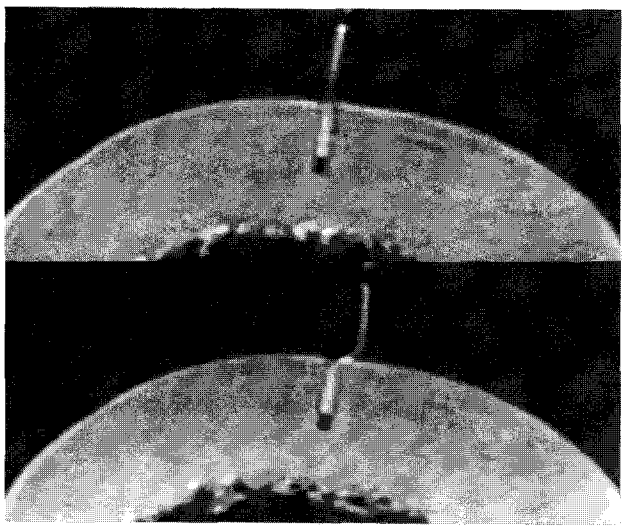

FIG. 10. MR image of a straight cannula inserted into a specimen. A ceramic zirconia (ZrO_2) cannula (transverse to B_o; inner diameter, 2.10 mm; outer diameter, 3.13 mm) containing a copper sulfate solution (1 g/l=1 kg/m^3) is inserted into the outer surface of a melon. The ceramic, the copper sulfate solution, and the melon (approximately spherical) all have susceptibilities close to that of water. In the lower panel, the readout gradient is perpendicular to the axis of the cannula and the discontinuity of the induced field of the melon at its surface creates a discontinuity in the image. In the upper panel, the readout gradient is parallel to cannula axis, and although the image of the cannula is foreshortened, the discontinuity is absent.

encoding direction. It is assumed here, as is ordinarily the case in MRI, that the perturbation producing $\Delta B_z(x,y,z)$ does not change the immediate chemical environment of the nuclei producing the NMR signal. If changes in chemical bonding do occur, changes in the local Lorentz field[49,51,141] contribute to $\Delta B_z(x,y,z)$.

Positions within the object to be imaged are represented by x, y and z: x' and y' represent positions within the two-dimensional image to be generated from the MRI data. The signal frequency f_o corresponding to the field value B_o is assigned the image position $x'=0$, and the image position, x', is determined from the measured frequency, f, by the formula

$$f-f_o=\gamma[G_R x+\Delta B_z(x,y,z)]=\gamma G_R x' \quad \text{or,}$$

$$x'(x,y,z)=x+\Delta B_z(x,y,z)/G_R,$$

and the position error, $\Delta x=x-x'=\Delta B_z(x,y,z)/G_R$.

It is assumed that the selected slice is perpendicular to the z axis; that x is the frequency encoded or readout direction; that y is the phase-encoded direction; and that the frequency, f, is within the receiver bandwidth. G_R is the strength of the readout gradient. Ideally, the extraneous field, $\Delta B_z(x,y,x)=0$, and the above formula then gives $x'(x,y,z)=x$ and $\Delta x=0$. However, if the presence of a foreign body results in $\Delta B_z(x,y,z)\neq 0$, then $x'(x,y,z)\neq x$ and the image is distorted in the direction of the readout gradient. The degree of distortion is determined by the ratio $\Delta B_z/G_R \approx \Delta\chi B_o/G_R$ and can therefore be reduced by increasing G_R or by decreasing B_o. Because decreasing B_o decreases the signal-to-noise ratio in MRI this second option is not particularly useful. In the orthogonal direction, y, the position information is developed from phase-encoding, G_y pulses: The image position, y', is not affected by ΔB_z and $y'=y$.

To determine the impact of $\Delta B_z(x,y,z)$ on the image it is necessary to relate G_R to the imaging field of view (FOV) and the receiver bandwidth, BW. The proton resonant frequency is determined by the relation $f=(\gamma/2\pi)\,B$, where γ is the proton gyromagnetic ratio. Once chemical shift and susceptibility effects are accounted for, the best current value[368] for $\gamma/2\pi$ is 42.576375 MHz/T: For $B_o=1.5$ T, the resonant frequency is 63.865 MHz. The readout gradient, G_R, is required to produce a frequency variation equal to BW between spins at opposite edges of the FOV and therefore

$$G_R=2\pi\mathrm{BW}/(\gamma\ \mathrm{FOV})=(B_o/\mathrm{FOV})(\mathrm{BW}/f_o).$$

At any point in the image a foreign object produces a position error $\Delta x=x-x'=\Delta B_z(x,y,z)/G_R$. For ellipsoids with $\Delta\chi\ll 1$ it was shown above that the extreme values of $\Delta B_z(x,y,z)$ are $\Delta B_z^{\mathrm{pole}} \approx B_o(1-\alpha)\Delta\chi$ and $\Delta B_z^{\mathrm{equator}} = -B_o\alpha\Delta\chi$ and the extreme possible values for $\Delta B_z(x,y,z)$ are $\pm\Delta\chi B_o$. Therefore, $\Delta\chi B_o/G_R$ is a rough but convenient measure of the maximum position errors produced when an object of susceptibility $\Delta\chi$ is present. This quantity, along with G_R, is tabulated in Table XI as a function of FOV for $B_o=1.5$ T and $\Delta\chi=9.05\times10^{-6}$ which corresponds to the susceptibility difference between human tissues and free space. For ellipsoids the extreme position errors are

$$\Delta x/\mathrm{FOV}=(1-\alpha)\Delta\chi f_o/\mathrm{BW} \quad \text{(at the poles)},$$

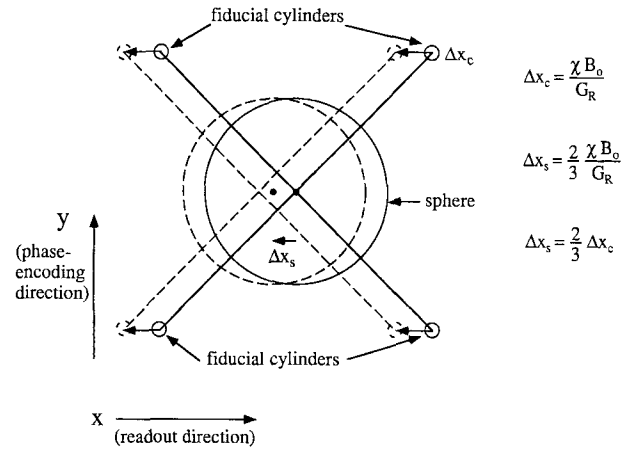

FIG. 11. Stereotactic test phantom. A test phantom to measure positional accuracy can be constructed using an array of tubes containing a copper sulfate solution; however, shape-dependent and susceptibility-dependent positional shifts affect the faithfulness of the image. The phantom utilizes, as fiducial markers, four tubes, each a long cylinder parallel to B_o, at the corners of a square and a sphere of the same solution centered in this array. In object space the diagonals of the square intersect at the center of the sphere as shown by the solid diagonal lines; the image positions of the sphere and the cylinders, however, are shifted by different amounts because of the difference in demagnetizing factors; the image of the sphere is shifted only 2/3 as much as that of the cylinders. Therefore, in the image (dashed lines), the diagonals drawn for the square array do not pass through the center of the sphere.

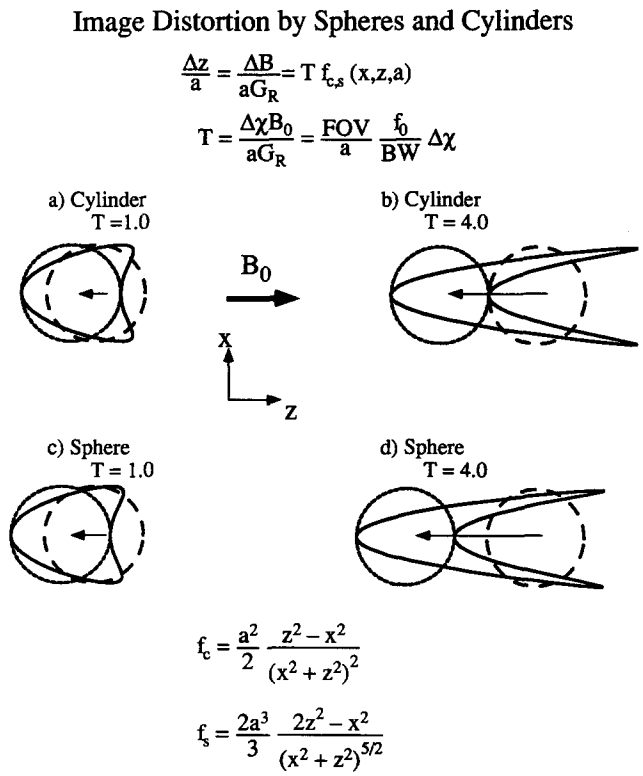

FIG. 12. Image distortion by spheres and cylinders in spin-echo imaging. The imaging plane is assumed to contain the direction of B_o; it is perpendicular to the axis of the cylinder and passes through the center of the sphere; the radius of each object is a. The coarse dashed lines indicate the image position for spins at the spherical or cylindrical surface in the absence of field perturbation ($\Delta\chi=0$). In the presence of field perturbation spins just inside the surface will map to the circular location indicated by the fine dashed lines: Spins just outside the surface will map to the V-shaped solid lines. T is a dimensionless measure of the image distortion; the functions $f_c(x,z,a)$ (for cylinders) and $f_s(x,z,a)$ (for spheres) give the image distortion in the z direction for spins just outside the perturbing object; there is no distortion in the x direction.

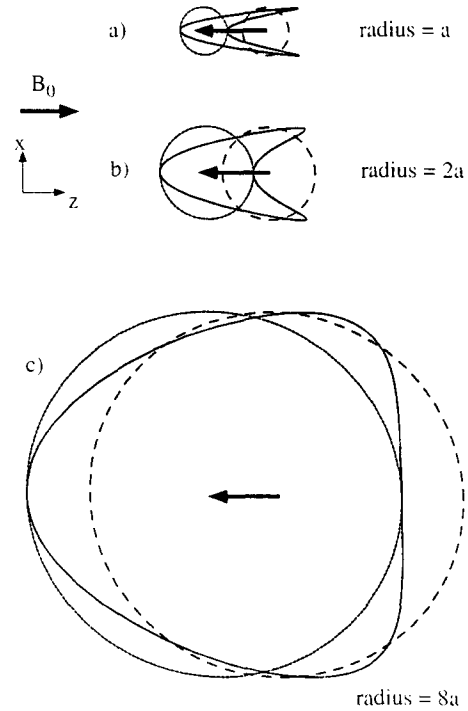

FIG. 13. Effect of cylinder diameter on the susceptibility artifact in spin-echo imaging. For fixed imaging parameters (i.e., G_R, BW, and FOV) the maximum image displacement at the sample surface, $B_o\Delta\chi/(2G_R)$, is independent of the radius (arrows). Calculated image distortions for three cylinders (all with the same negative susceptibility and centered at the same z location) with their axes perpendicular to B_o are shown with fine dashed lines for internal spins and continuous lines for the spins just outside the cylinder. Smaller cylinders have greater apparent shape distortion.

$$\Delta x/\mathrm{FOV} = -\alpha\Delta\chi f_o/\mathrm{BW} \text{ (at the equator).}$$

For $B_o=1.5$ T and BW=32 kHz, the gradients produce a total field excursion of 7.52×10^{-4} T (7.52 G) across the FOV. Expressed as fractions of B_o and f_o, the variation of B and f across the FOV is about 500 ppm and $(\Delta x/\mathrm{FOV})_{\max}\approx\Delta\chi/500$ ppm. Typically, the FOV is divided into 256 pixels, corresponding to a Δf pre pixel of 12.5 Hz per pixel or about 2 ppm of f_0 per pixel. If $\Delta\chi\ll1$ ppm, then $\Delta B_{\max}/B_o$ and $\Delta f_{\max}/f_o$ are also $\ll1$ ppm: In this case the frequency and position errors are much less than one pixel and are negligible. On the other hand, if $\Delta\chi$ is larger, e.g., $\Delta\chi\approx500$ ppm, position errors similar in size to the FOV can occur and the induced field may push the MR frequency for some regions outside the receiver bandwidth: Such regions are not represented in the image.

Patients produce their own perturbing field but, of course, they are not uniform ellipsoids. However, a rough estimate of the spatial average of the induced internal field can be made by taking $\alpha\approx1/4$ for B_o parallel to the long axis of the body. This approach indicates that images of human patients, with $B_o=1.5$ T and BW=32 kHz, are displaced roughly 1.4% of the FOV, i.e., 5.6 mm for a 40 cm FOV and 1.1 mm for an 8 cm FOV, from the position that would result if human tissues had precisely zero susceptibility. For $N=256$, this corresponds to a shift of 3.6 pixels. This effect can be readily demonstrated, using a conventional imager, by changing the sign or direction of the readout gradient, and observing the resulting shift in image position.

In the presence of field perturbations, $\Delta B_z(x,y,z)$, spatial relations present in the object are not necessarily maintained in the image. This distortion can arise from shape-dependent demagnetizing effects even when all the objects have the same susceptibility (Figs. 10 and 11). Under ideal circumstances MRI should be able to determine position information for image-guided stereotactic surgery to within the limits set by the slice thickness and the pixel size. Position errors associated with susceptibility effects must be considered to achieve this ideal level of accuracy. However, susceptibility effects are not the only source of position errors in MRI. The inhomogeneity of B_o, the nonlinearity of gradient fields and the presence of eddy currents associated with gradient switching, also affect the positional accuracy.

C. Image distortion

Objects with different shapes, but the same susceptibility, distort the image differently (Fig. 5). The perturbation fields produced by ellipsoidal objects (e.g., spheres and cylinders)

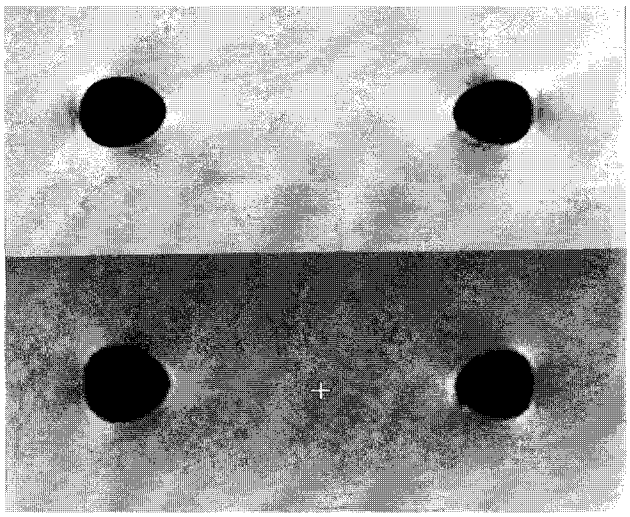

FIG. 14. Spin-echo (SE) images. Alumina (left) and air in a test tube (right) each have susceptibilities differing by about 10 ppm from that of water but the signs are opposite: air is paramagnetic and alumina is diamagnetic with respect to water and the circular cross sections of these two objects are distorted in opposite directions along the readout direction (horizontal). Because of refocusing in the spin-echo technique the distortion in the long echo (T_E=40 ms) in the bottom panel is no greater than in the short echo (T_E=12 ms) in the top panel. The imaging parameters for Figs. 14–19 are B_o=1.5 T, FOV=20 cm, T_R=1000 ms, slice thickness=3 mm, and imaging matrix=256×256. The cylinder orientation and field direction are as in Fig. 12.

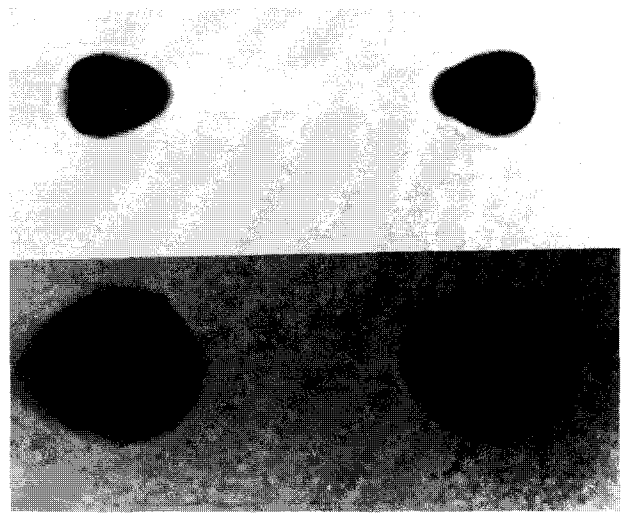

FIG. 15. Gradient-recalled echo (GRE) images. The configuration and imaging parameters are as in Figs. 12 and 14. The flip angle is 90°. Unlike spin-echo imaging, there is no radio-frequency refocusing in GRE imaging and, as a result, the long echo image (T_E=100 ms) in the lower panel is more degraded than the short echo image (T_E=20 ms) in the upper panel.

will be uniform inside the object and the image from any MR signal originating inside the object will be translated but not distorted. An image through a circular cross section of an ellipsoid of revolution is a translated circle superimposed on the image of the external spins (Fig. 12). If, as is often the case, there are no mobile protons inside the ellipsoid, there is no signal from the interior. The spins just outside the ellipsoid's surface do not map in a continuous fashion with those just inside this surface because of the surface discontinuity of the perturbed field (Figs. 7 and 8). Therefore, the image produced by spins immediately outside an object of circular cross section is not circular, but is elongated in a spear-shaped (or, alternatively, a V-shaped or chevron-shaped) fashion. If $\Delta\chi$ is not too large the image is simply distorted; if $\Delta\chi$ is large enough, by an amount which depends on the size and shape of the object, signals from spins near the object are mapped to the same image location as distant spins and some regions of the image become double exposures.[34,36]

The exact shape of the distorted boundary depends on the demagnetizing factor and is somewhat different for transverse cylinders and spheres (Fig. 12). Because ΔB_z is negative in some regions and positive in others, (Fig. 6) there are some regions which map toward increasing values of x and others which map toward decreasing values of x: Also there are locations, with ΔB_z=0, where the image position is not affected by the induced field. The degree of apparent distortion for objects of similar shape and susceptibility depends on their size. The image displacement in the readout direction is fixed and is independent of the object's diameter (Fig. 13). Therefore, under fixed imaging conditions, small objects appear to be relatively more distorted than similarly shaped larger objects.

VII. MRI OF MAGNETICALLY COMPATIBLE MATERIALS

Susceptibility information is not readily available for many materials that are potentially useful in MR-guided surgery. Therefore, the image distortion produced by several of

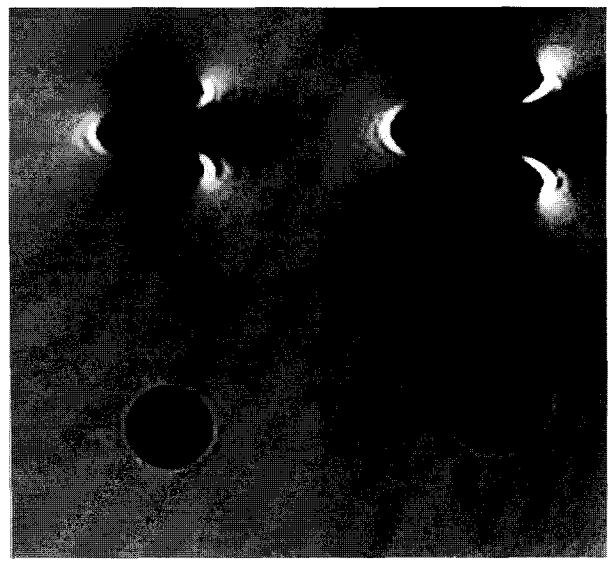

FIG. 16. Magnetic field distortion. The imaging effects of two engineering thermoplastic polymers that show excellent susceptibility matching to water are shown in the lower panel, acetal (left) and PEEK (poly-ether–ether–ketone—right). The upper panel shows the distortion caused by aluminum (left, $\Delta\chi$=30 ppm) and tungsten (right, $\Delta\chi$=86 ppm). These are spin-echo images with T_E=12 ms.

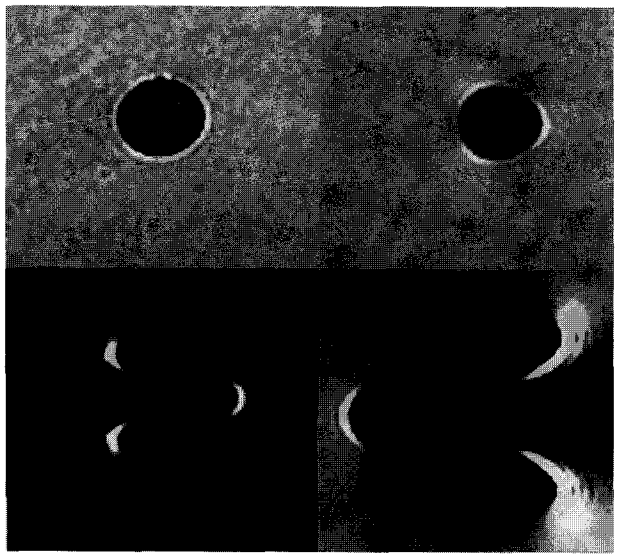

FIG. 17. Magnetic field distortion. The upper panel shows the effect of the thermoplastic polymer polysulfone which has a good susceptibility match to water (left) and of quartz which has $\Delta\chi=-7$ ppm. The lower panel shows the oppositely directed effects of bismuth ($\Delta\chi=-155$ ppm) and titanium ($\Delta\chi=191$ ppm). These are spin-echo images with $T_E=12$ ms.

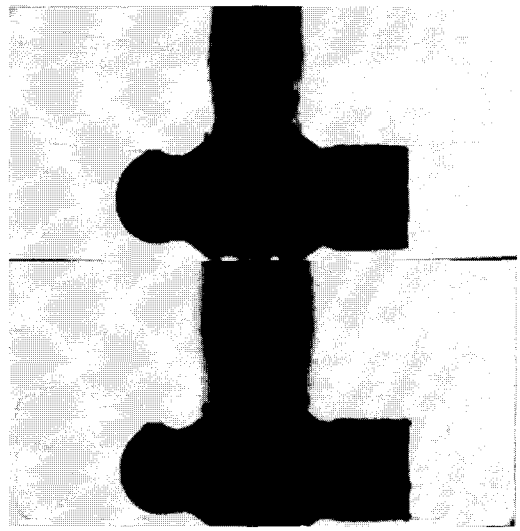

FIG. 19. Magnetic field compatibility of zirconia. This wooden-handled ceramic zirconia hammer (Coors Ceramics, Golden, CO) has the normal strength required for this application: A steel hammer would be impossible to image. However, the zirconia susceptibility is sufficiently close to that of water that even in gradient-echo images (90° flip angle, $T_E=20$ ms in the upper panel and 60 ms in the lower panel) no distortion from the ceramic hammerhead is detected. Some effect of the wooden handle is apparent in the longer echo image.

these materials was investigated using a commercial MR imager (SIGNA, General Electric, Milwaukee, WI). Cylindrical samples (12 to 19 mm in diameter), and transverse to the main magnetic field (1.5 T), were placed in a water bath doped with copper sulfate (1 g/l=1 kg/m^3) and were imaged in a plane perpendicular to the cylinder axis using either conventional spin-echo[368] (SE) or gradient-recalled echo[369] (GRE) techniques. None of the samples was itself a source of MR signal. Samples with the same susceptibility as water produce an undistorted image; simply a dark circle in the

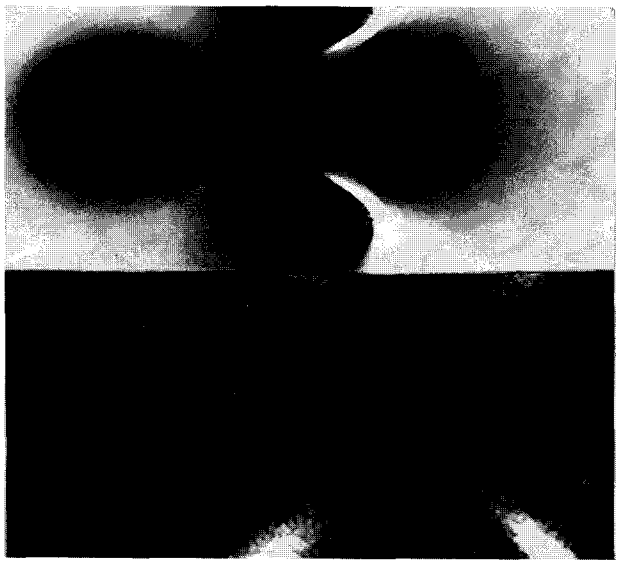

FIG. 18. Magnetic field distortion. The upper panel shows severe image distortion produced by a cylinder of "nonmagnetic" stainless steel (303). The bottom panel shows the extreme effect of a cylinder of cobalt powder. Cobalt is ferromagnetic and the sample experienced strong forces within the magnet and required careful mounting to restrain it; it produces a huge field perturbation and, except along the lines at ±45° which have $\Delta B_z=0$, most of the NMR signal is outside the receiver bandwidth. These are spin-echo images with $T_E=12$ ms.

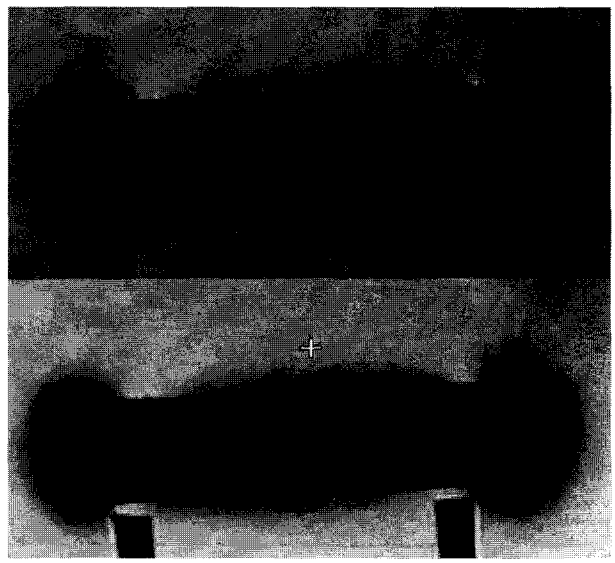

FIG. 20. Ferromagnetic surface contamination. A cylindrical copper rod (length 8 cm, diameter 1.91 cm), perpendicular to B_o is imaged while immersed in a water bath. Initially (upper panel) the imaged surface appears rough and uneven, but after a thin layer of the surface is machined away (lower panel) the surface roughness is absent. The probable explanation is that the rod initially had small fragments of ferromagnetic iron or steel embedded in its surface left over from the manufacturing process; this contamination is removed by the surface machining. The susceptibility of nonmagnetic materials is easily overwhelmed by small amounts of ferromagnetic contamination.

TABLE XII. Materials magnetically compatible with MRI. When examined by MRI these materials exhibit varying degrees of magnetic compatibility. The susceptibilities are based on published data when available and otherwise on measured image distortions. Materials in the first group produce essentially no image abnormality on either spin-echo or gradient-echo imaging. Materials in the second group produce noticeable image distortion, but for most applications it would not be significant. Materials in the third group produce obvious artifacts, but would still be acceptable for many applications.

Group 1. $\lvert\Delta\chi\rvert<3$ ppm	
Nylon	Vespel (acetal)
Silicon nitride (Si_3N_4)	Zirconia (ZrO_2)
Teflon	Plexiglass
Polysulfone	PEEK (poly-ether–ether–ketone)
Magnesia (MgO)	Wood (birch/maple)
Steatite	Copper
Carbon fiber composites[a]	
Group 2. $\lvert\Delta\chi\rvert<10$ ppm	
Alumina (Al_2O_3)	Quartz (SiO_2)
Silicon	Lead
Air	Zinc
Brass	
Group 3. $\lvert\Delta\chi\rvert<200$ ppm	
Titanium	Tantalum
Molybdenum	Zirconium
Tungsten	Bismuth
Graphite (polycrystalline)	Aluminum
Carbon fiber composites[b]	

[a]Applied field parallel to graphite atomic planes.
[b]Applied field normal to graphite atomic planes.

uniform background provided by the water bath. If $\Delta\chi=\chi_{sample}-\chi_{water}\neq 0$, the applied static field is perturbed and the image is distorted: The degree of distortion provides an estimate $\Delta\chi$.[7,34] This method can be used to quickly evaluate the magnetic compatibility of any material proposed for use in MR-guided surgery.

In SE images the expected circular sample outline is distorted into a spear-shaped figure pointing in the direction of the readout gradient. For materials, such as as air and alumina, for which $\Delta\chi$ is similar magnitude but opposite in sign, the orientation of the spear artifact is reversed (Fig. 14). In SE images, the 180° radio-frequency pulse refocuses spins that have been dephased by field inhomogeneities and, as a result, the distortion of these images does not increase as a function of echo time[35] (Fig. 14). Refocusing radio-frequency pulses are not used in GRE images and, as a result, for these images the degradation worsens as the echo time increases (Fig. 15). Figures 16–19 illustrates the image distortion produced by several different materials.

Minute contaminations by ferromagnetic substances can drastically alter the susceptibility of a magnetically compatible material. Copper has a magnetic susceptibility very close to that of water: Figure 20 shows images of a copper rod immersed in water. Visual inspection of the rod showed no evidence of surface contamination, but MR images taken prior to removing a thin layer of the surface indicate the probable presence of contaminating iron or steel particles introduced during the manufacturing process. Many ceramic materials incorporate an inert binding material, such as clay, in the manufacturing process. It is found that ceramic silicon nitride provided by some vendors has an almost perfect susceptibility match to water, while that from other vendors is markedly paramagnetic, probably as a result of minute quantities of iron oxide incorporated in the binding material. Magnetic susceptibility is not ordinarily specified during material acquisition; this opens the possibility of lot-to-lot variations in samples from a given vendor as well as variations from one vendor to another.

Several materials produce images with essentially no detectable distortion and for these materials $\Delta\chi$ is estimated to be less than 3 ppm (Table XII). These materials are expected to be magnetically compatible with any MRI sequence likely to be used in surgery. Particularly significant in this group of materials are ceramics, such as zirconia and silicon nitride, which produce no detectable image degradation and have the potential of being fabricated into very strong instruments. The biocompatibility of zirconia has been extensively studied.[371–376]

VIII. MICROSCOPIC SUSCEPTIBILITY INHOMOGENEITIES IN TISSUES

Variations in the susceptibility that occur over small distances, a few microns or less, affect MRI differently from the large scale, macroscopic variations in χ discussed above. Diffusion of water molecules through microscopically inhomogeneous fields[83–140] leads to a dephasing of nuclear spins that is not cancelled by the use of spin echoes. This results in an irreversible loss of signal and a decrease in the transverse relaxation time, T_2. Each water molecule diffusing through a microscopically inhomogeneous region experiences a fluctuating magnetic field that varies rapidly with respect to T_E but slowly compared to $1/f_o$: The result is a decrease in T_2 without a corresponding decrease in T_1. During a time, t, molecules diffuse an average distance $d=\sqrt{(6Dt)}$, where D is the diffusion constant. For water in tissues diffusion is restricted by the presence of macromolecules and membrane barriers at the subcellular level and, D is approximately 1.2×10^{-5} cm^2/s, which is about one-third of its value in pure water. The susceptibility-enhanced relaxation is determined by the amount of dephasing that occurs during the time, T_E, that elapses between the excitation pulse and the data acquisition. In MRI, T_E is normally in the range from 10 to 200 ms. For $T_E=50$ ms the expression above gives $d=19$ microns: A distance much larger than the 2–3 micron diameter typical of blood capillaries and also larger than many typical cells, Therefore, during a T_E interval each water molecule diffuses over a region comparable in size to the cellular volume and experiences whatever magnetic field fluctuations exist there.

If the variations of χ are on a coarse scale ($\gg\sqrt{(6DT_E)}$, the $\Delta B_z(x,y,z)$ that is experienced by a given nucleus is effectively constant during the T_E interval. In this case, the phase error is cancelled by the 180° B_1 pulse used in spin-echo imaging, and there is no signal loss caused by inhomogeneity effects. If the inhomogeneities are on a fine scale,

$\ll\sqrt{(6DT_E)}$, different perturbing fields are experienced before and after the the 180° pulse, and the phase errors are not completely cancelled by the 180° pulse. Because of the random nature of the diffusion process, the excess phase varies from nucleus to nucleus, leading to an overall loss of signal. Therefore, variations in susceptibility on a microscopic scale produce field variations proportional to $\Delta\chi B_o$ and the resulting MR contrast mechanism is more prominent at higher field strengths. This mechanism has been proposed to explain the short T_2 values characteristic of tissues containing trabecular bone, such as the vertebral bodies; of tissues, such as liver, spleen, and the basal ganglia that contain intracellular deposits of iron stored in ferritin and hemosiderin; and, in the field of functional MRI, of tissue contrast associated with deoxyhemoglobin in the microcirculation.

IX. SUMMARY

The magnetic susceptibility of human tissues and other materials is important to MR-guided surgery and to many other applications of MRI. The quantitative analysis of susceptibility-dependent effects is hampered by the lack of published information on many materials and by traditional inconsistencies in the conventions used to report susceptibility data. The range of susceptibility values acceptable for instruments that are to be used for MR-guided surgery depends on the stringency of the application. MRI magnetic compatibility of the first kind refers to the absence of significant forces and torques on devices used within and near the magnet; MRI magnetic compatibility of the second kind refers to the absence of significant image degradation when devices are present within the imaging region. The susceptibility of human tissues is restricted to a very small range. However, microscopic susceptibility variations of only 2 ppm or even less, particularly at high field strengths, over regions comparable to a diffusion length, produce easily detected signal losses; macroscopic variations on the order of 9 ppm can create position errors in the mm range.

By use of MR imaging, a number of materials have been identified that produce almost no discernible image deterioration, even when they are located within the object being imaged and, even when gradient-echo imaging, which is specially sensitive to field inhomogeneities, is used. It is likely that further study will disclose a number of materials, such as ceramics, thermoplastic polymers and composites that have excellent susceptibility matches with human tissues and that provide a wide range of desirable electrical conductivity, mechanical strength, biocompatibility, and other properties. Magnetic susceptibility is not ordinarily tightly controlled during manufacturing processes and the magnetic properties of materials with very small susceptibilities can be strongly modified by minute quantities of ferromagnetic contaminants: MR imaging itself is a useful method of quality control for materials which must meet stringent susceptibility criteria.

ACKNOWLEDGMENTS

It is a pleasure to acknowledge helpful discussions and technical assistance provided by K. W. Rohling, P. B. Roemer, P. Sandström, M. Sandström, M. Moore, J. S. Philo, E. Schneider, T. Linz, L. Levinson, L. Gleason, Z. Leber, F. A. Jolesz, L. Macuirles, R. Kikinis, H. E. Cline, K. G. Vosburgh, R. Newman, P. Jaskolski, D. Mack, L. Levinson, S. J. Kalia, L. Laitinen, P. Strubin, H. Teichman, S. P. Souza, R. E. Argersinger, D. R. Eisner, T. M. Moriarty, W. A. Edelstein, and J. A. Agresta.

[1]F. A. Jolesz and F. Shtern, "The operating room of the future: Report of the National Cancer Institute Workshop—Imaging-guided stereotactic tumor diagnosis and treatment," Invest. Radiol. **27**, 326–328 (1992).
[2]R. Lufkin, L. Teresi, and W. Hanafee, "New needle for MR-guided aspiration cytology of the head and neck," Am. J. Roentgenol. **149**, 380–382 (1987).
[3]F. A. Jolesz, A. R. Bleier, P. Jakab, P. W. Ruenzel, K. Huttl, and G. J. Jako, "MR imaging of laser tissue interactions," Radiology **168**, 249–253 (1988).
[4]R. Lufkin, L. Teresi, L. Chiu, and W. Hanfee, "A technique for MR-guided needle placement," Am. J. Roentgenol. **151**, 193–196 (1988).
[5]G. Duckwiler, R. B. Lufkin, L. Teresi, E. Spickler, J. Dion, F. Viñuela, J. Bentson, and W. Hanafee, "Head and neck lesions: MR-guided aspiration biopsy," Radiology **170**, 519–522 (1989).
[6]S. Y. C. To, R. B. Lufkin, and L. Chiu, "Technical note: MR compatible winged infusion set," Comput. Med. Imaging Graph. **13**, 469–472 (1989).
[7]Y. Anzai, R. B. Lufkin, R. E. Saxton, H. Fetterman, K. L. Farahani, L. J. Layfield, F. A. Jolesz, W. H. Hanafee, and D. J. Castro, "Nd:YAG interstitial laser phototherapy guided by magnetic resonance imaging in an *ex vivo* model: Dosimetry of laser–MR–tissue interaction," Laryngoscope **101**, 755–760 (1991).
[8]K. Hynynen, A. Darkazanli, E. Unger, and J. F. Schenck, "MRI-guided noninvasive ultrasound surgery," Med. Phys. **20**, 107–116 (1992).
[9]R. Wenokur, J. C. Andrews, E. Abemayor, J. Bailet, L. Layfield, R. F. Canalis, B. Jabour, and R. B. Lufkin, "Magnetic resonance imaging-guided fine needle aspiration for the diagnosis of skull base lesions," Skull Base Surgery **2**, 167–170 (1992).
[10]G. Hathout, R. B. Lufkin, B. Jabour, J. Andrews, and D. Castro, "MR-guided cytology in the head and neck at high field strength," JMRI **2**, 93–94 (1992).
[11]H. E. Cline, J. F. Schenck, K. Hynynen, R. D. Watkins, S. P. Souza, and F. A. Jolesz, "MR-guided focused ultrasound surgery," J. Comput. Assist. Tomogr. **16**, 956–965 (1992).
[12]K. Hynynen, C. Damianou, A. Darkazanli, E. Unger, and J. F. Schenck, "The feasibility of using MRI to monitor and guide noninvasive ultrasound surgery," Ultrasound in Med. Biol. **19**, 91–92, (1993).
[13]H. E. Cline, J. F. Schenck, R. D. Watkins, K. Hynynen, and F. A. Jolesz, "Magnetic resonance-guided thermal surgery," Magn. Reson. Med. **30**, 98–106 (1993).
[14]H. E. Cline, K. Hynynen, R. D. Watkins, W. J. Adams, J. F. Schenck, R. H. Ettinger, W. R. Freund, J. P. Vetro, and F. A. Jolesz, "Focused US system for MR imaging-guided tumor ablation," Radiology **194**, 731–737 (1995).
[15]A. M. Pitt, J. L. Fleckenstein, R. G. Greenlee, D. K. Burns, W. W. Bryan, and R. Haller, "MRI-guided biopsy in inflammatory myopathy: Initial results," Magn. Reson. Imaging **11**, 1093–1099 (1993).
[16]J. C. Gilbert, B. Rubinsky, M. S. Roos, S. T. S. Wong, and K. M. Brennan, "MRI-monitored cryosurgery in the rabbit brain," Magn. Reson. Imaging **11**, 1155–1164 (1993).
[17]H. E. Cline, K. Hynynen, E. Schneider, C. J. Hardy, S. Maier, R. D. Watkins, and F. A. Jolesz, "Simultaneous magnetic resonance phase and temperature maps in muscle," Magn. Reson. Med. **35**, 309–315 (1996).
[18]K. Hynynen, W. R. Freund, H. E. Cline, A. H. Chung, R. D. Watkins, J. P. Vetro, and F. A. Jolesz, "A clinical, noninvasive, MR imaging-monitored ultrasound surgery method," RadioGraphics **16**, 185–195, (1996).

[19]P. B. Roemer, J. F. Schenck, F. A. Jolesz, E. T. Laskaris, R. W. Newman, S. M. Blumenfeld, and K. G. Vosburgh, "A system for MRI-guided interventional procedures," in *Book of Abstracts* (Society of Magnetic Resonance, Berkeley, CA, 1994), p. 420.

[20]Th. Kahn, F. Ulrich, M. Bettag, R. Schober, and U. Möder, "MR-imaging guided laser-induced thermotherapy (LITT) in brain tumors—three year experience," in *Book of Abstracts* (Society of Magnetic Resonance, Berkeley, CA, 1994), p. 422.

[21]S. Wildermuth, K. Zweifel, V. D. Köchli, D. A. Leung, G. C. McKinnon, J. F. Debatin, G. K. von Schulthess, and J. Hodler, "EPI MR-monitoring of percutaneous laser discectomy in cadavers," in *Book of Abstracts* (Society of Magnetic Resonance, Berkeley, CA, 1994), p. 423.

[22]Th. J. Vogel, P. Fischer, U. Knöbber, M. Mack, C. Philipp, and R. Felix, "Interventional MR-guided laser-induced thermotherapy (LITT) for recurrent nasopharyngeal carcinoma—First clinical results of a new designed therapeutic modality," in *Book of Abstracts* (Society of Magnetic Resonance, Berkeley, CA, 1994), p. 424.

[23]J. De Porter, "The proton resonance frequency method for noninvasive MRI thermometry: Study of susceptibility effects," in *Book of Abstracts* (Society of Magnetic Resonance, Berkeley, CA, 1994), p. 426.

[24]J. F. Schenck, F. A. Jolesz, P. B. Roemer, *et al.*, "Superconducting open-configuration MR imaging system for image-guided therapy," Radiology **195**, 805–814 (1995).

[25]M. G. Abele, J. H. Jensen, and H. Rusinek, "Open permanent magnet for surgical applications," in *Book of Abstracts* (Society of Magnetic Resonance, Berkeley, CA, 1995), p. 1154.

[26]J. S. Lewin, J. L. Duerck, and J. R. Haaga, "Needle localization in MR guided therapy: Effect of field strength, sequence design, and magnetic field orientation," in *Book of Abstracts* (Society of Magnetic Resonance, Berkeley, CA, 1995), p. 1155.

[27]H.-B. Gehl, C. Frahm, U. H. Melchert, and H.-D. Weiss, "Suitability of different MR-compatible needles and magnet designs for MR-guided punctures," in *Book of Abstracts* (Society of Magnetic Resonance, Berkeley, CA, 1995), p. 1156.

[28]N. M. deSouza, A. S. Hall, G. A. Coutts, R. Puni, S. D. Taylor-Robinson, and I. R. Young, "Endoscopic magnetic resonance imaging of the upper gastrointestinal tract using a dedicated surface receiver coil," in *Book of Abstracts* (Society of Magnetic Resonance, Berkeley, CA, 1995), p. 1157.

[29]C. L. Emery, D. L. G. Hill, S. F. Keevil, P. E. Summers, J. A. McGlashan, R. Walsh, C. Diamantopoulos, P. J. Liepens, D. J. Hawkes, and M. J. Gleeson, "Preliminary work on MR guided flexible microendoscopic sinus surgery," in *Book of Abstracts* (Society of Magnetic Resonance, Berkeley, CA, 1995), p. 1158.

[30]G. Lenz and C. Dewey, "Study of new titanium alloys for interventional MRI procedures," in *Book of Abstracts* (Society of Magnetic Resonance, Berkeley, CA, 1995), p. 1159.

[31]S. Wildermuth, J. F. Debatin, D. A. Leung, E. Hofmann, C. L. Dumoulin, R. D. Darrow, W. D. Schöpke, G. Uhlschmid, G. C. McKinnon, and G. K. von Schulthess, "MR-guided percutaneous intravascular interventions: *In vivo* assessment of potential applications," in *Book of Abstracts* (Society of Magnetic Resonance, Berkeley, CA, 1995), p. 1161.

[32]D. Kondziolka, P. K. Dempsey, L. D. Lunsford, J. R. W. Kestle, E. J. Dolan, E. Kanal, and R. W. Tasker, "A comparison between magnetic resonance imaging and computed tomography for stereotactic coordinate determination," Neurosurgery **30**, 402–407 (1992).

[33]T. S. Sumanaweera, G. H. Glover, T. O. Binford, and J. R. Adler, "MR susceptibility misregistration correction," IEEE Trans. Med. Imaging **12**, 251–259 (1993).

[34]J. F. Schenck, "Quantitative analysis of intensity artifacts in spin-echo images produced by variations in magnetic susceptibility within the field of view: Equations for the rapid determination of susceptibilities and analogies with catastrophe optics and optical caustic curves," in *Book of Abstracts* (Society of Magnetic Resonance in Medicine, Berkeley, CA, 1993), p. 350.

[35]T. S. Sumanaweera, G. H. Glover, P. F. Hemler, P. A. van den Elsen, D. Martin, J. R. Adler, and S. Napel, "Geometric distortion correction for improved frame-based stereotaxic target localization accuracy," Magn. Reson. Med. **34**, 106–114 (1995).

[36]K. M. Lüdeke, P. Röschmann, and R. Tischler, "Susceptibility artifacts in MR imaging," Magn. Reson. Imaging **3**, 329–343, (1985).

[37]M. O'Donnell and W. A. Edelstein, "NMR imaging in the presence of magnetic field inhomogeneities and gradient field nonlinearities," Med. Phys. **12**, 20–26 (1985).

[38]I. J. Cox, G. M. Bydder, D. G. Gadian, *et al.* "The effect of magnetic susceptibility variations in NMR imaging and NMR spectroscopy *in vivo*," J. Magn. Reson. **70**, 163–168 (1986).

[39]H. W. Park, Y. M. Ro, and Z. H. Cho "Measurement of the magnetic susceptibility effect in high-field NMR imaging," Phys. Med. Biol. **33**, 339–349 (1988).

[40]A. Ericsson, A. Hemmingson, B. Jung, and G. O. Sperber, "Calculation of MRI artifacts caused by static field disturbances," Phys. Med. Biol. **33**, 1103–1112 (1988).

[41]Z. H. Cho, D. J. Kim, and Y. K. Kim, "Total inhomogeneity correction including chemical shifts and susceptibility by view angle tilting," Med. Phys. **15**, 7–11 (1988).

[42]L. F. Czervionke, D. L. Daniels, F. W. Wehrli, L. P. Mark, L. E. Hendrix, J. A. Strandt, A. L. Williams, and V. M. Haughton, "Magnetic susceptibility artifacts in gradient-recalled echo MR imaging," Am. J. Neuroradiol. **9**, 1145–1155 (1988).

[43]R. E. Wendt III, M. R. Wilcott III, W. Nitz, P. H. Murphy, and R. N. Bryan, "MR imaging of susceptibility-induced magnetic field inhomogeneities," Radiology **168**, 837–841 (1988).

[44]D. T. Edmonds and M. R. Wormald, "Theory of resonance in magnetically inhomogeneous specimens and some useful calculations," J. Magn. Reson. **77**, 223–232 (1988).

[45]C. H. Durney, J. Bertolina, D. C. Ailion, R. Christman, A. G. Cutillo, A. H. Morris, and S. Hashemi, "Calculation and interpretation of inhomogeneous line broadening in models of lungs and other heterogeneous structures," J. Magn. Reson. **85**, 554–570 (1989).

[46]K. Farahani, U. Sinha, S. Sinha, L. C.-L. Chiu, and R. B. Lufkin, "Effect of field strength on susceptibility artifacts in magnetic resonance imaging," Comput. Med. Imaging and Graphics **14**, 409–413 (1990).

[47]P. T. Callaghan, "Susceptibility-limited resolution in nuclear magnetic resonance microscopy," J. Magn. Reson. **87**, 304–318 (1990).

[48]S. Posse and W. P. Aue, "Susceptibility artifacts in spin-echo and gradient-echo imaging," J. Magn. Reson. **88**, 473–492 (1990).

[49]S. C.-K. Chu, Y. Xu, J. A. Balschi, and C. S. Springer, Jr., "Bulk magnetic susceptibility shifts in NMR studies of compartmentalized samples: Use of paramagnetic reagents," Magn. Reson. Med. **13**, 239–262 (1990).

[50]N. Yamada, S. Imakita, T. Sakuma, Y. Nishimura, Y. Yamada, H. Naito, T. Nishimura, and M. Takamiya, "Evaluation of the susceptibility effect on the phase images of a simple gradient echo," Radiology **175**, 561–565 (1990).

[51]Y. Xu, J. A. Balschi, and C. S. Springer, Jr., "Magnetic susceptibility shift selected imaging: MESSI," Magn. Reson. Med. **16**, 80–90 (1990).

[52]C. Derosier, G. Delegue, T. Munier, C. Pharaboz, and G. Cosnard, "IRM, distorsion géométrique de l'image et stéréotaxie (MRI, geometric distortion of the image and stereotaxy)," J. Radiol. **72**, 349–353 (1991).

[53]D. C. Noll, C. H. Meyer, J. M. Pauly, D. G. Nishimura, and A. Macovski, "A homogeneity correction method for magnetic resonance imaging with time-varying gradients," IEEE Trans. Med. Imaging **10**, 629–637 (1991).

[54]G. H. Glover and E. Schneider, "Three-point Dixon technique for true water/fat decomposition with B_0 inhomogeneity correction," Magn. Reson. Med. **18**, 371–383 (1991).

[55]C. J. Bergin, D. C. Noll, J. M. Pauly, G. H. Glover, and A. Macovski, "MR imaging of lung parenchyma: A solution to susceptibility," Radiology **183**, 673–676 (1992).

[56]J. M. Pope, R. R. Walker, and T. Kron, "Artifacts in chemical shift selective imaging," Magn. Reson. Imaging **10**, 695–698 (1992).

[57]N. Yamada, S. Imakita, T. Nishimura, M. Takamiya, and H. Naito, "Evaluation of the susceptibility effect on gradient echo phase images *in vivo*: A sequential study of cerebral hematoma," Magn. Reson. Imaging **10**, 559–571 (1992).

[58]R. Bhagwandien, R. Van Ee, R. Beermsa, C. J. G. Bakker, M. A. Moerland, and J. J. W. Lagendijk, "Numerical analysis of the magnetic field for arbitrary magnetic susceptibility distributions in 2D," Magn. Reson. Imaging **10**, 299–313 (1992).

[59]C. J. G. Bakker, M. A. Moerland, R. Bhaghwandien, and R. Beermsa, "Analysis of machine-dependent and object-induced geometric distortion in 2DFT MR imaging," Magn. Reson. Imaging **10**, 597–608 (1992).

[60]H. Chang and J. M. Fitzpatrick, "A technique for accurate magnetic resonance imaging in the presence of field inhomogeneities," IEEE Trans. Med. Imaging **11**, 319–329 (1992).

[61]R. Bhagwandien, M. A. Moerland, C. J. G. Bakker, R. Beermsa, and J. J. W. Lagendijk, "3D numerical analysis of the magnetic field for arbitrary magnetic susceptibility distributions," in *Book of Abstracts* (Society of

Magnetic Resonance in Medicine, Berkeley, CA, 1993), p. 349.
[62]T. Sumanaweera, S. Napel, G. Glover, and S. Song, "A new method to quantify the geometric accuracy of MRI in tissue using MRI itself," in *Book of Abstracts* (Society of Magnetic Resonance in Medicine, Berkeley, CA, 1993), p. 745.
[63]C. J. G. Bakker, R. Bhagwandien, and M. A. Moerland, "3D analysis of susceptibility artifacts in spin-echo and gradient-echo magnetic resonance imaging," in *Book of Abstracts* (Society of Magnetic Resonance in Medicine, Berkeley, CA, 1993), p. 746.
[64]O. Buef, Y. Crémillieux, A. Briguet, M. Lissac, and J. L. Coudert, "Correlation between magnetic susceptibility and image disturbances caused by prosthetic materials," in *Book of Abstracts* (Society of Magnetic Resonance in Medicine, Berkeley, CA, 1993), p. 805.
[65]C. S. Li, T. A. Frisk, and M. B. Smith, "Computer simulations of susceptibility effects: Implications for lineshapes and frequency shifts in localized spectroscopy of the human head," in *Book of Abstracts* (Society of Magnetic Resonance in Medicine, Berkeley, CA, 1993), p. 912.
[66]R. Bhagwandien, M. A. Moerland, C. J. G. Bakker, R. Beermsa, and J. J. W. Lagendijk, "Numerical analysis of the magnetic field for arbitrary magnetic susceptibility distributions in 3D," Magn. Reson. Imaging **12**, 101–107 (1994).
[67]T. Sumanaweera, G. Glover, S. Song, J. Adler, and S. Napel, "Quantifying MRI geometric distortion in tissue," J. Magn. Reson. **31**, 40–47 (1994).
[68]R. Bhagwandien, "Object induced geometry and intensity distortions in magnetic resonance imaging," Ph.D. thesis, University of Utrecht, 1994.
[69]P. F. J. New, B. R. Rosen, T. J. Brady, F. S. Buonanno, J. P. Kistler, C. T. Burt, W. S. Hinshaw, J. H. Newhouse, G. M. Pohost, and J. M. Traveras, "Potential hazards and artifacts of ferromagnetic and nonferromagnetic surgical and dental materials and devices in nuclear magnetic resonance imaging," Radiology **147**, 139–148 (1983).
[70]W. Pavlicek, M. Geisinger, L. Castle, G. P. Borkowski, T. F. Meaney, B. L. Bream, and J. H. Gallagher, "The effects of nuclear magnetic resonance on patients with cardiac pacemakers," Radiology **147**, 149–153 (1983).
[71]G. P. Teitelbaum, W. G. Bradley, Jr., and B. D. Klein, "MR imaging artifacts, ferromagnetism, and magnetic torque of intravascular filters, stents, and coils," Radiology **166**, 657–664 (1988).
[72]F. Shellock, "MR imaging of metallic implants and materials: A compilation of the literature," Am. J. Roentgenol. **151**, 811–814 (1988).
[73]S. J. Karlik, T. Heatherley, F. Pavan, J. Stein, F. Lebron, B. Rutt, L. Carey, R. Wexler, and A. Gelb, "Patient anesthesia and monitoring at a 1.5-T MRI installation," Magn. Reson. Med. **7**, 210–221 (1988).
[74]R. L. Becker, J. F. Norfray, G. P. Teitelbaum, W. G. Bradley, Jr., J. B. Jacobs, L. Wacaser, and R. L. Rieman, "MR imaging in patients with intracranial aneurysm clips," Am. J. Neuroradiol. **9**, 885–889 (1988).
[75]D. A. Clayman, M. E. Murakami, and F. S. Vines, "Compatibility of cervical spine braces with MR imaging: A study of nine nonferrous devices," Am. J. Neuroradiol. **11**, 385–390 (1990).
[76]E. Kanal and F. G. Shellock, "Safety considerations in MR imaging," Radiology **176**, 593–606 (1990).
[77]F. G. Shellock and J. S. Curtis, "MR imaging and biomedical implants, materials, and devices: An updated review," Radiology **180**, 541–550 (1990).
[78]N. J. Kagetsu and A. W. Litt, "Important considerations in measurement of attractive force on metallic implants in MR images," Radiology **179**, 505–508 (1991).
[79]A. S. Smith, G. C. Hurst, J. L. Duerk, and P. J. Diaz, "MR of ballistic materials—Imaging artifacts and potential hazards," Am. J. Neuroradiol. **12**, 567–572 (1991).
[80]R. P. Klucznik, D. A. Carrier, R. Pyka, and R. W. Haid, "Placement of a ferromagnetic intracerebral aneurysm clip in a magnetic field with a fatal outcome," Radiology **187**, 855–856 (1993).
[81]E. Kanal and F. Shellock, "MR imaging of patients with intracranial aneurysm clips," Radiology **187**, 612–614 (1993).
[82]F. G. Shellock, S. Morisoli, and M. Kanal, "MR procedures and biomedical implants, materials, and devices: 1993 update," Radiology **189**, 587–599 (1993).
[83]B. Drayer, P. Burger, P. R. Darwin, S. Riederer, R. Herfkens, and G. A. Johnson, "Magnetic resonance imaging of brain iron," Am. J. Neuroradiol. **7**, 373–380 (1986).
[84]B. P. Drayer, W. Olanow, P. Burger, G. A. Johnson, R. Herfkens, and S. Riederer, "Parkinson plus syndrome: Diagnosis using high field MR imaging of brain iron," Radiology **159**, 493–498 (1986).
[85]B. P. Drayer, P. Burger, B. Hurwitz, D. Dawson, J. Cain, J. Leong, R. Herfkens, and G. A. Johnson, "Magnetic resonance imaging in multiple sclerosis: Decreased signal in thalamus and putamen," Ann. Neurol. **22**, 546–550 (1988).
[86]J. F. Norfray, N. L. Charadonna, W. J. Heiser, S.-H. Song, B. V. Manyam, A. B. Devleschoward, and L. M. Eastwood, "Brain iron in patients with Parkinson disease: MR visualization using gradient modification," Am. J. Neuroradiol. **9**, 237–240 (1988).
[87]B. H. Braffman, R. I. Grossman, H. I. Goldberg, M. B. Stern, H. I. Hurtig, D. B. Hackney, L. T. Bilaniuk, and R. A. Zimmerman, "MR imaging of Parkinson disease with spin-echo and gradient-echo sequences," Am. J. Neuroradiol. **9**, 1093–1099 (1988).
[88]R. B. Dietrich and W. G. Bradley, Jr., "Iron accumulation in the basal ganglia following severe ischemic-anoxic insults in children," Radiology **168**, 203–206 (1988).
[89]J. F. Schenck, O. M. Mueller, S. P. Souza, C. L. Dumoulin, and M. A. Hussain, "Iron-dependent contrast in NMR imaging of the human brain at 4.0 tesla," in *Book of Abstracts* (Society of Magnetic Resonance in Medicine, Berkeley, CA, 1989), p. 9.
[90]S. Aoki, Y. Okada, K. Nishimura, A. J. Barkovich, B. O. Kjos, R. C. Brasch, and D. Norman, "Normal deposition of brain iron in childhood and adolescence: MR imaging at 1.5 T," Radiology **172**, 381–385 (1989).
[91]C. Chen, P. A. Hardy, M. J. Clauberg, J. G. Joshi, J. Parravano, J. H. N. Deck, R. M. Henkelman, L. E. Becker, and W. Kucharczyk, "*T*2 Values in the human brain: Comparison with quantitative assays of iron and ferritin," Radiology **173**, 521–526 (1989).
[92]A. Bizzi, R. A. Brooks, A. Brunetti, J. M. Hill, R. Alger, R. S. Miletich, T. L. Francavilla, and G. DiChiro, "Role of iron and ferritin in MR imaging of the brain: A study in primates at different field strengths," Radiology **177**, 59–65 (1990).
[93]J. F. Schenck, O. M. Mueller, S. P. Souza, and C. L. Dumoulin, "Magnetic resonance imaging of brain iron using a 4 tesla whole-body scanner," in *Iron Biominerals*, edited by R. B. Frankel and R. P. Blakemore (Plenum, New York, 1990), pp. 373–385.
[94]P. Pujol, C. Junqué, P. Vendrell, J. M. Grau, J. L. Martí-Vilalta, C. Olivé, and J. Gili, "Biological significance of iron-related magnetic resonance imaging changes in the brain," Arch. Neurol. **49**, 711–717 (1992).
[95]J. Vymazal, R. A. Brooks, O. Zak, C. McRill, C. Shen, and G. DiChiro, "*T*1 and *T*2 of ferritin at different field strengths: Effect on MRI," Magn. Reson. Med. **27**, 368–374 (1992).
[96]P. Schmalbrock, D. W. Chakeres, and V. A. Hacker, "3D-gradient echo MRI of the substantia nigra and basal ganglia," in *Book of Abstracts* (Society of Magnetic Resonance in Medicine, Berkeley, CA, 1992), p. 1326.
[97]G. Bartzokis, M. Aravagiri, W. H. Oldendorf, J. Mintz, and S. R. Marder, "Field dependent transverse relaxation rate increase may be a specific measure of tissue iron stores," Magn. Reson. Med. **29**, 459–464 (1993).
[98]R. J. Ordidge, J. M. Gorell, J. C. Deniau, R. A. Knight, and J. A. Helpern, "Assessment of relative brain iron concentrations using T_2-weighted and T_2^*-weighted MRI at 3 tesla," Magn. Reson. Med. **32**, 335–341 (1994).
[99]F. Q. Ye, W. R. W. Martin, J. Hodder, and P. S. Allen, "Brain iron imaging exploiting heterogeneous-susceptibility-enhanced proton relaxation," in *Book of Abstracts* (Society of Magnetic Resonance, Berkeley, CA, 1994), p. 5.
[100]J. Vymazal, M. Hajek, N. Patronas, J. N. Giedd, J. W. M. Bulte, R. A. Brooks, and G. Di Chiro, "Effect of brain iron on *T*1-weighted MRI," in *Book of Abstracts* (Society of Magnetic Resonance, Berkeley, CA, 1995), p. 513.
[101]Vymazal, M. Hajek, C. Baumgarner, V. Tran, N. Patronas, J. W. M. Bulte, and R. A. Brooks, "Effect of brain iron on MRI: An *in vivo–in vitro* correlation," in *Book of Abstracts* (Society of Magnetic Resonance, Berkeley, CA, 1995), p. 1085.
[102]F. Q. Ye, W. R. W. Martin, and P. S. Allen, "Proton transverse relaxation in brain tissue," in *Book of Abstracts* (Society of Magnetic Resonance, Berkeley, CA, 1995), p. 1234.
[103]Walecki, T. Kmiec, and J. Jusko, "MRI findings in children with Hallervorden–Spatz disease," in *Book of Abstracts* (Society of Magnetic Resonance, Berkeley, CA, 1995), p. 1235.
[104]M. Paley, R. Ordidge, I. D. Wilkinson, R. J. S. Chinn, M. A. Hall-Craggs, and M. J. G. Harrison, "PRIME: A multi-echo method for the measure-

ment of $T2$," in *Book of Abstracts* (Society of Magnetic Resonance, Berkeley, CA, 1995), p. 1259.
[105]J. F. Schenck, "Imaging of brain iron by magnetic resonance imaging: T_2 relaxation at different field strengths," J. Neurol. Sci. S **134**, 10–18 (1995).
[106]K. R. Thulborn, A. G. Sorensen, N. W. Kowall, A. McKee, A. Lai, R. C. McKinstry, J. Moore, B. R. Rosen, and T. J. Brady, "The role of ferritin and hemosiderin in the MR appearance of cerebral hemorrhage," Am. J. Neuroradiol. **11**, 1053–1059 (1989).
[107]K. R. Thulborn and S. W. Atlas, "Intracranial hemorrhage," in *Magnetic Resonance Imaging of the Brain and Spine*, 2nd ed., edited by S. W. Atlas (Raven, New York, 1996), pp. 265–314.
[108]W. G. Bradley, "MR appearance of hemorrhage in the brain," Radiology **189**, 15–26 (1993).
[109]F. W. Wehrli, J. C. Ford, M. Attie, H. Y. Kressel, and F. S. Kaplan, "Trabecular structure: Preliminary application of MR interferometry," Radiology **179**, 615–621 (1991).
[110]J. C. Ford and F. W. Wehrli, "*In vivo* quantitative characterization of trabecular bone by NMR interferometry and localized proton spectroscopy," Magn. Reson. Med. **17**, 543–551 (1991).
[111]J. C. Ford, F. W. Wehrli, and H.-W. Chung, "Magnetic field distribution in models of trabecular bone," Magn. Reson. Med. **30**, 373–379 (1993).
[112]H. Chung, F. W. Wehrli, J. L. Williams, and S. D. Kugelmass, "Relationship between NMR transverse relaxation, trabecular bone architecture and strength," Proc. Natl. Acad. Sci. (USA) **90**, 10250–10254 (1993).
[113]K. R. Thulborn, J. C. Waterton, P. M. Matthews, and G. K. Radda, "Oxygenation dependence of the transverse relaxation time of water protons in whole blood at high field," Biochim. Biophys. Acta **714**, 265–270 (1982).
[114]R. A. Brooks and G. DiChiro, "Magnetic resonance imaging of stationary blood: A review," Med. Phys. **14**, 903–913 (1987).
[115]A. Villringer, B. R. Rosen, J. W. Belliveau, J. L. Ackerman, R. B. Lauffer, R. B. Buxton, Y.-S. Chao, V. J. Wedeen, and T. J. Brady, "Dynamic imaging with lanthanide chelates in normal brain: Contrast due to magnetic susceptibility effects," Magn. Reson. Med. **6**, 164–174 (1988).
[116]R. R. Edelman, H. P. Mattle, D. J. Atkinson, T. Hill, J. P. Finn, C. Mayman, M. Ronthal, H. M. Hoogewoud, and J. Kleefeld, "Cerebral blood flow: Assessment with dynamic contrast-enhanced $T2^*$-weighted MR imaging at 1.5 T," Radiology **176**, 211–220 (1990).
[117]S. Ogawa, T.-M. Lee, A. S. Nayak, and P. Glynn, "Oxygenation-sensitive contrast in magnetic resonance image of rodent brain at high magnetic fields," Magn. Reson. Med. **14**, 68–78 (1990).
[118]J. W. Belliveau, B. R. Rosen, H. L. Kantor, R. R. Rzedzian, D. N. Kennedy, R. C. McKinstry, J. M. Vevea, M. S. Cohen, I. L. Pykett, and T. J. Brady, "Functional cerebral imaging by susceptibility-contrast NMR," Magn. Reson. Med. **14**, 538–546 (1990).
[119]R. Turner, D. LeBihan, C. T. W. Moonen, D. Despres, and J. Frank, "Echo-planar time course MRI of cat brain oxygenation changes," Magn. Reson. Med. **22**, 159–166 (1991).
[120]B. R. Rosen, J. W. Belliveau, H. J. Aronen, D. Kennedy, B. R. Buchbinder, A. Fischman, M. Gruber, J. Glas, R. M. Weisskoff, M. S. Cohen, F. H. Hochberg, and T. J. Brady, "Susceptibility contrast imaging of cerebral blood volume: Human experience," Magn. Reson. Med. **22**, 293–299 (1991).
[121]C. R. Fisel, J. L. Ackerman, R. B. Buxton, L. Garrido, J. W. Belliveau, B. R. Rosen, and T. J. Brady, "MR contrast due to microscopically heterogeneous magnetic susceptibility: Numerical simulations and applications to cerebral physiology," Magn. Reson. Med. **17**, 336–347 (1991).
[122]J. F. Schenck, "Health and physiological effects of human exposure to whole-body four-tesla magnetic fields during MRI," in *Biological and Safety Aspects of Nuclear Magnetic Resonance Imaging and Spectroscopy: Ann. N.Y. Acad. Sci.*, edited by R. L. Magin, R. P. Liburdy, and B. Persson (N.Y. Acad. Sci. New York, 1992), Vol. 649, pp. 285–301.
[123]M. Maeda, S. Itoh, H. Kimura, T. Iwasaki, N. Hayashi, K. Yamamoto, Y. Ishii, and T. Kubota, "Tumor vascularity in the brain: Evaluation with dynamic susceptibility-contrast MR imaging," Radiology **189**, 233–238 (1993).
[124]S. Ogawa, R. S. Menon, D. W. Tank, S.-G. Kim, J. M. Ellerman, and K. Urgubil, "Functional brain mapping by oxygenation level-dependent contrast magnetic resonance imaging: A comparison of signal characteristics with a biophysical model," Biophys. J. **64**, 803–812 (1993).
[125]R. M. Weisskoff and S. Kiihne, "MRI susceptometry: Image-based measurement of absolute susceptibility of MR contrast agents and human blood," Magn. Reson. Med. **24**, 375–383 (1992).
[126]P. A. Bandettini, E. C. Wong, R. S. Hinks, R. S. Tikofsky, and J. S. Hyde, "Time course EPI of human brain function during task activation," Magn. Reson. Med. **25**, 390–397 (1992).
[127]S. Ogawa, D. W. Tank, R. Menon, J. M. Ellerman, S.-G. Kim, H. Merkle, and K. Ugurbil, "Intrinsic signal changes accompanying sensory stimulation: Functional brain mapping with magnetic resonance imaging," Proc. Natl. Acad. Sci. USA **89**, 5951–5955 (1992).
[128]K. K. Kwong, J. W. Belliveau, D. A. Chesler, E. I. Goldberg, R. M. Weisskoff, B. P. Poncelet, D. N. Kennedy, B. E. Hoppel, M. S. Cohen, R. Turner, H. M. Cheng, T. J. Brady, and B. R. Rosen, "Dynamic magnetic resonance imaging of human brain activity during primary sensory stimulation," Proc. Natl. Acad. Sci. USA **89**, 5675–5679 (1992).
[129]B. E. Hoppel, R. M. Weisskoff, K. R. Thulborn, J. B. Moore, K. K. Kwong, and B. R. Rosen, "Measurement of regional blood oxygenation and cerebral hemodynamics," Magn. Reson. Med. **30**, 715–723 (1993).
[130]H. Sakuma, M. O'Sullivan, J. Lucas, M. F. Wendland, M. Saeed, M. C. Dulce, A. Watson, K. L. Bleyl, N. D. LaFrance, and C. B. Higgins, "Effect of magnetic susceptibility contrast medium on myocardial signal intensity with fast gradient-recalled echo and spin-echo MR imaging: Initial experience in humans," Radiology **190**, 161–166 (1994).
[131]R. P. Kennan, J. Zhong, and J. C. Gore, "Intravascular susceptibility contrast mechanisms in tissues," J. Magn. Reson. **31**, 9–21 (1994).
[132]J. Hennig, Th. Ernst, O. Speck, G. Deuschl, and E. Feifel, "Detection of brain activation using oxygenation sensitive functional spectroscopy," J. Magn. Reson. **31**, 85–90 (1994).
[133]E. O. Stejskal and J. E. Tanner, "Spin diffusion measurements: Spin echoes in the presence of a time-dependent field gradient," J. Chem. Phys. **42**, 288–292 (1965).
[134]R. C. Wayne and R. M Cotts, "Nuclear-magnetic-resonance study of self-diffusion in a bounded medium," Phys. Rev. **151**, 264–272 (1966).
[135]J. E. Tanner and E. O. Stejskal, "Restricted self-diffusion of protons in colloidal systems by the pulsed-gradient, spin-echo method," J. Chem. Phys. **49**, 1768–1777 (1968).
[136]K. J. Packer, "The effects of diffusion through locally inhomogenous magnetic fields on transverse nuclear spin relaxation in heterogeneous systems. Proton transverse relaxation in striated muscle tissue," J. Magn. Reson. **9**, 438–443 (1973).
[137]S. Majumdar and J. C. Gore, "Studies of diffusion in random fields produced by variations in susceptibility," J. Magn. Reson. **78**, 41–55 (1988).
[138]C. B. Ahn and Z. H. Cho, "A generalized formulation of diffusion effects in μm resolution nuclear magnetic resonance imaging," Med. Phys. **16**, 22–28 (1989).
[139]P. Hardy and R. M. Henkelman, "On the transverse relaxation rate enhancement induced by the diffusion of spins through inhomogeneous fields," Magn. Reson. Med. **17**, 348–356 (1991).
[140]J. Zhong and J. C. Gore, "Studies of restricted diffusion in heterogeneous media containing variations in susceptibility," J. Magn. Reson. **19**, 276–284 (1991).
[141]W. C. Dickinson, "The time average magnetic field at the nucleus in nuclear magnetic resonance experiments," Phys. Rev. **81**, 717–731 (1951).
[142]D. F. Evans, "Anomalous solvent shifts in high-resolution nuclear magnetic resonance spectra," Proc. Chem. Soc. 115–116 (April, 1958).
[143]D. F. Evans, "The determination of paramagnetic susceptibility of substances in solution by nuclear magnetic resonance," J. Chem. Soc. (London) **111**, 2003–2005 (1959).
[144]K. D. Bartle, D. W. Jones, and S. Maricic, "The determination of paramagnetic susceptibilities by high-resolution nuclear magnetic resonance," Croatica Chemica Acta **40**, 227–239 (1968).
[145]J. K. Becconsall, G. D. Daves, Jr., and W. R. Anderson, Jr., "Reference-independent nuclear magnetic resonance solvent shifts," J. Am. Chem. Soc. **92**, 430–432 (1970).
[146]T. H. Crawford and J. Swanson, "Temperature dependent magnetic measurements and structural equilibria in solution," J. Chem. Educ. **48**, 382–386 (1971).
[147]*Mathematical Papers of George Green*, edited by N. M. Ferrers (London, 1871; Reprinted, Chelsea, New York, 1970).
[148]W. Thomson, *Reprint of Papers on Electrostatics and Magnetism* (Macmillan, London, 1872).
[149]J. C. Maxwell, *A Treatise on Electricity and Magnetism*, 3rd ed. (Claren-

don, Oxford, 1891; Reprinted, Dover, New York, 1954).
[150]H. A. Lorentz, *The Theory of Electrons*, 2nd ed. (Teubner, Leipzig, 1916; Reprinted, Dover, New York, 1952).
[151]A. Gray, *Absolute Measurements in Electricity and Magnetism* (Macmillan, London, 1921; Reprinted, Dover, New York, 1967).
[152]E. C. Stoner, *Magnetism and Atomic Structure* (Methuen, London, 1926).
[153]W. D. MacMillan, *The Theory of the Potential* (Reprinted, Dover, New York, 1958).
[154]O. D. Kellogg, *Foundations of Potential Theory* (Springer, Berlin, 1929; Reprinted, Dover, New York, 1953).
[155]R. S. Edgar, *Field Analysis and Potential Theory* (Springer, Berlin, 1989).
[156]J. H. Van Vleck, *The Theory of Electric and Magnetic Susceptibilities* (Oxford University, London, 1932).
[157]E. C. Stoner, *Magnetism and Matter* (Methuen, London, 1934).
[158]N. F. Mott and H. Jones, *The Theory of the Properties of Metals and Alloys* (Clarendon, Oxford, 1936; Reprinted, Dover, New York, 1958) pp. 183–239.
[159]A. O'Rahilly, *Electromagnetic Theory: A Critical Examination of Fundamentals* (Longmans, Green and Company, London, 1938; Reprinted, Dover, New York, 1965).
[160]J. A. Stratton, *Electromagnetic Theory* (McGraw-Hill, New York, 1941), pp. 241–242.
[161]C. J. Gorter, *Paramagnetic Relaxation* (Elsevier, Amsterdam, 1947).
[162]M. Planck, *Theory of Electricity and Magnetism: Introduction to Theoretical Physics*, 2nd ed., Translated by H. L. Brose (Macmillan, New York, 1949), Vol. 3.
[163]R. M. Bozorth, *Ferromagnetism* (Van Nostrand, New York, 1951; Reprinted, IEEE, Piscataway, NJ, 1993).
[164]A. Sommerfeld, *Electrodynamics: Lectures on Theoretical Physics*, Translated by E. G. Ramberg (Academic, New York, 1952), Vol. 4.
[165]A. H. Wilson, *The Theory of Metals*, 2nd ed. (Cambridge University, Cambridge, 1953).
[166]E. T. Whittaker, *A History of the Theories of Aether and Electricity* (Thomas Nelson, London, 1951 and 1953; Reprinted, Dover, New York, 1989).
[167]P. M. Morse and H. Feshbach, *Methods of Theoretical Physics* (McGraw-Hill, New York, 1953).
[168]R. E. Peierls, *Quantum Theory of Solids* (Clarendon, Oxford, 1955), pp. 143–160.
[169]P. W. Selwood, *Magnetochemistry* (Interscience, New York, 1956).
[170]N. Cusack, *The Electrical and Magnetic Properties of Solids* (Longmans, London, 1958).
[171]L. F. Bates, *Modern Magnetism*, 4th ed. (Cambridge University, London, 1961).
[172]A. H. Morrish, *The Physical Principles of Magnetism* (Wiley, New York, 1965).
[173]E. M. Purcell, *Electricity and Magnetism* (McGraw-Hill, New York, 1965).
[174]R. S. Elliott, *Electromagnetics: History, Theory, and Applications* (McGraw-Hill, New York, 1966; Reprinted, IEEE Press, Piscataway, NJ 1993).
[175]N. Feather, *Electricity and Matter* (Edinburgh University, Edinburgh, 1968), pp. 453–455.
[176]B. D. Cullity, *Introduction to Magnetic Materials* (Addison-Wesley, Reading, 1972).
[177]L. N. Mulay and E. A. Boudreaux, *Theory and Applications of Molecular Diamagnetism* (Wiley, New York, 1976).
[178]E. A. Boudreaux and L. N. Mulay, *Theory and Applications of Molecular Paramagnetism* (Wiley, New York, 1976).
[179]C.-W. Chen, *Magnetism and Metallurgy of Soft Magnetic Materials* (North-Holland, Amsterdam, 1977; Reprinted, Dover, New York, 1985).
[180]L. D. Landau and E. M. Lifshitz, *Electrodynamics of Continuous Media*, 2nd ed. (Pergamon, Oxford, 1984).
[181]R. L. Carlin, *Magnetochemistry* (Springer, Berlin, 1986).
[182]D. Jiles, *Introduction to Magnetism and Magnetic Materials* (Chapman and Hall, London, 1991).
[183]S. T. Keith and P, Quédec, "Magnetism and magnetic materials," in *Out of the Crystal Maze: Chapters from the History of Solid State Physics*, edited by L. Hoddeson, E. Braun, J. Teichmann, and S. Weart (Oxford University, Oxford, 1992), pp. 359–442.
[184]S. Chapman and J. Bartels, *Geomagnetism*, (Clarendon, Oxford, 1940).
[185]T. Nagata, *Rock Magnetism*, 2nd ed. (Maruzen Company, Tokyo, 1961).
[186]E. Irving, *Paleomagnetism and its Application to Geological and Geophysical Problems* (Wiley, New York, 1964).
[187]F. D. Stacey and S. K. Banerjee, *The Physical Principles of Rock Magnetism* (Elsevier, Amsterdam, 1974).
[188]W. D. Parkinson, *Introduction to Geomagnetism* (Scottish Academic, Edinburgh, 1983).
[189]R. T. Merrill and M. W. McElhinny, *The Earth's Magnetic Field: Its History, Origin and Planetary Perspective* (Academic, Orlando, 1983).
[190]R. Thompson and F. Oldfield, *Environmental Magnetism* (Allen and Unwin, London, 1986).
[191]R. F. Butler, *Paleomagnetism: Magnetic Domains to Geologic Terranes* (Blackwell Scientific, Boston, 1992).
[192]C. Emiliani, *Planet Earth: Cosmology, Geology, and the Evolution of Life and Environment* (Cambridge University, Cambridge, 1992).
[193]F. D. Stacey, "The physical theory of rock magnetism," Adv. Phys. **12**, 45–133 (1963).
[194]W. O'Reilly, "Magnetic minerals in the crust of the earth," Rep. Prog. Phys. **39**, 857–908 (1976).
[195]J. H. Puffer, E. W. B. Russell, and M. R. Rampino, "Distribution and origin of magnetic spherules in air, waters and sediments of the greater New York City area and the North Atlantic Ocean," J. Sed. Petrol. **50**, 247–256 (1980).
[196]D. J. Dunlop, "The rock magnetism of fine particles," Phys. Earth Planet. Inter. **26**, 1–26 (1981).
[197]D. A. Clark, "Comments on magnetic petrophysics," Bull. Aust. Soc. Explor. Geophys. **14**, 49–62 (1983).
[198]C. R. Camacho, D. B. Plewes, and R. M. Henkelman, "Nonsusceptibility artifacts due to metallic objects in MRI," JMRI **5**, 75–88 (1995).
[199]J. F. Schenck, C. L. Dumoulin, R. W. Redington, H. Y. Kressel, R. T. Elliott, and I. L. McDougall, "Human exposure to 4.0-tesla magnetic fields in a whole-body scanner," Med. Phys. **19**, 1089–1098 (1992).
[200]Reference 180, p. 115.
[201]Reference 149, Vol. 2, pp. 63–66.
[202]C. P. Poole, Jr. and H. A. Farach, *Relaxation in Magnetic Resonance* (Academic, New York, 1971).
[203]H. A. Klein, *The Science of Measurement: A Historical Survey* (Simon and Schuster, New York, 1974; Reprinted, Dover, New York, 1988).
[204]G. Giorgi, "Unità razionali di elettromagnetismo," L'Elettricita (Milan) **20**(50), 787–788 (1901).
[205]A. E. Kennelly, "Historical outline of the electrical units," J. Eng. Educ. **19**, 229–275 (1928).
[206]A. E. Kennelly, "The oersted considered as a new international magnetic unit," Scientific Monthly (April, 1931).
[207]A. E. Kennelly, "Notes on the July 1932 meeting of the Committee on Symbols, Units, and Nomenclature of the International Union of Pure and Applied Physics to discuss magnetic units," Terr. Magn. Atmos. Elect. **37**, 447–453 (1932).
[208]A. E. Kennelly, "Conference of the Symbols, Units and Nomenclature (S. U. N.) Commission of the International Union of Pure and Applied Physics (I. P. U.) at Paris, in July, 1932, and its results," Proc. Natl. Acad. Sci. (USA) **19**, 144–149 (1933).
[209]R. T. Birge, "On electric and magnetic units and dimensions," Am. Phys. Teacher **2**, 41–48 (1934).
[210]R. T. Birge, "On the establishment of fundamental and derived units, with special reference to electric units. Part I," Am. Phys. Teacher **3**, 102–109 (1935).
[211]R. T. Birge, "On the establishment of fundamental and derived units, with special reference to electric units. Part II," Am. Phys. Teacher **3**, 171–179 (1935).
[212]A. E. Kennelly, "The MKS system of units," J. Instr. Elect. Enging. **78**, 235–244 (1936).
[213]A. E. Kennelly, "Magnetic formulae expressed in the M.K.S. system of units," Proc. Am. Phil. Soc. **76**, 343–377 (1936).
[214]SUN Commission, "Symbols and units," Phys. Today **9**(11), 23–27 (1956).
[215]SUN Commission, "SUN Commission Report, Document SUN 56–7," Phys. Today **10**(3), 30–34 (1957).
[216]T. I. Quickenden and R. C. Marshall, "Magnetochemistry in SI units," J. Chem. Educ. **49**, 114–116 (1972).
[217]J. Crangle, "SI Units in magnetism," Phys. Bull. **26**, 539–540 (1975).
[218]International Union of Pure and Applied Physics—S.U.N. Commission, "Symbols, units, and nomenclature in physics," Physica A **93**, 1–60 (1978).

[219]M. A. Payne, "SI and gaussian units, conversions and equations for use in geomagnetism," Phys. Earth Planet. Sci. **26**, P10–P16 (1981).
[220]N. Shive, "Suggestions for the use of SI units in magnetism," Eos **67**, 25–26 (1986).
[221]Reference 160, pp. 16–23 and 238–241.
[222]O. Heaviside, *Electrical Papers* (London, 1892; Reprinted, Chelsea, New York, 1970).
[223]O. Heaviside, *Electromagnetic Theory* (London, 1893, 1899, 1912; Reprinted, Dover, New York, 1950).
[224]Reference 150, pp. 2–20.
[225]P. J. Nahin, *Oliver Heaviside* (IEEE, New York, 1988).
[226]R. W. Whitworth and H. V. Stopes-Roe, "Experimental demonstration that the couple on a bar magnet depends on H not B," Nature **234**, 31–33 (1971).
[227]P. J. Smith, "B and H," Nature **250**, 535 (1974).
[228]Reference 160, pp. 241–242.
[229]Reference 176, p. 7.
[230]A. W. Rücker, "On the suppressed dimensions of physical quantities," Philos. Mag. (Series 5) **27**, 104–114 (1889).
[231]A. W. Porter, *The Method of Dimensions* (Methuen, London, 1933), pp. 66–71.
[232]S. L. Rock, E. F. Pearson, E. H. Appleman, C. L. Norris, and W. H. Flygare, "Molecular rotational Zeeman effect in HOF, a comparison with H_2O, F_2O, and other flourine containing molecules; and dipole moments of HOF and DOF," J. Chem. Phys. **59**, 3940–3945 (1973).
[233]L. C. Jackson, "Investigations on paramagnetism at low temperatures," Philos. Trans. A **224**, 1–48 (1923).
[234]H. R. Nettleton and S. Sugden, "The magnetic susceptibility of nickel chloride," Proc. R. Soc. A **173**, 313–323 (1939).
[235]L. J. E. Hofer, W. C. Peebles, and W. E. Dieter, "X-ray diffraction and magnetic studies of unreduced ferric oxide Fischer–Tropsch catalysts," J. Am. Chem. Soc. **68**, 1953–1956 (1946).
[236]D. McClelland and J. J. Donoghue, "The effect of neutron bombardment upon the magnetic susceptibility of several pure oxides," J. Appl. Phys. **24**, 963 (1953).
[237]L. R. Bickford, Jr., J. Pappis, and J. L. Stull, "Magnetostriction and permeability of magnetite and cobalt-substituted magnetite," Phys. Rev. **99**, 1210–1214 (1955).
[238]*Landolt–Börnstein Numerical Data and Functional Relationships in Science and Technology*, edited by K.-H. Hellwege and A. M. Hellwege New Series Vol. 12: Magnetic and other Properties of Oxides and Related Compounds (Springer, Heidelberg, 1980).
[239]S. K. Banerjee and B. M. Moskowitz, "Ferrimagnetic properties of magnetite," in *Magnetite Biomineralization and Magnetoreception in Organisms; A New Biomagnetism*, edited by J. L. Kirschvink, D. R. Jones, and B. J. MacFadden (Plenum, New York, 1985), pp. 17–41.
[240]*Landolt–Börnstein Numerical Data and Functional Relationships in Science and Technology*, edited by R. R. Gupta New Series Vol. 16, Diamagnetic Susceptibility (Springer, Heidelberg, 1986).
[241]K. O'Grady, R. G. Gibson, and P. C. Hobby, "Magnetic pigment dispersions (a tutorial review)," J. Magn. Magn. Mat. **95**, 341–355 (1991).
[242]J. Emsley, *The Elements*, 2nd ed. (Clarendon Press, Oxford, 1991).
[243]L. Pauling, R. E. Wood, and J. H. Sturdivant, "An instrument for determining the partial pressure of oxygen in a gas," Science **103**, 338 (1946).
[244]L. Pauling, R. E. Wood, and J. H. Sturdivant, "An instrument for determining the partial pressure of oxygen in a gas," J. Am. Chem. Soc. **68**, 795–798 (1946).
[245]L. A. Geddes and L. E. Baker, *Principles of Applied Biomedical Instrumentation*, 3rd ed. (Wiley, New York, 1989). p. 153 and pp. 288–291.
[246]Reference 180, p. 105–107.
[247]Reference 181, pp. 312–317.
[248]S. Dattagupta, *Relaxation Phenomena in Condensed Matter Physics* (Academic, Orlando, 1987), pp. 5–25.
[249]F. W. Byron, Jr., and R. W. Fuller, *Mathematics of Classical and Quantum Physics* (Addison-Wesley, Reading, 1969, 1970; Reprinted, Dover, New York, 1992), pp. 344–349.
[250]Reference 180, pp. 268–270.
[251]P. N. Butcher and D. Cotter, *The Elements of Nonlinear Optics* (Cambridge University, Cambridge, 1990).
[252]A. Abragam, *The Principles of Nuclear Magnetism* (Clarendon, Oxford, 1961).
[253]P. W. Atkins, *Molecular Quantum Mechanics*, 2nd ed. (Oxford University, Oxford, 1983), pp. 377–394.
[254]P. Langevin, "Magnétisme et théorie des électrons," Ann. Chim. Phys. (Series 8) **5**, 70–127 (1905).
[255]W. Pauli, "Theoretische Bemerkungen über den Diamagnetismus einatomiger Gase," Z. Phys. **2**, 201–205 (1920).
[256]W. Weltner, Jr., "Paramagnetism in diamagnetic molecules," J. Chem. Phys. **28**, 477–485 (1958).
[257]L. Landau, "Diamagnetismus der Metalle," Z. Phys. **64**, 629–637 (1930).
[258]W. Pauli, Jr., "Über Gasentartung und paramagnetismus," Z. Phys. **41**, 81–102 (1927).
[259]Reference 158, pp. 201–219.
[260]Reference 165, pp. 150–169.
[261]Reference 168, pp. 144–160.
[262]J. H. Van Vleck, "Magnetic properties of metals," Nuovo Cimento (Series 10) **6**, Supplement AL, 857–886 (1957).
[263]S. D. Silverstein, "Influence of electron interactions on metallic properties. II. Electron spin paramagnetism," Phys. Rev. **130**, 1703–1710 (1962).
[264]W. Jones and N. H. March, *Theoretical Solid State Physics* (Wiley, New York, 1973; Reprinted, Dover, New York, 1985), pp. 318–450.
[265]D. Y. Kojima and A. Isihara, "Density dependence of the magnetic susceptibilities of metals," Phys. Rev. B **20**, 489–500 (1979).
[266]I. Dzyaloshinsky, "A thermodynamic theory of "weak" ferromagnetism of antiferromagnetics," J. Phys. Chem. Solids **4**, 241–255 (1958).
[267]P. J. Flanders and W. J. Schuele, "Anisotropy in the basal plane of hematite single crystals," Philos. Mag. (8th Series) **9**, 485–490 (1964).
[268]T. Moriya, "Weak ferromagnetism," in *Magnetism: A Treatise on Modern Theory and Materials*, edited by G. T. Rado and H. Suhl (Academic, New York, 1963), Vol. 1, pp. 85–125.
[269]J. H. Van Vleck, "$\chi=C/(T+\Delta)$, the most overworked formula in the history of paramagnetism," Physica **69**, 177–192 (1973).
[270]C. Herring, "Exchange interactions among itinerant electrons," in *Magnetism: A Treatise on Modern Theory and Materials*, edited by G. T. Rado and H. Suhl (Academic, New York, 1966), Vol. IV, pp. 1–407.
[271]Reference 163, pp. 821–823.
[272]Reference 182, pp. 127–143.
[273]C. P. Bean, "Hysteresis loops of mixtures of ferromagnetic micropowders," J. Appl. Phys. **26**, 1381–1383 (1955).
[274]C. P. Bean and I. S. Jacobs, "Magnetic granulometry and superparamagnetism," J. Appl. Phys. **27**, 1448–1452 (1956).
[275]C. P. Bean and J. D. Livingston, "Superparamagnetism," J. Appl. Phys. **30** (Supplement), 120S–129S (1959).
[276]C. P. Bean and I. S. Jacobs, "Magnetization of a dilute suspension of a multidomain ferromagnetic," J. Appl. Phys. **31**, 1228–1230 (1960).
[277]Yu. D. Tropin, "Superparamagnetism below the blocking temperature," Izv. Earth Physics **7**, 61–63 (1967). Translation in Phys. Solid Earth, 1967, 458–459 (1967).
[278]A. Ya. Vlasov, G. V. Kovalenko, and V. A. Chikhachev, "The superparamagnetism of α-FeOOH," Izv. Earth Physics **7**, 64–69 (1967). Translation in Phys. Solid Earth 460–464 (1967).
[279]G. Pullaiah, E. Irving, K. L. Buchan, and D. J. Dunlop, "Magnetization changes caused by burial and uplift," Earth Planet. Sci. Lett. **28**, 133–143 (1975).
[280]R. F. Butler and S. K. Banerjee, "Theoretical single-domain size range in magnetite and titanomagnetite," J. Geophys. Res. **80**, 4049–4058 (1975).
[281]M. Lönnemark, A. Hemmingson, J. Carlsten, A. Ericsson, E. Holtz, and J. Klaveness, "Superparamagnetic particles as an MRI contrast agent for the gastrointestinal tract," Acta Radiol. **29**, 599–602 (1988).
[282]Cerdan, H. R. Lötscher, B. Künnecke, and J. Seelig, "Monoclonal antibody-coated magnetite particles as contrast agents in magnetic resonance imaging of tumors," Magn. Reson. Med. **12**, 151–163 (1989).
[283]Y. Kawamura, K. Endo, Y. Watanabe, T. Saga, T. Nakai, H. Hikita, K. Kagawa, and J. Konishi, "Use of magnetite particles as a contrast agent for MR imaging of the liver," Radiology **174**, 357–360 (1990).
[284]R. Weissleder, G. Elizondo, J. Wittenberg, C. A. Rabito, H. H. Bengele, and L. Josephson, "Ultrasmall superparamagnetic iron oxide: Characterization of a new class of contrast agents for MR imaging," Radiology **175**, 489–493 (1990).
[285]R. Weislaeder, G. Elizondo, J. Wittenberg, A. S. Lee, L. Josephson, and T. J. Brady, "Ultrasmall superparamagnetic iron oxide: An intravenous contrast agent for assessing lymph nodes with MR imaging," Radiology **175**, 494–498 (1990).
[286]J. T. Ferruci and D. Stark, "Iron oxide-enhanced MR imaging of the liver

and spleen: Review of the first five years," Am. J. Roentgenol. **155**, 943–950 (1990).
[287]T. Shen, R. Weissleder, M. Papisov, A. Bogdanov, Jr., and T. J. Brady, "Monocrystalline iron oxide nanocompounds (MION): Physicochemical properties," Magn. Reson. Med. **29**, 599–604 (1993).
[288]T. G. St. Pierre, D. H. Jones, and D. P. E. Dickson, "The behavior of superparamagnetic small particles in applied magnetic fields: A Mössbauer spectroscopic study of ferritin and haemosiderin," J. Magn. Magn. Mater. **69**, 276–284 (1987).
[289]D. D. Awschalom, D. P. DiVincenzo, and J. F. Smyth, "Macroscopic quantum effects in nanometer-scale magnets," Science **258**, 414–421 (1992).
[290]D. D. Awschalom, J. F. Smyth, G. Grinstein, D. P. DiVincenzo, and D. Loss, "Macroscopic quantum tunneling in magnetic proteins," Phys. Rev Lett. **68**, 3092–3095 (1992).
[291]A. Garg, "Have resonance experiments seen macroscopic quantum coherence in magnetic particles? The case from power absorption," Phys. Rev. Lett. **71**, 4249–4252 (1993).
[292]S. Morup and E. Tronc, "Superparamagnetic relaxation of weakly interacting particles," Phys. Rev. Lett. **72**, 3278–3281 (1994).
[293]Gider, D. D. Awschalom, T. Douglas, S. Mann, and M. Chaparala, "Classical and quantum magnetic phenomena in natural and artificial ferritin proteins," Science **268**, 77–80 (1995).
[294]A. P. Wills and G. F. Boeker, "The dependence of the diamagnetism of water upon its temperature," Phys. Rev. **46**, 907–909 (1934).
[295]S. Seely, "The variation of the diamagnetism of water with temperature," Phys. Rev. **52**, 662 (1937).
[296]T. P. Das and T. Ghose, "Magnetic properties of water molecule," J. Chem. Phys. **31**, 42–52 (1959).
[297]G. P. Arrighini, M. Maestro, and R. Moccia, "Magnetic properties of polyatomic molecules. I. Magnetic susceptibility of H_2O, NH_3, CH_4, H_2O_2," J. Chem. Phys. **49**, 882–889 (1968).
[298]R. Cini and M. Torrini, "Temperature dependence of the magnetic susceptibility of water," J. Chem. Phys. **49**, 2826–2830 (1968).
[299]H. Taft and B. P. Dailey, "Magnetic susceptibility of the H_2O molecule," J. Chem. Phys. **51**, 1002–1007 (1969).
[300]J. Verhoeven and A. Dymanus, "Magnetic properties and molecular quadrupole tensor of the water molecule by beam-maser Zeeman spectroscopy," J. Chem. Phys. **52**, 3222–3233 (1970).
[301]Y.-C. Pan and H. F. Hameka, "Calculation of the diamagnetic susceptibility of the water molecule," J. Chem. Phys. **53**, 1265–1269 (1970).
[302]C. W. Kern and M. Karplus, "The water molecule," in *Water: A Comprehensive Treatise*, edited by F. Franks, Vol. 1: The Physics and Physical Chemistry of Water (Plenum, New York, 1972), pp. 21–91.
[303]J. S. Philo and W. M. Fairbank, "Temperature dependence of the diamagnetism of water," J. Chem. Phys. **72**, 4429–4433 (1980).
[304]E. P. Day, "Equation for the magnetic susceptibility of water," J. Chem. Phys. **72**, 4434–4436 (1980).
[305]R. L. Conger and P. W. Selwood, "Proton relaxation in paramagnetic solutions," J. Chem. Phys. **20**, 383–387 (1952).
[306]A. W. Nolle and L. O. Morgan "Frequency dependence of proton spin relaxation in aqueous solutions of paramagnetic ions," J. Chem. Phys. **26**, 642–648 (1957).
[307]L. O. Morgan and A. W. Nolle, "Proton spin relaxation in aqueous solutions of paramagnetic ions. II. Cr^{+++}, Mn^{++}, Ni^{++}, Cu^{++}, and Gd^{+++}," J. Chem. Phys. **31**, 365–368 (1959).
[308]R. Hausser and F. Noack, "Kernmagnetische relaxation und korrelation im system Wasser–Sauerstoff," Z. Naturforsch. Teil A **20**, 1668–1675 (1965).
[309]K. Krynicki, "Proton spin-lattice relaxation in pure water between 0 °C and 100 °C," Physica **32**, 167–178 (1966).
[310]J. A. Glasel "Nuclear magnetic resonance studies on water and ice," in *Water: A Comprehensive Treatise*, edited by F. Franks Vol. 1: The Physics and Physical Chemistry of Water (Plenum, New York, 1972), pp. 215–254.
[311]C. Hindman, A. Svirmickas, and M. Wood, "Relaxation processes in water. A study of the proton spin-lattice relaxation time," J. Chem. Phys. **59**, 1517–1522 (1973).
[312]J. S. Philo, U. Dreyer, and T. M. Schuster, "Diamagnetism of human apo-, oxy-, and (carbonmonoxy)-hemoglobin," Biochemistry **23**, 865–872 (1984).
[313]Reference 171, p. 86.
[314]J. S. Philo (personal communication).
[315]J. O. Christoffersson, L. E. Olsson, and S. Sjöberg, "Nickel-doped agarose gel phantoms in MR imaging," Acta Radiol. **32**, 426–431 (1991).
[316]F. E. Senftle and A. Thorpe, "Magnetic susceptibility of normal liver and transplantable hepatoma tissue," Nature **190**, 410–413 (1961).
[317]F. E. Senftle and W. P. Hambright, "Magnetic susceptibility of biological materials," in *Biological Effects of Magnetic Fields*, edited by M. F. Barnothy (Plenum, New York, 1969), Vol. 2, pp. 261–306.
[318]G. M. Brittenham, D. E. Farrell, J. W. Harris, E. S. Feldman, E. H. Danish, W. A. Muir, J. H. Tripp, and E. M. Bellon, "Magnetic-susceptibility of human iron stores," N. Eng. J. Med. **307**, 1671–1675 (1982).
[319]L. Pauling and C. D. Coryell, "The magnetic properties and structure of hemoglobin, oxyhemoglobin, and carbonmonoxyhemoglobin," Proc. Natl. Acad. Sci. USA **22**, 210–216 (1936).
[320]Reference 171, p. 155.
[321]K. Lonsdale, "Diamagnetic anisotropy of conjugated compounds," J. Chem. Soc. **1**, 364–368 (1939).
[322]K. Lonsdale, "Diamagnetic anisotropy of organic molecules," Proc. R. Soc. London A **171**, 541–568 (1939).
[323]Z. Gottesfeld and M. Neeman, "Ferritin effect on the transverse relaxation of water: NMR microscopy at 9.4 T," Magn. Reson. Med. **35**, 514–520 (1996).
[324]L. Michaelis, C. D. Coryell, and S. Granick, "The magnetic properties of ferritin and some other colloidal ferric compounds," J. Biol. Chem. **148**, 463–480 (1943).
[325]T. G. St. Pierre, J. Webb, and S. Mann, "Ferritin and hemosiderin: Structural and magnetic studies of the iron core," in *Biomineralization: Chemical and Biochemical Perspectives*, edited by S. Mann, J. Webb, and R. J. P. Williams (VCH, Weinheim, 1989), pp. 295–344.
[326]F. Moatamed and F. B. Johnson, "Identification and significance of magnetite in human tissues," Arch. Pathol. Lab. Med. **110**, 618–621 (1986).
[327]J. L. Kirschvink, A. Kobayishi-Kirschvink, and B. J. Woodford, "Magnetite biomineralization in the human brain," Proc. Natl. Acad. Sci. USA **89**, 7683–7687 (1992).
[328]D. Cohen, "Ferromagnetic contamination in the lungs and other organs of the body," Science **180**, 745–748 (1973).
[329]A. P. Freedman, S. E. Robinson, and R. J. Johnston, "Non-invasive magnetopneumographic estimation of lung dust loads and distribution in bituminous coal workers," J. Occupational Med. **22**, 613–618 (1980).
[330]D. Cohen and I. Nemoto, "Ferrimagnetic particles in the lung Part 1: The magnetizing process," IEEE Trans. Biomed. Engin. **31**, 261–273 (1984).
[331]D. Cohen, I. Nemoto, L. Kaufman, and S. Arai "Ferrimagnetic particles in the lung Part 2: The relaxation process," IEEE Trans. Biomed. Engin. **31**, 274–284 (1984).
[332]G. Lund, J. D. Nelson, J. D. Wirtschafter, and P. A. Williams, "Tattooing of eyelids: Magnetic resonance imaging artifacts," Ophthalmic Surg. **17**, 550–553 (1986).
[333]D. C. Sacco, D. A. Steiger, E. M. Bellon, P. E. Coleman, and E. M. Haacke, "Artifacts caused by cosmetics in MR imaging of the head," Am. J. Roentgenol. **148**, 1001–1004 (1987).
[334]J. G. Jackson and J. D. Acker, "Permanent eyeliner and MR imaging," Am. J. Roentgenol. **149**, 1080 (1987) (letter).
[335]D. E. Wolfley, K. J. Flynn, J. Cartwright, and J. A. Tschen, "Eyelid pigment implantation: Early and late histopathology," Plast. Reconstr. Surg. **82**, 770–774 (1988).
[336]J. K. Stanley, *Metallurgy and Magnetism* (American Society for Metals, Cleveland, 1949).
[337]K. Hoselitz, *Ferromagnetic Properties of Metals and Alloys* (Clarendon, Oxford, 1952).
[338]G. L. Salinger and J. C. Wheatley, "Magnetic susceptibility of materials commonly used in the construction of cryogenic apparatus," Rev. Sci. Instrum. **32**, 872–874 (1961).
[339]C. A. Zapffe, A. M. Bounds, W. W. Brandel *et al.*, "Wrought stainless steels," in *Metals Handbook*, 8th ed. (American Society for Metals, Metals Park, Novelty, OH, 1961), Vol. 1: Properties and Selection of Metals, pp. 408–431.
[340]*Smithells Metals Reference Handbook*, 6th ed., edited by E. A. Brandes (Butterworths, London, 1983).
[341]P. M. Unterweiser and H. M. Cobb, *Worldwide Guide to Equivalent Irons and Steels*, 2nd ed. (ASM International, Metals Park, Ohio, 1987).
[342]S. D. Washko and G. Aggen, "Wrought stainless steels," in *Metals Handbook*, 10th ed. (ASM International, Materials Park, OH, 1990), Vol.

1: Properties and Selection of Irons, Steels, and High-Performance Alloys, pp. 841–907.
[343]N. Ohashi, "Modern steelmaking," Am. Scient. **80**, 540–555 (1992).
[344]F. Herbst, "Permanent magnets," Am. Scient. **81**, 252–260 (1993).
[345]E. I. Kondorsky and V. L. Sedov, "Antiferromagnetism of iron in face-centered crystalline lattice and the causes of anomalies in invar physical properties," J. Appl. Phys. **31**, 331S–335S (1960).
[346]Y. Ishikawa, Y. Endoh, and T. Takimoto, "Antiferromagnetism of a γ iron–nickel–chromium alloy (non-magnetic stainless steel)," J. Phys. Chem. Solids **31**, 1225–1234 (1970).
[347]R. Kohlhaas, A. A. Raible, and W. Rocker, "Zum antiferromagnetismus austenitischer Eisenwerkstoffe (About the antiferromagnetic behavior of some austenitic steels)," Z. Angew. Phys. **30**, 254–257, (1970).
[348]L. A. A. Warnes and H. W. King, "The low temperature magnetic properties of austenitic Fe–Cr–Ni alloys: 1. The effect of nickel concentration in Fe–Ni–20 wt% Cr alloys," Cryogenics **16**, 473–481 (1976).
[349]L. A. A. Warnes and H. W. King, "The low temperature magnetic properties of austenitic Fe–Cr–Ni alloys: 2. The prediction of Néel temperatures and maximum susceptibilities," Cryogenics **16**, 659–667 (1976).
[350]R. J. Diefendorf, "Carbon/graphite fibers," in *Engineered Materials Handbook*, edited by T. J. Reinhart, *et al.* (ASM International, Metals Park, Ohio, 1987), Vol. 1, pp. 49–53.
[351]M. S. Dresselhaus, G. Dresselhaus, K. Sugihara, I. L. Spain, and H. A. Goldberg, *Graphite Fibers and Filaments* (Springer, Berlin, 1988).
[352]L. E. McCallister and S. Awasthi, "Carbon–carbon composites," in *Encyclopedia of Advanced Materials*, edited by D. Bloor, R. J. Brook, M. C. Flemings, and S. Mahajan (Elsevier Science, Tarrytown, 1994).
[353]D. J. Johnson, "Carbon fibers," in *Encyclopedia of Advanced Materials*, edited by D. Bloor, R. J. Brook, M. C. Flemings and S. Mahajan (Elsevier, Tarrytown, 1994).
[354]L. H. Peebles, *Carbon Fibers: Formation, Structure, and Properties* (CRC, Boca Raton, 1995).
[355]J. W. McLure, "Electronic structure and magnetic properties of monocrystalline graphite," J. Chim. Phys. **57**, 859–865 (1960).
[356]E. Poquet, N. Lumbroso, J. Hoarau, A. Marchand, A. Pacault, and D. E. Soule, "Étude du diamagnétisme de monocristaux de graphite," J. Chim. Phys. **57**, 866–872 (1960).
[357]J. W. McClure and B. B. Hickman, "Analysis of magnetic susceptibility of carbon fibers," Carbon **20**, 373–378 (1982).
[358]J. F. Schenck, K. W. Rohling, T. M. Moriarty, E. Alexander III, and F. A. Jolesz, "Carbon fiber biopsy cannulas for MR-compatible neurosurgical procedures," in *Book of Abstracts* (Society of Magnetic Resonance, Berkeley, CA, 1995), p. 1160.
[359]B. Keisch, "Mössbauer effect studies in fine arts," J. Phys. Paris **35** (C6), 151–164 (1974).
[360]V. Rusanov, V. Angelov, V. Jordanov, and S. Ormandjiev, "Mössbauer test for forgery," Nature **349**, 199 (1991).
[361]E. C. Stoner, "The demagnetizing factors for ellipsoids," Philos. Mag. (Series 7) **37**, 803–821 (1945).
[362]R. M. Bozorth and D. M. Chapin, "Demagnetizing factors of rods," J. Appl. Phys. **13**, 320–326 (1942).
[363]J. A. Osborn, "Demagnetizing factors of the general ellipsoid," Phys. Rev. **67**, 351–357 (1945).
[364]R. I. Joseph and E. Schlömann, "Demagnetizing field in nonellipsoidal bodies," J. Appl. Phys. **36**, 1579–1593 (1965).
[365]Reference 153, pp. 407–462.
[366]Reference 167, pp. 1304–1309.
[367]Reference 180, pp. 19–29.
[368]E. R. Cohen and B. N. Taylor, "The fundamental physical constants," Phys. Today **42**, BG 8–8d (1989).
[369]D. B. Plewes and J. Bishop, "Spin-echo MR imaging," in *The Physics of MRI*, Medical Physics Monograph No. 21, edited by M. J. Bronskill and P. Sprawls (American Institute of Physics, Woodbury 1993), pp. 166–187.
[370]G. H. Glover, "Gradient echo imaging," in *The Physics of MRI*, Medical Physics Monograph No. 21, edited by M. J. Bronskill and P. Sprawls (American Institute of Physics, Woodbury, 1993), pp. 188–205.
[371]S. F. Hulbert, S. J. Morrison, and J. J. Klawitter, "Tissue reaction to three ceramics of porous and non-porous structures," J. Biomed. Mater. Res. **6**, 347–374 (1972).
[372]P. Christel, A. Meunier, M. Heller, J. P. Torre, and C. N. Peille, "Mechanical properties and short-term *in-vivo* evaluation of yttrium-oxide-partially-stabilized zirconia," J. Biomed. Mater. Res. **23**, 45–61 (1989).
[373]P. S. Christel, "Zirconia: The second generation of ceramics for total hip replacement," Bull. Hosp. Jt. Dis. Orthop. Inst. **49**, 170–177 (1989).
[374]A. Suda, T. Sato, M. Takagi, and O Suzuki, "Biocompatibility of zirconia dispersed hydroxyapatitie ceramics," J. Jpn. Orthop. Assoc **64**, 75–84 (1990).
[375]V. S. Nagarajan and K. J. Rao, "Characterization of sol–gel derived zirconia with additions of yttria and ceria. Origin of high fracture toughness in ceria-stabilized samples," Philos. Mag. A **65**, 771–781 (1992).
[376]K. Hayashi, N. Matsuguchi, K. Uenoyama, and Y. Sugioka, "Re-evaluation of the biocompatibility of bioinert ceramics *in vivo*," Biomaterials **13**, 195–200 (1992).